



SCUOLA INTERNAZIONALE SUPERIORE DI STUDI AVANZATI  
INTERNATIONAL SCHOOL FOR ADVANCED STUDIES

**Quantum Effects and Broken Symmetries**  
**in**  
**Frustrated Antiferromagnets**

Thesis submitted for the degree of  
*Doctor Philosophiæ*

**Candidate:**  
Luca Capriotti

**Supervisor:**  
Prof. Sandro Sorella

October 2000



## Abstract

We investigate the interplay between frustration and zero-point quantum fluctuations in the ground state of two spin-half frustrated spin systems: the triangular and the  $J_1-J_2$  Heisenberg antiferromagnets. These are the simplest examples of two-dimensional spin models in which quantum effects may be strong enough to destroy the classical long-range Néel order, thus stabilizing a ground state with symmetries and correlations different from their classical counterparts.

In this thesis the ground-state properties of these frustrated models are studied using finite-size spin-wave theory, exact diagonalization, and quantum Monte Carlo methods. In particular, in order to control the sign-problem instability, which affects the numerical simulation of frustrated spin systems and fermionic models, we have used the recently developed Green function Monte Carlo with Stochastic Reconfiguration. This technique, which represents the state-of-the-art among the zero-temperature quantum Monte Carlo methods, has been developed and tested in detail in the present thesis.

In the triangular Heisenberg antiferromagnet, by performing a systematic size-scaling analysis, we have obtained strong evidences for a gapless spectrum and a finite value of the thermodynamic order parameter, thus confirming the existence of long-range Néel order. Our best estimate is that in the thermodynamic limit the antiferromagnetic order parameter  $m^\dagger = 0.41 \pm 0.02$  is reduced by about 59% from its classical value and the ground state energy per site is  $e_0 = -0.5458 \pm 0.0001$  in unit of the exchange coupling. In addition, the good agreement between the finite-size spin-wave results and the exact and quantum Monte Carlo data supports the reliability of the spin-wave expansion to describe both the ground state and the low-energy spin excitations of the triangular Heisenberg antiferromagnet.

In the  $J_1-J_2$  Heisenberg model, our results indicate the opening of a finite gap in the thermodynamic excitation spectrum at  $J_2/J_1 \simeq 0.4$ , marking the melting of the antiferromagnetic Néel order and the onset of a non-magnetic ground state. In order to characterize the nature of the latter quantum-disordered phase we have computed the susceptibilities for the most important crystal symmetry breaking operators. A genuine and somehow unexpected ‘plaquette resonating valence bond’ (RVB), with spontaneously broken translation symmetry and no broken rotation symmetry, comes out from our numerical simulations as the most plausible ground state in the regime of strong frustration. In the ordered phase, instead, the effectiveness of the spin-wave theory in reproducing the low-energy excitation spectrum suggests that the uniform spin susceptibility of the model is very close to the linear spin-wave prediction.



# Contents

<b>Introduction</b>	<b>1</b>
<b>1 Spontaneous symmetry breaking in a quantum antiferromagnet</b>	<b>7</b>
1.1 The Lieb-Mattis property . . . . .	7
1.1.1 Marshall-Peierls sign rule . . . . .	8
1.1.2 Ordering of the energy levels . . . . .	11
1.2 Order parameters and susceptibilities . . . . .	12
1.2.1 Exact bounds on the susceptibilities . . . . .	13
1.3 Néel order and Anderson's towers of states . . . . .	15
1.4 Resonating Valence Bond states . . . . .	17
<b>2 Numerical methods</b>	<b>21</b>
2.1 The Lanczos method . . . . .	23
2.2 Monte Carlo sampling . . . . .	25
2.3 Variational Monte Carlo . . . . .	26
2.3.1 Variational improvement by Lanczos iteration . . . . .	28
2.4 The Green function Monte Carlo . . . . .	28
2.4.1 Statistical implementation of the power method . . . . .	29
2.4.2 The Stochastic Reconfiguration . . . . .	35
2.4.3 The limit $\Lambda \rightarrow \infty$ for the power method: imaginary time evolution	40
2.5 Numerical tests . . . . .	41
2.5.1 The limit of small $\Delta\tau$ and large number of walkers . . . . .	41
2.5.2 Convergence to the exact result and size consistency . . . . .	45
<b>3 The triangular Heisenberg antiferromagnet</b>	<b>49</b>
3.1 Finite-size spin-wave theory . . . . .	50
3.1.1 Application to the triangular antiferromagnet . . . . .	51
3.1.2 Low-energy spin-wave spectrum . . . . .	53

## ii Contents

3.1.3	Spin-wave variational wavefunctions . . . . .	56
3.2	Quantum Monte Carlo calculation . . . . .	58
3.2.1	From Marshal-Peierls to Huse-Elser sign rule . . . . .	58
3.2.2	The reconfiguration scheme . . . . .	60
3.2.3	Ground-state energy and spin gap . . . . .	61
3.2.4	Staggered magnetization . . . . .	63
3.3	Conclusions . . . . .	66
<b>4</b>	<b>The <math>J_1 - J_2</math> Heisenberg model</b>	<b>67</b>
4.1	Finite-size spin-wave results . . . . .	68
4.2	Transition to a quantum disordered state induced by frustration . . . . .	70
4.2.1	Spin-wave susceptibilities and low-energy spectra . . . . .	70
4.2.2	Size-scaling of the spin gap . . . . .	72
4.3	The nature of the non-magnetic phase . . . . .	73
4.3.1	The method of generalized susceptibilities . . . . .	74
4.3.2	Stability of Plaquette vs Columnar RVB . . . . .	76
4.4	Conclusions . . . . .	79
	<b>Conclusions</b>	<b>81</b>
	<b>Acknowledgments</b>	<b>83</b>
	<b>(Further) Acknowledgments and Greetings</b>	<b>85</b>
<b>A</b>	<b>An important property of non-positive Hamiltonian matrices</b>	<b>89</b>
<b>B</b>	<b>The uniform spin susceptibility</b>	<b>91</b>
<b>C</b>	<b>Properties of a stochastic matrix</b>	<b>93</b>
<b>D</b>	<b>Stochastic Reconfiguration conditions</b>	<b>95</b>
D.1	Formal proof of the SR conditions . . . . .	95
D.2	Existence and uniqueness of a solution for the SR . . . . .	96
<b>E</b>	<b>Details of the GFMCSR algorithm</b>	<b>101</b>
<b>F</b>	<b>Optimization of the one Lanczos step variational parameter</b>	<b>105</b>
	<b>Bibliography</b>	<b>107</b>

# Introduction

The physics of quantum antiferromagnets is a very old topic, dating back to the early days of quantum mechanics itself. Nonetheless, after many years of intensive study, the interest in this research field is still high, with several new problems arising from the behavior of low-dimensional magnetic materials. This is also due to the existence of simple toy-models in which the interplay between antiferromagnetism, symmetry, dimensionality and strong quantum correlations leads to fascinating effects in the low-temperature physics, often reproducing the behavior of real systems. Among them, the nearest-neighbor Heisenberg Hamiltonian,

$$\hat{\mathcal{H}} = J \sum_{n.n.} \hat{\mathbf{S}}_i \cdot \hat{\mathbf{S}}_j, \quad (1)$$

where  $\hat{\mathbf{S}}_i = (\hat{S}_i^x, \hat{S}_i^y, \hat{S}_i^z)$  are spin- $s$  operators and  $J$  is the (positive) exchange integral, has certainly played a central role as an ideal test ground to investigate the influence of quantum effects on the mechanism of spontaneous symmetry breaking. In fact, in contrast to the ferromagnetic state, the classical Néel state is not an eigenstate of the Heisenberg Hamiltonian and therefore, in general, the ground state of the latter does not have a purely classical representation. Hence, quantum effects may play an important role in modifying the zero-temperature properties of the model from the classical ( $s \rightarrow \infty$ ) limit. In particular, reduced dimensionality and a small spin value might enhance zero-point quantum fluctuations up to the point of destroying the classical Néel order, thus stabilizing a ground state with symmetries and correlations different from its classical counterpart.

Indeed, in one dimension and for  $s = 1/2$ , a famous exact solution found by Bethe in 1931 [1] showed that quantum effects prevent the onset of true long-range antiferromagnetic order, giving instead a power-law decay of the spin-spin correlation functions. Despite Bethe's promise to generalize his solution to the two-dimensional square lattice case, appearing in the conclusions of his paper, this was never done, and the issue of the existence of long-range order in the ground state of the two-dimensional Heisenberg model has been left unsolved for many years. The rigorous proof of the ordered nature of

## 2 Introduction

the ground state of the square Heisenberg antiferromagnet was given in fact, for  $s \geq 1$ , only in 1986 [2], and has not been extended yet to the spin-half case where zero-point quantum fluctuations are stronger.

This problem became a hot topic when possible connections between a non-magnetic ground state and the mechanism of high- $T_c$  superconductivity were put forward by Anderson in 1987 [3]. In fact, since the stoichiometric compounds of the high- $T_c$  superconductors are good realizations of a  $s = 1/2$  square Heisenberg antiferromagnet, this conjecture focused the attention on the properties of this system. Fortunately enough, at that time the development of modern computers was such that the use of numerical techniques could compensate for the lack of exact analytical results. In particular, quantum Monte Carlo methods have been of crucial importance, by allowing one to perform a systematic size-scaling of the physical observables and therefore to reach a definite conclusion [4]. As a result, even if a rigorous proof is still lacking, there is at present a general consensus about the ordered nature of the ground state of the spin-half square Heisenberg antiferromagnet: in two dimensions, reduced dimensionality and a low spin value do not seem enough to stabilize, within the Heisenberg model, a non-magnetic ground state.

Better candidates for a realization of disordered ground states in two dimensions are frustrated spin models. In these systems, in fact, the usual antiferromagnetic alignment between spins is hindered by the geometry of the lattice or by the presence of competing interactions. As a result, a general feature introduced by frustration is a less stable classical minimum energy configuration which is more likely to be destabilized by zero-point quantum fluctuations for a small spin value. Among this class of systems two prototypical examples are given by the triangular Heisenberg antiferromagnet, and the  $J_1 - J_2$  Heisenberg model. The nature of the ground state in these frustrated spin models represents the main topic of this thesis.

The triangular Heisenberg antiferromagnet is described by the Hamiltonian (1), where  $i$  and  $j$  are the sites of a triangular lattice. Due to the geometry of the lattice (see Fig. 1), the classical minimum energy configuration of this model is not the usual Néel state with antiparallel spins on neighboring sites. In fact, if two spins on an elementary triangular plaquette minimize their exchange energy by aligning antiparallel, the third one cannot do the same because it cannot be antiparallel to both of them, simultaneously. As a result, the minimum energy configuration consists of coplanar spins forming  $\pm 2\pi/3$  angles between nearest-neighbors and this leads to a  $\sqrt{3} \times \sqrt{3}$  periodic Néel state with the spins ferromagnetically aligned on each of the three sublattices (Fig. 1). The resulting state, having an energy per bond twice than the optimal one, is far less stable than that

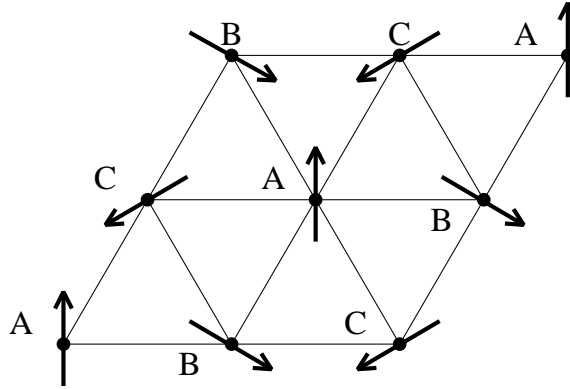


Figure 1: The classical Néel state consists of coplanar spins forming  $\pm 2\pi/3$  angles between nearest neighbors. This leads to a  $\sqrt{3} \times \sqrt{3}$  periodicity with the spins on the three sublattices A,B,C ferromagnetically aligned.

on the square lattice.

In the  $J_1 - J_2$  model, instead, frustration arises on the square lattice because of the presence of competing interactions, the Hamiltonian being

$$\hat{\mathcal{H}} = J_1 \sum_{n.n.} \hat{\mathbf{S}}_i \cdot \hat{\mathbf{S}}_j + J_2 \sum_{n.n.n.} \hat{\mathbf{S}}_i \cdot \hat{\mathbf{S}}_j, \quad (2)$$

where  $J_1$  and  $J_2$  are the antiferromagnetic couplings between nearest- and next-nearest-neighbors, respectively. Classically, the minimum energy configuration has the conventional Néel order for  $J_2/J_1 < 0.5$  [Fig. 2 (a)]. By increasing further the frustrating interaction  $J_2$  this configuration is destabilized and, for  $J_2/J_1 > 0.5$ , the system decouples into two Néel ordered sublattices. At the purely classical level, the energy of the latter configuration is independent of the relative orientations of the staggered magnetizations on the two sublattices. However, this degeneracy is partially lifted by zero-point quantum fluctuations even at the lowest order in  $1/s$  so that in the  $s \rightarrow \infty$  limit the minimum energy configuration is the so-called *collinear* state [Fig. 2 (b)] with the spin ferromagnetically aligned in one direction and antiferromagnetically in the other, corresponding to a magnetic wavevector  $\mathbf{Q} = (\pi, 0)$  or  $\mathbf{Q} = (0, \pi)$  [5]. Exactly at  $J_2/J_1 = 0.5$  any classical state having zero total spin on each elementary square plaquette is a minimum of the total energy. These states include both the Néel and the collinear states but also many others with no long-range order. The occurrence of a non-magnetic ground state in the quantum case, for a small spin value, is therefore likely around this value of the  $J_2/J_1$  ratio.

The recent experimental finding of real compounds described by the triangular and the  $J_1 - J_2$  Heisenberg antiferromagnets have renewed the interest in these frustrated

## 4 Introduction

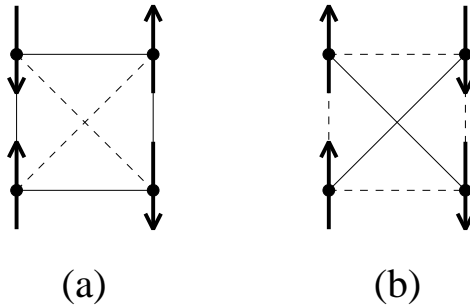


Figure 2: The two sublattices Néel (a) and the collinear (b) classical states.

spin systems. In particular the  $\text{K/Si(111)-}\sqrt{3} \times \sqrt{3}\text{-B}$  interface [6, 7] has turned out to be a good experimental realization of a spin-half Heisenberg antiferromagnet on a triangular lattice. In fact, due to strong electronic correlations, the surface states consist of a triangular arrangement of half-filled dangling bonds, which are localized and carry local  $s = 1/2$  magnetic moments coupled antiferromagnetically. Recent experimental realizations of the spin-half  $J_1\text{-}J_2$  Heisenberg model have been found instead in the  $\text{Li}_2\text{VO}_2\text{SiO}_4$  and  $\text{Li}_2\text{VOGeO}_4$  compounds [8]. These are three-dimensional systems formed by stacked square planes of  $V^{4+}$  ( $s = 1/2$ ) ions with a weak inter-plane interaction. The structure of the  $V^{4+}$  planes suggests that both the superexchange couplings between first and second neighbors can be significant and indeed, the first experimental results have indicated that these antiferromagnetic couplings are of the same order of magnitude [8]. In addition, the possibility of performing measurements under pressure will also allow one in the near future [9] to tune the  $J_2/J_1$  ratio and to investigate the properties of these systems in various regimes of frustration.

In this work the problem of the nature of the ground state of these frustrated spin systems is tackled using various techniques, namely: the finite-size spin-wave theory, exact diagonalization of small clusters by the Lanczos algorithm, and several zero-temperature quantum Monte Carlo methods. The finite-size spin-wave theory has been recently proposed [10] as a generalization of one of the oldest analytical techniques in the study of quantum magnetism [11]. In particular, this spin-wave expansion allows one to deal with finite clusters while avoiding the spurious Goldstone modes divergences in a straightforward way. Even if these results are biased by the long-range order hypothesis, nevertheless useful information on the thermodynamic ground state can be extracted from the comparison with the numerical results on finite systems or from the occurrence of a breakdown of the  $1/s$  expansion.

The Lanczos method allows the exact evaluation of static and dynamical properties of the finite-size system and, especially when combined with a careful analysis of the symmetry of the low-energy excited states [12], can provide clear indications about the nature of the ground state. However, due to memory constraints, exact diagonalization techniques are limited in two dimensions to very small clusters ( $\sim 30$  sites) so that it is in general difficult to perform a systematic size scaling of the important physical observables. In order to numerically investigate larger systems, different approaches are therefore necessary.

In the unfrustrated cases, quantum Monte Carlo has turned out to be an essential instrument for studying both the ground-state and the finite-temperature properties of a quantum antiferromagnet [13]. Unfortunately, in the frustrated cases standard stochastic techniques cannot be applied, as their reliability is strongly limited by the well-known *sign problem*. This numerical instability originates from the vanishing of the signal-to-noise ratio in the Monte Carlo sampling which occurs within bosonic models in the presence of frustration or, in general, in fermionic systems.

Presently, the sign problem can be controlled only at the price of introducing some kind of approximation. Apart from purely variational calculations, the simplest approximation scheme in the framework of one of the most efficient zero-temperature algorithms – the Green function Monte Carlo [14] – is the fixed-node (FN) technique [15]. This method allows one to obtain variational estimates of the energy by defining an effective Hamiltonian with no sign problem, depending on a variational guess on the ground-state wavefunction (the *guiding wavefunction*). However, the fixed-node results are usually strongly biased by this ansatz so that it is in general difficult to extract reliable information about the ground-state correlations whenever they are not well reproduced by the variational guess. In order to overcome this difficulty, here we have used the recently developed Green function Monte Carlo with Stochastic Reconfiguration [16, 17], which allows one to release the fixed-node approximation in a controlled way and to obtain much more accurate estimates of the ground-state correlations, thus reproducing also ground-state properties that are not contained at the variational level in the guiding wavefunction.

By using these numerical techniques, in this thesis we provide two clear examples of systems in which the combined effect of frustration and quantum fluctuations *do not* or *do* change the zero-temperature long-range properties of their classical counterparts. In particular we find that the thermodynamic ground state of the spin-half triangular Heisenberg antiferromagnet is most likely long-range ordered although with a remarkable reduction of the order parameter with respect to the classical case. On the other

## 6 Introduction

hand, in the  $J_1 - J_2$  Heisenberg model, quantum fluctuations turn out to be strong enough to melt the antiferromagnetic Néel order, driving the ground state into a non-magnetic phase of purely quantum-mechanical nature which we have characterized as a *plaquette RVB*.

# Chapter 1

## Spontaneous symmetry breaking in a quantum antiferromagnet

In this chapter we will review the basic concepts concerning the mechanism of the spontaneous symmetry breaking in a quantum antiferromagnet that will be used in the present work to investigate the ground-state properties of the triangular and of the  $J_1 - J_2$  Heisenberg models. Starting from the Lieb-Mattis theorem for the bipartite Heisenberg antiferromagnet, we will introduce some general features of the finite-size spectrum of the Heisenberg Hamiltonian. In particular, we will focus on the importance of the structure of the low-lying excited states, explaining also how the finite-size ground-state properties can be consistent with a broken symmetry in the thermodynamic limit.

### 1.1 The Lieb-Mattis property

One of the few rigorous results on the ground-state properties of the Heisenberg model on a bipartite lattice is the Lieb-Mattis theorem. Here we will reproduce the demonstration of this important result, following the paper by E. Lieb and D. Mattis [18] who extended and generalized the original results obtained by W. Marshall [19].

Let us consider the Heisenberg Hamiltonian

$$\hat{\mathcal{H}} = \sum_{(i,j)} J_{ij} \hat{\mathbf{S}}_i \cdot \hat{\mathbf{S}}_j, \quad (1.1)$$

where the sum runs over all the bonds on a  $d$ -dimensional *bipartite* lattice,  $\hat{\mathbf{S}}_i$  are spin- $s$  operators;  $J_{ij}$  is the (symmetric) exchange matrix such that  $J_{ij} > 0$ , if  $i$  and  $j$  belong to different sublattices, and  $J_{ij} < 0$ , otherwise. We will assume that the Hamiltonian cannot be split into sets of noninteracting spins, restricting also for simplicity, to the case

## 8 Spontaneous symmetry breaking in a quantum antiferromagnet

in which the number of sites of the two sublattices is the same. In the following  $N$  will denote the total number of sites of the lattice.

Since the Hamiltonian (1.1) commutes with all the three components of the total spin operator,

$$\hat{S} = \sum_i \hat{S}_i, \quad (1.2)$$

it is known from the theory of the angular momentum that we can construct two operators which commute with each other and with  $\hat{\mathcal{H}}$ . For example, choosing the quantization axis along the  $z$ -direction, we can consider the total spin squared,  $\hat{S}^2$ , and its component along the  $z$ -axis,  $\hat{S}^z$ , whose eigenvalues  $S(S+1)$  and  $M$  are good quantum numbers for the eigenstates of the Hamiltonian,

$$|\psi_n\rangle = |n, S, M, \dots\rangle, \quad (1.3)$$

such that  $\hat{\mathcal{H}}|\psi_n\rangle = E_n|\psi_n\rangle$ . If the couplings  $J_{ij}$  are translationally or rotationally invariant, also the lattice momentum and the eigenvalues of the generators of the crystal point group label the eigenstates of the Hamiltonian. However this restriction is not needed to derive the following results.

### 1.1.1 Marshall-Peierls sign rule

In the hypothesis stated above, the first strong result one can prove is about the signs of the coefficients of the expansion of the ground state of (1.1) in the so-called Ising basis whose states are specified by assigning the value of the  $S_i^z$  at each lattice site, i.e.,  $|x\rangle = \prod_{i=1}^N |m_i\rangle$  with  $\hat{S}_i^2|m_i\rangle = s(s+1)|m_i\rangle$  and  $\hat{S}_i^z|m_i\rangle = m_i|m_i\rangle$  where  $|m_i| \leq s$ . Within this basis it is easy to distinguish between the subspaces with different values of the projection of the total spin on the  $z$ -axis,  $M$ . In fact, in order to restrict to a particular  $M$  sector, one has to use only the states of the basis,  $|x\rangle$ , such that  $\sum_i m_i = M$ . In addition, sorting the basis in order to group together the states with the same  $M$ , the Hamiltonian matrix assumes a simpler block-diagonal form, i.e., a block for each  $M$  sector. Let us restrict therefore to a particular  $M$  subspace.

The first step of the proof is to perform a unitary transformation,

$$\hat{U}^\dagger = \exp \left[ -i\pi \sum_{i \in B} (s + \hat{S}_i^z) \right], \quad (1.4)$$

whose physical meaning is to flip the quantization axis on the B sublattice. This defines a spatially varying reference frame pointing along the local Néel direction [Fig. 2 (a)]. The transformed Hamiltonian then results

$$\hat{U}^\dagger \hat{\mathcal{H}} \hat{U} = \hat{\mathcal{H}}_d + \hat{\mathcal{H}}_o, \quad (1.5)$$

where the diagonal part,

$$\hat{\mathcal{H}}_d = \sum_{(i,j)} J_{ij} \hat{S}_i^z \hat{S}_j^z, \quad (1.6)$$

is invariant in the new representation, while the off-diagonal spin-flip term,

$$\hat{\mathcal{H}}_o = -\frac{1}{2} \sum_{(i,j)} J_{ij} (\hat{S}_i^+ \hat{S}_j^- + h.c.), \quad (1.7)$$

acquires instead an overall minus sign. Therefore, in this representation, the Hamiltonian has non-positive off-diagonal matrix elements. In this case, using the hypothesis that the Hamiltonian cannot be split into sets of noninteracting spins<sup>1</sup>, one can demonstrate (see Appendix A) that the ground-state expansion over the chosen basis  $|\tilde{\psi}_M\rangle = \sum_x f_x |x\rangle$  has non-vanishing positive amplitudes, i.e.,  $f_x > 0$ .

The latter result has two important consequences: in each  $M$  subspace the ground state of the Hamiltonian (1.1) *i*) is *non-degenerate*, and *ii*) obeys, in the original representation, the well-known *Marshall-Peierls sign rule*, i.e.,

$$|\psi_M\rangle = \hat{\mathcal{U}} |\tilde{\psi}_M\rangle = \sum_x e^{i\pi N(x)} f_x |x\rangle = \sum_x (-1)^{N(x)} f_x |x\rangle, \quad (1.8)$$

where  $N(x) = \sum_{i \in B} (s + m_i)$ , and the sum is restricted to the configurations  $|x\rangle$  such that  $\sum_i m_i = M$ . Notice that the unessential constant term  $s$  in the definition of  $\hat{\mathcal{U}}$  have allowed us to write a real ground-state wavefunction. In particular, for  $s = 1/2$ ,  $N(x)$  is simply the number of spins up on the B sublattice, say  $N_\uparrow(x)$ . In this case, the ground-state projections on two Ising configurations differing for a single spin flip have opposite signs. Notice that the rotational invariance of the Hamiltonian has never been used in the proof so that this result is valid in general even in presence of an easy-plane anisotropy, i.e., for the more general XXZ Hamiltonian, or in presence of an arbitrary magnetic field in the  $z$  direction.

In contrast, for frustrated spin systems, like the  $J_1 - J_2$  model and the Heisenberg triangular antiferromagnet, the same proof does not hold. In fact, in both systems the off-diagonal part of the Hamiltonian cannot be made non-positive defined by any known unitary transformation. In the  $J_1 - J_2$  model, the unitary transformation (1.4) does not change the signs of the next-nearest-neighbors spin-flip term. In the triangular antifer-

---

<sup>1</sup>This formally means that each  $M$  block of the Hamiltonian cannot be block diagonalized by performing a permutation of the vectors of the basis. In this case each block is said *irreducible* [20] and every state of the basis spanning the  $M$  subspace is connected to all the others by successive application of the Hamiltonian.

## 10 Spontaneous symmetry breaking in a quantum antiferromagnet

romagnet, under the transformation corresponding to the one in Eq. (1.4)

$$\hat{U}^\dagger = \exp \left[ -\frac{2\pi i}{3} \left( \sum_{i \in B} \hat{S}_i^z - \sum_{i \in C} \hat{S}_i^z \right) \right] \quad (1.9)$$

where B and C label two of the three sublattices as shown in Fig. 1<sup>2</sup>, the Hamiltonian reads

$$\begin{aligned} \hat{U}^\dagger \hat{H} \hat{U} &= -\frac{J}{4} \sum_{\langle i,j \rangle} (\hat{S}_i^+ \hat{S}_j^- + h.c.) + J \sum_{\langle i,j \rangle} \hat{S}_i^z \hat{S}_j^z \\ &+ i \sum_{\langle i,j \rangle} C_{i,j} (\hat{S}_i^+ \hat{S}_j^- - h.c.) \end{aligned} \quad (1.10)$$

with  $C_{i,j} = \pm\sqrt{3}/4$ . The transformed Hamiltonian then displays an extra current-like term which is off-diagonal and has no definite sign. Therefore for frustrated spin systems the Marshall-Peierls sign rule cannot be demonstrated and in general it does not hold exactly. In addition, the impossibility to find a unitary transformation allowing us to map the Hamiltonian into an operator with non-positive defined off-diagonal matrix elements has also dramatic consequences on the computability of such frustrated systems with standard quantum Monte Carlo methods. This is the origin of the so-called *sign-problem instability* (see also Sec. 2.4).

However, as originally pointed out by Richter and co-workers [21], the Marshall-Peierls sign-rule survives in the  $J_1 - J_2$  model in very good approximation up to relatively large values of the frustration. By means of the Lanczos technique (see Sec. 2.1), for  $s = 1/2$ ,  $N = 32$  and  $36$ , we have calculated the weight of the states satisfying the Marshall-Peierls sign-rule in the expansion of the (normalized) exact ground state  $|\psi_0\rangle$ , namely:

$$\langle s \rangle = \sum_x |\psi_0(x)|^2 (-1)^{N_\uparrow(x)} \text{sgn}[\psi_0(x)], \quad (1.11)$$

with  $\psi(x) = \langle x|\psi \rangle$  and the notations introduced in this chapter. Our results, shown in Tab. 1.1, put further evidence to the previous findings of Ref. [21] and indicate that the Marshall-Peierls sign rule is verified almost exactly up to  $J_2/J_1 \simeq 0.3 \div 0.4$ , even for  $N = 36$ . Moreover, even if the average sign  $\langle s \rangle$  eventually vanishes in the thermodynamic limit, its small size dependence suggests that this property is likely to be conserved also for the lattice sizes ( $N \simeq 100$ ) presently accessible with the stochastic numerical techniques used in this work (see Chap. 2). As it will be explained in Sec. 2.4.1, a reasonable guess on the phases of the exact ground state is in general very

---

<sup>2</sup>As the unitary transformation in Eq. (1.4) this mapping defines a spatially varying coordinate system pointing along the local Néel direction.

$J_2/J_1$	0.1	0.2	0.3	0.4	0.5
$N = 32$	1	1	$\sim (1 - 10^{-8})$	$\sim 0.9998$	0.973
$N = 36$	1	1	$\sim (1 - 10^{-8})$	$\sim 0.9995$	0.961

Table 1.1: Weight of the states satisfying the Marshall-Peierls sign-rule,  $\langle s \rangle$ , in the ground state of the  $J_1 - J_2$  Heisenberg model. Data are reported for  $s = 1/2$ ,  $N = 32$  and  $N = 36$ , and various values of the frustration.

useful to improve the efficiency of the approximated quantum Monte Carlo techniques that have to be used in presence of the sign problem.

In the triangular case, instead, the phases obtained by applying the operator (1.9) to a state with positive-definite amplitudes on the Ising basis, as in Eq. (1.8), are very far from being exact, especially in the spin-isotropic limit (see Sec. 3.2.1).

### 1.1.2 Ordering of the energy levels

It follows from the spin rotational invariance of the Hamiltonian (1.1) that each energy level,  $E(S)$ , belonging to the total spin  $S$  subspace is  $(2S + 1)$ -fold degenerate: in any  $S$  sector there is a degenerate level for each value of  $M$  in the range  $-S \leq M \leq S$ . Therefore, in a given  $M$  subspace every energy eigenstate with total spin  $S \geq |M|$  must be contained. In the hypothesis stated above, it is possible to prove that the lowest energy in each  $M$  subspace belongs to  $S = M$ , i.e., it has the minimum total spin allowed.

In order to prove this result we will show that the ground state of  $\hat{\mathcal{H}}$  in an  $M$  subspace is not orthogonal to the ground state of a rotational invariant soluble Hamiltonian, which is known to belong to the  $S = M$  sector. Therefore, so does the former since two eigenfunctions having different quantum numbers are in general orthogonal. Let us consider the infinite-range Heisenberg Hamiltonian on a bipartite lattice

$$\hat{\mathcal{H}}_\infty = J \sum_{i \in A, j \in B} \hat{\mathbf{S}}_i \cdot \hat{\mathbf{S}}_j, \quad (1.12)$$

with  $J$  positive constant. This Hamiltonian is rotationally invariant and exactly soluble since it is equivalent to a two spin problem:

$$\hat{\mathcal{H}}_\infty = J(\hat{\mathbf{S}}^2 - \hat{\mathbf{S}}_A^2 - \hat{\mathbf{S}}_B^2) \quad (1.13)$$

where  $\hat{\mathbf{S}}_A^2$  and  $\hat{\mathbf{S}}_B^2$  are the total spin squared on the  $A$  and  $B$  sublattices, respectively. The eigenvalues of this special Hamiltonian are

$$E_\infty(S) = \frac{J}{2}[S(S + 1) - S_A(S_A + 1) - S_B(S_B + 1)], \quad (1.14)$$

## 12 Spontaneous symmetry breaking in a quantum antiferromagnet

and are monotonically increasing with the total spin  $S$ . Then, the ground state of  $\hat{\mathcal{H}}_\infty$ , in each  $M$  subspace, has  $S = M$  total spin. Moreover, both  $\hat{\mathcal{H}}$  and  $\hat{\mathcal{H}}_\infty$  satisfy the requirements for the Marshall-Peierls sign rule. Hence, their ground state in any  $M$  sector are not orthogonal since their overlap involves the sum of positive numbers. It follows that they have necessarily the same total spin quantum number  $S = M$ . Therefore in a given  $M$  subspace the lowest energy of the Heisenberg Hamiltonian has the minimum total spin allowed.

This implies in turn that  $E(S) < E(S+1)$ . In fact, among the degenerate eigenfunctions with  $E(S+1)$ , there is a representative in the  $M = S$  subspace. The latter has not the minimum total spin allowed for that subspace and therefore it has an energy higher than  $E(S)$ . This proves that the energy levels of the Heisenberg antiferromagnet (1.1) *increase monotonically with the total spin* and, in particular, that *the absolute ground state is a singlet and non-degenerate* (Lieb-Mattis property)<sup>3</sup>.

The above proof on the ordering of the energy levels is a direct consequence of the Marshall-Peierls sign rule and therefore it breaks in presence of frustration. However the Lieb-Mattis property turns out to be verified even for frustrated spin systems. In particular, for symmetry reasons, the ground state on any *finite size* of the spin-isotropic Heisenberg antiferromagnet is believed to possess all the symmetries of the Hamiltonian and in particular to be a singlet, rotationally invariant, and non-degenerate [22]. Even if there is no rigorous theorem proving this property in general, the latter turns out to be true on a finite size whenever the cluster is large enough, it has an even number of sites, and the boundary conditions do not frustrate the antiferromagnetic long-range order [12]. In any case, however, these symmetry properties concern in general the ground states *on finite sizes only*. In the thermodynamic limit, the situation can change drastically if there is no gap in the excitation spectrum. In this case, in fact, a family of excited states collapses onto the ground state and may break its symmetric character. This will be illustrated in the following sections.

### 1.2 Order parameters and susceptibilities

A zero-temperature spontaneously broken symmetry occurs when the ground state has a lower degree of symmetry than the corresponding Hamiltonian. In this case, one can define an *extensive* operator,  $\hat{O}$ , breaking some symmetry of the Hamiltonian and such that the so-called *order parameter*, *i.e.*, the ground-state expectation value  $m = \langle \psi_0 | \hat{O} | \psi_0 \rangle / N$ , has a finite value. In general, whenever the symmetry-breaking operator

---

<sup>3</sup>In fact, having  $S = 0$ , it has only a representative in the  $M = 0$  subspace

$\hat{O}$  does not commute with the Hamiltonian, the symmetry breaking can happen only in the thermodynamic limit. In fact, in that case, the ground-state expectation value of  $\hat{O}$  is zero on *any finite size* by symmetry. This will be the case for the symmetry-breaking operators considered in this thesis.

The occurrence of a spontaneously broken symmetry can be detected by adding to the Hamiltonian  $\hat{\mathcal{H}}$  an *ordering field*  $\delta$ :

$$\hat{\mathcal{H}}_\delta = \hat{\mathcal{H}} - \delta \hat{O}. \quad (1.15)$$

Since on a finite size the ground-state expectation value of  $\hat{O}$  vanishes for  $\delta = 0$ , the ground-state energy per site has corrections proportional to  $\delta^2$ ,

$$e(\delta) \simeq e_0 - \frac{1}{2} \chi_O \delta^2, \quad (1.16)$$

$\chi_O$  being the (positive-definite) generalized susceptibility associated to the operator  $\hat{O}$ , namely:

$$\chi_O = \frac{2}{N} \langle \psi_0 | \hat{O} (E_0 - \hat{\mathcal{H}})^{-1} \hat{O} | \psi_0 \rangle, \quad (1.17)$$

where  $E_0$  is the ground-state energy of  $\hat{\mathcal{H}}$ .

If symmetry breaking occurs in the thermodynamic limit then

$$\lim_{\delta \rightarrow 0} \lim_{N \rightarrow \infty} \frac{1}{N} \langle \psi_0 | \hat{O} | \psi_0 \rangle = m \neq 0, \quad (1.18)$$

and the finite-size susceptibility has to diverge with the system size. In fact, by the Hellmann-Feynman theorem, the ground-state expectation value of  $\hat{O}$  at finite field is  $\langle \hat{O} \rangle_\delta / N = -de(\delta)/d\delta$ , so that, if symmetry breaking occurs in the thermodynamic limit, an infinitesimal field  $\delta$  must give a finite  $\langle \hat{O} \rangle_\delta / N \sim \chi_O \delta$  implying that the susceptibility has to diverge in the thermodynamic limit. Moreover, it is possible to show that the finite-size susceptibility must diverge at least as the volume squared  $N^2$ . This will be proven in the next section.

### 1.2.1 Exact bounds on the susceptibilities

Since on a finite size  $\langle \psi_0 | \hat{O} | \psi_0 \rangle = 0$ , it is convenient to introduce as the order parameter the quantity  $p = \sqrt{\langle \psi_0 | \hat{O}^2 | \psi_0 \rangle} / N$ . The latter is finite in general on any finite size and extrapolate to a finite value in the thermodynamic limit in presence of long-range order, i.e., whenever  $m$ , given by Eq. (1.18), is finite. In this section we will show that, whenever symmetry breaking occurs in the thermodynamic limit, the corresponding

## 14 Spontaneous symmetry breaking in a quantum antiferromagnet

susceptibility must diverge as  $N \rightarrow \infty$  and, in particular, it is bounded from below by the order parameter times the system volume squared, namely  $\chi_O > \text{const } p^4 N^2$ .

Let us define the following decomposition:

$$p^2 = \frac{1}{N^2} \langle \psi_0 | \hat{O}^2 | \psi_0 \rangle = \frac{1}{N^2} \sum_{n \neq 0} |\langle \psi_0 | \hat{O} | \psi_n \rangle|^2 = \frac{1}{N} \int d\omega S(\omega) \quad (1.19)$$

with

$$S(\omega) = \frac{1}{N} \sum_{n \neq 0} |\langle \psi_0 | \hat{O} | \psi_n \rangle|^2 \delta(\omega - \omega_n), \quad (1.20)$$

where we have introduced a complete set of eigenstates of the Hamiltonian  $|\psi_n\rangle$  with eigenvalues  $E_n$ , we have used the symmetry of the ground state (i.e.,  $\langle \psi_0 | \hat{O} | \psi_0 \rangle = 0$ ) and set  $\omega_n = E_n - E_0$ . By the Cauchy-Schwartz inequality we have:

$$\begin{aligned} \int d\omega S(\omega) &= \int d\omega \omega^{1/2} S(\omega)^{1/2} \omega^{-1/2} S(\omega)^{1/2} \\ &\leq \left[ \int d\omega \omega S(\omega) \int d\omega \omega^{-1} S(\omega) \right]^{1/2}. \end{aligned} \quad (1.21)$$

Now,

$$\int d\omega \omega^{-1} S(\omega) = \frac{1}{N} \sum_{n \neq 0} \frac{1}{\omega_n} |\langle \psi_0 | \hat{O} | \psi_n \rangle|^2 \equiv \frac{\chi_O}{2}, \quad (1.22)$$

where  $\chi_O$  by Eq. (1.17) is the susceptibility associated to the operator  $\hat{O}$ . In addition it is straightforward to show that

$$\int d\omega \omega S(\omega) = \frac{1}{N} \sum_{n \neq 0} \omega_n |\langle \psi_0 | \hat{O} | \psi_n \rangle|^2 = \frac{1}{2N} \langle [\hat{O}, [\hat{\mathcal{H}}, \hat{O}]] \rangle \equiv \frac{f_0}{2}, \quad (1.23)$$

so that, using Eqs. (1.21) and (1.22), we have

$$p^2 = \frac{1}{N} \int d\omega S(\omega) \leq \frac{1}{2N} \sqrt{\chi_O f_0}. \quad (1.24)$$

Hence, we have obtained the following lower bound for the susceptibility:

$$\chi_O \geq \frac{4p^4}{f_0} N^2. \quad (1.25)$$

Therefore, if the order parameter is finite in the thermodynamic limit, the susceptibility must diverge at least as the volume squared, provided  $f_0$  is a constant. This happens whenever the commutator of  $\hat{\mathcal{H}}$  and  $\hat{O}$  is an extensive quantity as it is the case for the magnetization in the Heisenberg model and for all the symmetry-breaking operators treated in this work.

Moreover it is also possible to construct an upper bound for the generalized susceptibility  $\chi_O$  associated to a symmetry-breaking operator  $\hat{O}$ . In fact, using Eqs. (1.22) and (1.19), we have

$$\frac{\chi_O}{2} = \frac{1}{N} \sum_{n \neq 0} \frac{1}{\omega_n} |\langle \psi_0 | \hat{O} | \psi_n \rangle|^2 \leq \frac{1}{\Delta} \int d\omega S(\omega) = \frac{Np^2}{\Delta}, \quad (1.26)$$

where  $\Delta$  is the energy gap between the ground state and the first excitation. An energy gap in the thermodynamic excitation spectrum is therefore incompatible with a spontaneously broken symmetry. The physical meaning of this quite general result is the following: in presence of a gap in the excitation spectrum, the ground state, which has generally all the symmetries of the Hamiltonian on *any finite size*, has clearly no mean to develop a spontaneously broken symmetry in the thermodynamic limit. In this case, the susceptibility is bounded [Eq. (1.26)]. In contrast, in presence of a gapless excitation spectrum, a family (or a *tower*) of excited states can collapse in the thermodynamic limit onto the ground state and can break its symmetric character. In fact, these states acquire in general a phase factor under some operation of the symmetry group of the Hamiltonian and they can give rise to a symmetry-broken superposition. Whenever this happens, the related susceptibility must diverge as the volume squared [Eq. (1.25)]. In this case from Eqs. (1.25) and (1.26) we get a remarkable relation for the size-dependence of the spin gap, namely

$$\Delta \leq \frac{f_0}{2p^2} N^{-1}. \quad (1.27)$$

The mechanism underlying the spontaneous symmetry breaking leading to the onset of long-range Néel order in the thermodynamic ground state of a quantum antiferromagnet will be discussed in more detail in the following section.

### 1.3 Néel order and Anderson's towers of states

As we have already noticed, the occurrence of a spontaneous symmetry breaking in the thermodynamic ground state, can be evidenced from the structure of the finite-size energy spectrum.

On any finite size, the ground state of a quantum antiferromagnet is generally believed to be a singlet, rotationally invariant and non-degenerate, i.e., non-magnetic. This is rigorously stated by the Lieb-Mattis theorem (Sec. 1.1) only for the Heisenberg square antiferromagnet but nonetheless it can be numerically verified on small clusters also in presence of frustration for the triangular Heisenberg antiferromagnet [12] and for the  $J_1 - J_2$  model itself [23] (see also Sec. 1.2). Therefore, as originally pointed out by

## 16 Spontaneous symmetry breaking in a quantum antiferromagnet

Anderson [11], the spontaneously symmetry breaking mechanism necessarily involves the low-energy portion of the excitation spectrum: in particular, a whole *tower of states* has to collapse in the thermodynamic limit onto the ground state faster than the low-lying excitations involving a spatial modulation of the classical Néel state (the so-called *magnons*). In fact, since in general these states acquire phase factors under rotations in the spin space, they can sum up to a nontrivial state in which the spins point in a definite direction, giving rise to Néel-like long-range order.

In particular, it is well known [24, 25, 26, 27] that in this case the low-lying excited states of energy  $E(S)$  and spin  $S$  are predicted to behave as the spectrum of a free quantum rotator (or *quantum top*) as long as  $S \ll \sqrt{N}$ ,

$$E(S) - E_0 = \frac{S(S+1)}{2IN}, \quad (1.28)$$

where  $E_0 = E(0)$  is the energy of the ground state,  $|\psi_0\rangle$ , and  $I$  is known as the *momentum of inertia* per site and is an intensive quantity.

This equation, which is in agreement with the bound (1.27), can be justified in a semiclassical picture of the long-range ordered ground state of a quantum antiferromagnet. To this purpose, let us consider the nearest-neighbor Heisenberg antiferromagnet on the square lattice, and separate in the Fourier transformed Hamiltonian the  $\mathbf{k} = 0$ , and  $\mathbf{Q} = (\pi, \pi)$  contributions (i.e., the only ones allowed by the sublattice translation invariance of the classical Néel state) from the others:

$$\hat{\mathcal{H}} = \hat{\mathcal{H}}_0 + \hat{\mathcal{V}}, \quad (1.29)$$

where

$$\hat{\mathcal{H}}_0 = \frac{4J}{N}(\hat{\mathbf{S}}^2 - \hat{\mathbf{S}}_A^2 - \hat{\mathbf{S}}_B^2), \quad (1.30)$$

$\hat{\mathbf{S}}^2$  is the total spin square, and  $\hat{\mathbf{S}}_A^2$  and  $\hat{\mathbf{S}}_B^2$  are the total spin square of the A and B sublattices, respectively;

$$\hat{\mathcal{V}} = 2J \sum_{\mathbf{k} \neq 0, \mathbf{Q}} \gamma_{\mathbf{k}} \hat{\mathbf{S}}_{\mathbf{k}} \cdot \hat{\mathbf{S}}_{-\mathbf{k}}, \quad (1.31)$$

where  $\hat{\mathbf{S}}_{\mathbf{k}} = 1/\sqrt{N} \sum_i \hat{\mathbf{S}}_i \exp(\mathbf{k} \cdot \mathbf{r}_i)$ ,  $\mathbf{r}_i$  is the position of the site  $i$ , and  $\gamma_{\mathbf{k}} = (\cos k_x + \cos k_y)/2$ . For each value of the total spin  $S$  the lowest eigenstate of  $\hat{\mathcal{H}}_0$  is the classical-like state fully polarized on each magnetic sublattice with energy:

$$E_0(S) = -\frac{1}{4}(N+4) + \frac{4JS(S+1)}{N}. \quad (1.32)$$

This is in agreement with the quantum top law (1.28). Of course, since  $\hat{\mathbf{S}}_A^2$  and  $\hat{\mathbf{S}}_B^2$  do not commute with  $\hat{\mathcal{V}}$ , such eigenstates are not eigenstates of  $\hat{\mathcal{H}}$ . Nonetheless we can look

at them as the first approximation to the low-lying excited states in each  $S$  sector. The perturbation  $\hat{V}$  dresses these classical-like states with quantum fluctuations decreasing the average value of the sublattice magnetization and lowering their energy towards the exact result. However, as long as the energy scale of these states is well separated by the low-lying excitations with  $\mathbf{k} \neq 0, \mathbf{Q}$  such renormalizations are not expected to modify the behavior (1.28). These excitations are known as *magnons* or *spin-waves* (see Sec. 3.1), and involve a spatial modulation of the classical Néel state. In the Heisenberg antiferromagnet the dispersion relation of the softest magnons is linear in the wavevector so that, in two dimensions, they have an energy scaling as  $1/\sqrt{N}$ . This implies that the constraint on the value of  $S$  for the validity of Eq. (1.28) is  $S \ll \sqrt{N}$ .

The quantum top law is similar to the definition of the uniform spin susceptibility (see Appendix B). The latter, in fact, can be calculated, by taking *first* the infinite-volume limit of the energy per site  $e(m) = E(S)/N$  at fixed magnetization  $m = S/N$  and then letting  $m \rightarrow 0$  in the expansion

$$e(m) = e_0 + \frac{m^2}{2\chi}, \quad (1.33)$$

which is quite similar to Eq. (1.28). However an identification between  $I$  and  $\chi$  is possible if the excitation spectrum smoothly connects the low-energy portion which corresponds to total spin  $S \sim \mathcal{O}(1)$ , with the regime of macroscopic spin excitations:  $S \sim mN$  (with  $m \ll 1$ ) [28]. This is an highly nontrivial statement which is actually verified by the underlying low-energy effective model of the quantum antiferromagnet, known as nonlinear  $\sigma$  model (NL $\sigma$ M) [26, 27, 29, 28, 22]. Therefore, the quantity

$$\frac{1}{\chi_S} = 2N \frac{E(S) - E_0}{S(S+1)} \quad (1.34)$$

must approach the inverse of the spin susceptibility for infinite size and for any spin excitation with  $S \ll N$ .

## 1.4 Resonating Valence Bond states

A simple and clear picture of a non-magnetic ground state can be given in terms of the so-called *Resonating Valence Bond* (RVB) wavefunctions [30]. Here, for simplicity, we will restrict ourselves to the case of the spin-half square antiferromagnet even if these states can be used also for a generic value of the spin  $s$  [31] and different lattice geometries [32].

The RVB wavefunctions are linear superpositions of valence bond states in which each spin forms a singlet bond with another spin on the opposite sublattice. These

## 18 Spontaneous symmetry breaking in a quantum antiferromagnet

states form in general a (overcomplete) basis of the  $S = 0$  subspace so that any singlet wavefunction can be represented in terms of them. In particular, with such RVB wavefunctions it is possible to describe either a long-range ordered or a non-magnetic state by varying the bond-length distribution [31]. In order to clarify this point, let us consider the following class of RVB wavefunctions for a system of  $N$  spins:

$$|\psi_{RVB}\rangle = \sum_{i_\alpha \in A, j_\beta \in B} h(r_1) \dots h(r_n) (i_1 j_1) \dots (i_n, j_n), \quad (1.35)$$

where  $n = N/2$ ,  $r_m$  is the distance between the spins forming the  $m^{\text{th}}$  singlet bond  $(i_m j_m)$ , and  $h(r_m)$  is a bond weight factor, function of its length. The latter wavefunction has no long-range order whenever the short-ranged bonds are the dominant one in the superposition (1.35). More precisely, it has been numerically shown by Liang, Doucot and Anderson [33] that the RVB state (1.35) has no long-range antiferromagnetic order for bonds that decay as rapidly as  $h(r) \sim r^{-p}$ , with  $p \geq 5$ . Instead, if the weight functions decay slowly enough with the length of the bond, then the RVB wavefunction has a finite value of the thermodynamic order parameter squared. In particular, if the weight factors  $h(r)$  are independent of the bond length, the RVB wavefunction is the projection of the Néel state onto the singlet subspace.

Therefore, the simplest physical picture of a non-magnetic ground state can be given in terms of a RVB wavefunction with short-ranged bonds. In addition, such bonds can be either homogeneously spatially distributed on the lattice, with short-range correlations among each other (*spin liquid*) [Fig. 1.1 (a)], or they can break some symmetries of the Hamiltonian, with the dimers frozen in some special patterns [Fig. 1.1 (b)]. In Chap. 4 we will provide an example of the latter situation.

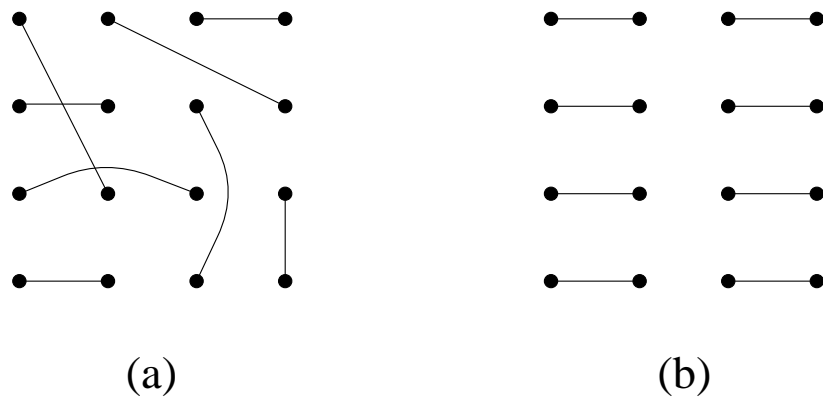


Figure 1.1: An example of a spin liquid (a) and of a symmetry-broken (b) non-magnetic RVB state. Each stick represents a singlet bond.



# Chapter 2

## Numerical methods

The various numerical methods that allow one to investigate the ground-state properties of a lattice Hamiltonian can be grossly divided into two main branches: the exact diagonalizations and the stochastic (Monte Carlo) techniques.

The first family includes all kinds of brute force diagonalizations of the Hamiltonian matrix, providing the exact physical properties of the finite-size ground state. However, due to memory limitations, the numerical calculation of the entire spectrum of a matrix is possible only for very small systems as the linear dimension of this matrix grows exponentially with the system size. The use of iterative procedures converging to the ground state of the Hamiltonian, like the power method or the very efficient Lanczos technique (Sec. 2.1), allows one to study clusters of the order of  $\sim 30$  sites for the most common strongly correlated models (Heisenberg,  $t-J$ , Hubbard, etc.). However this is far from being enough for the determination of the physical properties in the thermodynamic limit.

Recent progress has been made by using exact diagonalization within the so-called density matrix renormalization group technique (DMRG) [34], which allows one to obtain almost exact – at least in one dimension – large-size ground-state properties. However, the DMRG results, although quite accurate, are not exact in two dimensions. Moreover, for technical reasons it is possible to consider only particular boundary conditions (open in one direction and periodic in the other), which certainly make the DMRG calculation still far to be representative of the thermodynamic limit.

The simplest stochastic technique is the variational Monte Carlo (VMC) method (Sec. 2.3), which is a statistical sampling of a variational wavefunction  $\psi_G(x)$ , defined on a given basis  $|x\rangle$ <sup>1</sup>. From this point of view, the Green function Monte Carlo (GFMC)

---

<sup>1</sup>In the simulations of strongly correlated Hamiltonians each element  $|x\rangle$  of the basis set is typically represented by a simple *configuration*, defined by the electron positions and spins.

technique [14] can be considered as a development of the VMC, because it allows one to sample statistically the exact ground state of a many body Hamiltonian  $\hat{\mathcal{H}}$ , instead of being restricted to a variational wavefunction. In fact, the ground state of a given Hamiltonian  $\hat{\mathcal{H}}$  can be obtained by applying the propagator  $e^{-\hat{\mathcal{H}}\tau}$  to a trial wavefunction  $|\psi_G\rangle$  and sampling statistically the state  $|\psi_\tau\rangle = e^{-\hat{\mathcal{H}}\tau}|\psi_G\rangle$  for large imaginary time  $\tau$ . As explained in detail in Sec. 2.4, in the GFMC numerical scheme a Markov process is defined, acting on the elements of a chosen basis  $|x\rangle$  such that the ground state is sampled by a set of *random walkers*  $(w_i, x_i)$ , *i.e.*, a weight  $w_i$  is associated at each configuration  $x_i$  in order to represent the amplitude of the wavefunction on the element  $x_i$  of the Hilbert space. The algorithm is efficient even for large system sizes, provided all the matrix elements of the Hamiltonian in the chosen basis,  $H_{x,x'}$ , are non-positive; otherwise the numerical method suffers from the numerical instability known as the *sign problem*. Unfortunately, with very few exceptions, this happens in general for fermionic models and for frustrated spin systems [17].

In this case the imaginary time propagation can still have a statistical meaning at the price of having walkers with weights  $w_i$  which are no longer restricted to be positive. As a result, the average weight sign  $\langle s \rangle_n = \langle \sum_i w_i \rangle_n / \sum_i \langle |w_i| \rangle_n$  at a Markov iteration  $n$  is exponentially decreasing with  $n$ , implying a dramatic decrease of the signal-to-noise ratio for all correlation functions. Presently, the above mentioned instability can be avoided only at the price of introducing some kind of approximations. Among them the fixed-node (FN) GFMC [35], recently extended to lattice Hamiltonians [15], allows one to handle approximately the negative off-diagonal matrix elements of the Green function with the introduction of an effective FN Hamiltonian with no sign problem, depending on a trial state  $|\psi_G\rangle$ . Unfortunately, for strongly frustrated spin systems the results obtained with the FN GFMC are strongly biased by the choice of the variational guess  $|\psi_G\rangle$  [17, 36, 37].

The Green function Monte Carlo with Stochastic Reconfiguration (GFMC SR) [16, 17] allows one to release the FN approximation in a controlled way and to obtain much more accurate estimates not only of the energy but also of the ground-state correlation functions. The idea underlying the Stochastic Reconfiguration (SR) procedure is that, given a certain state  $\psi_n(x)$ , its representation in terms of the walkers' population is not unique. In particular it is possible to represent statistically the same state with an ensemble of walkers either with vanishing average sign  $\langle s \rangle_n$  or with an average sign close to 1. Indeed the task accomplished by the SR procedure is to change the walker population every few iterations in order to stabilize  $\langle s \rangle_n$  to a value close to 1. This can be done in principle without changing the information content of the walkers' population,

i.e., the sampled wavefunction. In practice, to limit the numerical effort, the SR is performed with the constraint that only a certain number  $p$  of expectation values of correlation functions is propagated consistently with the exact dynamics. Of course this introduces a certain amount of bias that can however be systematically reduced by increasing the number of reconfigured operators, so that the method becomes exact if all the correlation functions are included in the SR.

In this chapter the Lanczos method and the mentioned quantum Monte Carlo techniques, will be treated in detail.

## 2.1 The Lanczos method

From a general point of view, the ground state  $|\psi_0\rangle$  of a lattice Hamiltonian  $\hat{\mathcal{H}}$  can be obtained by iterating the well-known *power method*

$$|\psi_0\rangle = (\Lambda - \hat{\mathcal{H}})^n |\psi_G\rangle, \quad (2.1)$$

where  $|\psi_G\rangle$  is a trial wavefunction non-orthogonal to  $|\psi_0\rangle$  and  $\Lambda$  is a suitable constant, allowing the convergence to the ground state for large  $n$ . In fact, by expanding the trial state on the basis of eigenstates of the Hamiltonian,  $|\psi_m\rangle$ , such that  $\hat{\mathcal{H}}|\psi_m\rangle = E_m|\psi_m\rangle$ , we have

$$(\Lambda - \hat{\mathcal{H}})^n |\psi_G\rangle = (\Lambda - E_0)^n \left[ c_0 |\psi_0\rangle + \sum_{m \neq 0} c_m \left( \frac{\Lambda - E_m}{\Lambda - E_0} \right)^n |\psi_m\rangle \right], \quad (2.2)$$

with  $c_m = \langle \psi_m | \psi_G \rangle$ ; therefore, for large  $n$ , the ground-state component is filtered out from  $|\psi_G\rangle$  provided  $|(\Lambda - E_m)/(\Lambda - E_0)| < 1$  for any  $m$ , and  $c_0 \neq 0$ .

Starting from the power method, it is possible to define a much more efficient iterative procedure for the determination of the lowest eigenstate of Hermitian matrices, especially those of very large dimension and sparse character<sup>2</sup>. The basic idea of this technique, known as the Lanczos method [38], is that it is in general possible, given an Hamiltonian, to construct a special orthogonal basis (the Lanczos basis) which is a smart choice for the expansion of its lowest eigenvector. In particular the Lanczos algorithm generates a sequence of tridiagonal matrices, representing the Hamiltonian in the truncated Lanczos basis, with the property that their lowest eigenvalues (eigenvectors) are better and better estimates of the lowest eigenvalue (eigenvector) of the original operator. In this section we will recall only the essential features of this technique, following Refs. [39, 40], to which we address the reader for further details.

---

<sup>2</sup>A  $L \times L$  matrix is usually said sparse if the number of nonzero entries is of order  $L$  instead of  $L^2$ .

## 24 Numerical methods

To illustrate the procedure, let us consider an Hamiltonian  $\hat{\mathcal{H}}$  and an initial state  $|\phi_0\rangle$  not orthogonal to the ground state of  $\hat{\mathcal{H}}$ ,  $|\psi_0\rangle$ . In practice, this requirement can be satisfied simply using a state with *randomly* chosen amplitudes in the chosen basis set. Of course, if some information is known on physical grounds about the ground-state quantum numbers, it is convenient to start with a random state in the corresponding subspace.

A new vector of the Lanczos basis,  $|\phi_1\rangle$ , is constructed by applying the operator  $\hat{\mathcal{H}}$  to the initial state and subtracting its projection on the initial state, i.e.,

$$|\phi_1\rangle = \hat{\mathcal{H}}|\phi_0\rangle - a_0|\phi_0\rangle, \quad (2.3)$$

with  $a_0 = \langle\phi_0|\hat{\mathcal{H}}|\phi_0\rangle/\langle\phi_0|\phi_0\rangle$ , so that  $\langle\phi_0|\phi_1\rangle = 0$ . Similarly, we construct the second vector of the basis set,  $|\phi_2\rangle$ , by applying  $\hat{\mathcal{H}}$  to the vector  $|\phi_1\rangle$  and then orthogonalizing the resulting state to both  $|\phi_0\rangle$  and  $|\phi_1\rangle$ , namely

$$|\phi_2\rangle = \hat{\mathcal{H}}|\phi_1\rangle - a_1|\phi_1\rangle - b_1^2|\phi_0\rangle, \quad (2.4)$$

with  $a_1 = \langle\phi_1|\hat{\mathcal{H}}|\phi_1\rangle/\langle\phi_1|\phi_1\rangle$  and  $b_1^2 = \langle\phi_1|\phi_1\rangle/\langle\phi_0|\phi_0\rangle$ .

The key point of the Lanczos procedure turns out in the construction of the third state of the new basis,  $|\phi_3\rangle$ , obtained by the orthogonalization of  $\hat{\mathcal{H}}|\phi_2\rangle$  to the previous states  $|\phi_0\rangle$ ,  $|\phi_1\rangle$ , and  $|\phi_2\rangle$ . In fact  $\hat{\mathcal{H}}|\phi_2\rangle$  is by construction orthogonal to  $|\phi_0\rangle$  since, by Eq. (2.3), being  $\langle\phi_2|\phi_0\rangle = \langle\phi_1|\phi_0\rangle = 0$ ,  $\langle\phi_2|\hat{\mathcal{H}}|\phi_0\rangle = 0$ . Therefore, the iteration procedure leads to a three term relation, i.e., the operator  $\hat{\mathcal{H}}$  is represented in the Lanczos basis by a tridiagonal matrix. Then, the state after  $n + 1$  iteration will be obtained by orthogonalizing the state  $\hat{\mathcal{H}}|\phi_n\rangle$  only to the two predecessors  $|\phi_n\rangle$  and  $|\phi_{n+1}\rangle$ , namely

$$|\phi_{n+1}\rangle = \hat{\mathcal{H}}|\phi_n\rangle - a_n|\phi_n\rangle - b_n^2|\phi_{n-1}\rangle, \quad (2.5)$$

where the coefficients  $a_n$  and  $b_n^2$  are given by

$$a_n = \frac{\langle\phi_n|\hat{\mathcal{H}}|\phi_n\rangle}{\langle\phi_n|\phi_n\rangle}, \quad b_n^2 = \frac{\langle\phi_n|\phi_n\rangle}{\langle\phi_{n-1}|\phi_{n-1}\rangle}, \quad (2.6)$$

and  $b_0 = 0$ ,  $|\phi_{-1}\rangle = 0$ . In the Lanczos basis the operator is therefore represented by the following tridiagonal matrix:

$$H = \begin{bmatrix} a_0 & b_1 & 0 & 0 & \dots \\ b_1 & a_1 & b_2 & 0 & \dots \\ 0 & b_2 & a_2 & b_3 & \dots \\ 0 & 0 & b_3 & a_3 & \dots \\ \dots & \dots & \dots & \dots & \dots \end{bmatrix}. \quad (2.7)$$

At any given iteration  $n$ , the diagonalization of the latter matrix leads to the optimal approximation, in the truncated Lanczos basis  $\{|\phi_n\rangle\}$ , of the lowest eigenstate of  $\hat{\mathcal{H}}$ ,  $|\psi_0\rangle$ . The variational principle<sup>3</sup> guarantees the monotonic convergence to the exact ground state for large  $n$ .

Therefore, by successive diagonalizations of small order tridiagonal matrices it is possible to infer the lowest eigenvalue of  $\hat{\mathcal{H}}$  and the corresponding eigenfunction. In fact, with a small number of iterations ( $\sim 100$ ) it is typically possible to get practically exact ground-state energies of lattice Hamiltonians defined on Hilbert spaces of  $\sim 10^7$  states. Such large matrices can be diagonalized only by iterative procedures, and the Lanczos algorithm allows a much faster convergence than ordinary power methods. The convergence properties of the Lanczos algorithm are discussed in detail in Refs. [41, 42].

The most serious drawback of the Lanczos method, as well as of the other exact diagonalization algorithms, comes from memory limitations which restricts the applicability of this technique only to small clusters. In fact, for interesting lattice Hamiltonians the dimension of the associated Hilbert space grows exponentially with the system size. By using the symmetries of the Hamiltonian it is possible to block diagonalize the corresponding matrix, therefore restricting the calculation to smaller subspaces. It is then possible to evaluate the exact ground state of up to  $\sim 30$  electrons in simple strongly correlated models like: the Heisenberg, the  $t - J$ , the Hubbard models and related ones [39]. A clear treatment of the group theory underlying the use of the symmetries in the Lanczos diagonalization can be found in Ref. [43].

## 2.2 Monte Carlo sampling

In its simplest formulation, the Monte Carlo method is a way to approximate the mean value of a function  $f(x)$  with respect to a probability distribution  $P(x)$ ,

$$\langle f \rangle = \sum_x f(x)P(x), \quad (2.8)$$

where  $P(x)$  satisfies the conditions:  $P(x) \geq 0$  and  $\sum_x P(x) = 1$ . In order to do so, we can generate, according to the probability distribution  $P(x)$ , a sample  $X$  of independent values  $x$ , and approximate  $\langle f \rangle$  as

$$\langle f \rangle \simeq \bar{f}_X = \frac{1}{N_X} \sum_{x \in X} f(x), \quad (2.9)$$

---

<sup>3</sup>See also Sec. 2.3

where  $N_X$  is the number of configurations  $x$  in the sample. The Central Limit Theorem [44] ensures that, for big enough samples, the values  $\bar{f}_X$  are normal distributed around the true value  $\langle f \rangle$ , and converge for  $N_X \rightarrow \infty$  towards  $\langle f \rangle$ , namely:

$$\langle f \rangle \simeq \frac{1}{N_X} \sum_{x \in X} f(x) \pm \frac{\sigma}{\sqrt{N_X}}, \quad (2.10)$$

where  $\sigma = (\langle f^2 \rangle - \langle f \rangle^2)^{1/2}$  is the variance and can be estimated, using Eq. (2.10), as:

$$\sigma \simeq \left[ \frac{1}{N_X} \sum_{x \in X} f(x)^2 - \left( \frac{1}{N_X} \sum_{x \in X} f(x) \right)^2 \right]^{1/2}. \quad (2.11)$$

Although in principle Eq. (2.10) is valid in general, its practical utility is governed by the signal-to-noise ratio. In fact, the ratio of the variance to the mean,  $\sigma/\langle f \rangle$ , must be sufficiently small so that the relative error may be controlled with a feasible sample size (i.e., with a reasonable simulation time). As we will also see later on, for some cases the integrand in Eq. (2.8) has nearly canceling positive and negative contributions which are separately very large in magnitude. In this cases standard Monte Carlo methods become practically useless, and this is known as the *sign problem*. For problems with dominantly positive integrands, however, the choice of  $P(x)$  in Eq. (2.8) is largely arbitrary, and this freedom may be effectively exploited to reduce the variance. For example, if we choose  $P(x)$  such that  $f(x)$  is almost constant, then the variance will be small and the Monte Carlo sampling will converge rapidly [44]. The selection of  $P(x)$  to reduce the variance is known as *importance sampling*.

### 2.3 Variational Monte Carlo

The Rayleigh-Ritz variational principle is one of the most powerful non-perturbative method in quantum mechanics: given an Hamiltonian  $\hat{\mathcal{H}}$ , its expectation value over any trial wavefunction  $|\psi_G\rangle$ ,  $E_G$ , is greater than the ground-state energy,  $E_0$ :

$$E_G = \frac{\langle \psi_G | \hat{\mathcal{H}} | \psi_G \rangle}{\langle \psi_G | \psi_G \rangle} \geq E_0. \quad (2.12)$$

This important result can be easily derived by expanding the trial state in a complete set of eigenstates of the Hamiltonian  $|\psi_n\rangle$  with energies  $E_n$ . In fact,

$$\frac{\langle \psi_G | \hat{\mathcal{H}} | \psi_G \rangle}{\langle \psi_G | \psi_G \rangle} = \sum_n E_n \frac{|\langle \psi_n | \psi_G \rangle|^2}{\langle \psi_G | \psi_G \rangle} = E_0 + \sum_n (E_n - E_0) \frac{|\langle \psi_n | \psi_G \rangle|^2}{\langle \psi_G | \psi_G \rangle} \geq E_0, \quad (2.13)$$

since  $E_n \geq E_0$ . Therefore, among a set of wavefunctions the best approximation to the ground state is the one with the lowest expectation value of the energy.

In general, variational expectation values cannot be calculated analytically, but they must be computed introducing a complete set of states,  $|x\rangle$ , and summing over these states explicitly,

$$\frac{\langle \psi_G | \hat{\mathcal{H}} | \psi_G \rangle}{\langle \psi_G | \psi_G \rangle} = \frac{\sum_{x,x'} \psi_G(x) H_{x,x'} \psi_G(x')}{\sum_x \psi_G(x)^2}, \quad (2.14)$$

where  $H_{x,x'} = \langle x | \hat{\mathcal{H}} | x' \rangle$ ,  $\psi_G(x) = \langle x | \psi_G \rangle$  and we have restricted ourselves to the case of real wavefunctions, for simplicity. Unfortunately, the dimension of the Hilbert space grows exponentially with the system size, so that the exact evaluation of variational expectation values (2.14) is possible only for very small clusters. In order to extend the variational calculation to large system sizes, one must follow a stochastic approach: the variational Monte Carlo (VMC).

In the most simple formulation, the Monte Carlo evaluation of the variational expectation values can be done by rearranging Eq. (2.14) as

$$\frac{\langle \psi_G | \hat{\mathcal{H}} | \psi_G \rangle}{\langle \psi_G | \psi_G \rangle} = \frac{\sum_x \psi_G(x)^2 E_x}{\sum_x \psi_G(x)^2}, \quad (2.15)$$

where  $E_x$  is the so-called *local energy*:

$$E_x = \frac{\langle \psi_G | \hat{\mathcal{H}} | x \rangle}{\langle \psi_G | x \rangle} = \sum_{x'} \psi_G(x') H_{x',x} / \psi_G(x). \quad (2.16)$$

Then, as shown in Sec. 2.2, the sum in Eq. (2.15) can be evaluated by choosing a sample of  $N_X$  configurations  $x$  according to the distribution  $P(x) = \psi_G(x)^2 / \sum_x \psi_G(x)^2$  and then averaging the corresponding values of the local energy, namely:

$$\frac{\langle \psi_G | \hat{\mathcal{H}} | \psi_G \rangle}{\langle \psi_G | \psi_G \rangle} \simeq \frac{1}{N_X} \sum_{x \in X} E_x. \quad (2.17)$$

Similarly, all the other physical expectation values,

$$\langle \hat{O}^k \rangle = \frac{\langle \psi_G | \hat{O}^k | \psi_G \rangle}{\langle \psi_G | \psi_G \rangle} = \frac{\sum_x \psi_G(x)^2 \hat{O}_x^k}{\sum_x \psi_G(x)^2}, \quad (2.18)$$

can be obtained on the given variational wavefunction, provided the local estimator  $\hat{O}_x^k = \langle \psi_G | \hat{O}^k | x \rangle / \langle \psi_G | x \rangle$  of the correlation function  $\hat{O}^k$  can be computed in an efficient way.

The simplest way to generate samples according to the probability distribution  $P(x)$  is by mean of the *Metropolis algorithm* [45]: starting from a configuration  $x$ , a new configuration  $x'$  is accepted if a random number  $\xi$ , between zero and one, satisfies the condition  $\xi < P(x')/P(x) = \psi_G(x')^2/\psi_G(x)^2$ , otherwise  $x' = x$ . This simple procedure generates configurations  $x$  that, after some equilibration, are distributed statistically according to the square of the variational wavefunction.

### 2.3.1 Variational improvement by Lanczos iteration

As discussed in Sec. 2.1, the Lanczos basis is a smart choice to expand the ground state of an Hamiltonian  $\hat{\mathcal{H}}$ . Therefore, as originally suggested by Heeb and Rice [46], any given variational wavefunction  $|\psi_G\rangle$  can be improved by applying  $n$  times the Hamiltonian to it and using the variational principle to optimize the amplitudes,  $\alpha_i$ , of the truncated expansion in the Lanczos basis:

$$|\alpha_1, \alpha_2, \dots, \alpha_n\rangle = \sum_{i=1}^n \alpha_i \hat{\mathcal{H}}^i |\psi_G\rangle . \quad (2.19)$$

In this work we have used the simplest *one Lanczos step* (LS) wavefunction,

$$|\psi_\alpha\rangle = (1 + \alpha \hat{\mathcal{H}}) |\psi_G\rangle , \quad (2.20)$$

where  $\alpha$  is a variational parameter. The Monte Carlo sampling of this wavefunction is particularly easy. In fact,

$$\psi_\alpha(x) = \langle x | (1 + \alpha \hat{\mathcal{H}}) |\psi_G\rangle = \psi_G(x) (1 + \alpha E_x) , \quad (2.21)$$

where  $E_x$  is the local energy given by Eq. (2.16), so that at each Monte Carlo step, in order to evaluate the ratio  $P(x')/P(x)$ , we have only to calculate the local energy on both the configurations  $x'$  and  $x$ . Then, the variational expectation value of the Hamiltonian over the state  $|\psi_\alpha\rangle$  can be obtained by averaging the local energy defined by the LS wavefunction, namely:

$$E_x^\alpha = \sum_{x'} \psi_\alpha(x') H_{x',x} / \psi_\alpha(x) . \quad (2.22)$$

Moreover it turns out that the optimal variational parameter  $\alpha$  can be efficiently determined with only two variational calculations. This is discussed in Appendix F.

## 2.4 The Green function Monte Carlo

As shown in Sec. 2.1, the simplest algorithm allowing one to converge to the ground state of a model Hamiltonian is the power method. However, similarly to the variational or the Lanczos techniques, the exact implementation of the power method clashes with the difficulties related to the dimensions of the Hilbert space, so that it is limited in practice to small clusters. A stochastic approach is therefore needed in order to study large system sizes. This is represented by the Green function Monte Carlo (GFMC).

The first step along this way is to define an iterative procedure implementing the power method (2.1):

$$\psi_{n+1}(x') = \sum_x G_{x',x} \psi_n(x) , \quad (2.23)$$

where  $G_{x',x}$  is the lattice Green function, which is simply related to the Hamiltonian matrix in the given basis  $|x\rangle$

$$G_{x',x} = \Lambda \delta_{x',x} - H_{x',x} . \quad (2.24)$$

A stochastic approach is therefore possible if one can sample statistically the matrix-vector iterations (2.23). The property that allows a statistical approach is that physical lattice Hamiltonians are represented by very sparse matrices: though the total number of nonzero elements of  $G_{x',x}$  is prohibitive, the number of non-vanishing entries in each column is a neglectable fraction of the total Hilbert space dimension. Thus all the nonzero  $G_{x',x}$ , for fixed column index  $x$ , can be computed even for large size.

In practice, in the statistical implementation of the power method, it is convenient to consider in the iteration (2.23), in place of the original matrix  $G$ , the slightly more involved non-symmetric one

$$\bar{G}_{x',x} = \psi_G(x') G_{x',x} / \psi_G(x) , \quad (2.25)$$

where  $\psi_G$  is the so-called *guiding wavefunction*, that has to be as simple as possible to be efficiently implemented in the calculation of the matrix elements and, as we will see, as close as possible to the ground state of  $\hat{\mathcal{H}}$ . In fact, the power method is not restricted to symmetric matrices, and  $\bar{G}$ , though non-symmetric, has the same spectrum of  $G$  as for any eigenvector  $\psi_k(x)$  of  $G$  with energy  $\Lambda - E_k$ ,  $\psi_G(x) \psi_k(x)$  is a right eigenvector of  $\bar{G}$  with the same eigenvalue. As shown later on, by sampling statistically the iteration (2.23) with  $\bar{G}$  instead of  $G$  it is possible to reduce the variance of the energy (importance sampling).

In the following, given any operator  $\hat{O}^k$ , we will indicate with

$$\bar{O}_{x',x}^k = \psi_G(x') O_{x',x}^k / \psi_G(x) \quad (2.26)$$

its matrix elements transformed according to the guiding wavefunction.

### 2.4.1 Statistical implementation of the power method

In order to define a statistical implementation of the matrix multiplication (2.23), the standard approach is first to determine the Green function matrix elements  $\bar{G}_{x',x}$  connected to  $x$  which are different from zero. These matrix elements can be generally

written in terms of three factors,

$$\bar{G}_{x',x} = s_{x',x} p_{x',x} b_x, \quad (2.27)$$

where  $b_x$  is a positive normalization factor,  $s_{x',x}$  takes into account the signs of the Green function and  $p_{x',x}$  is a *stochastic matrix*. All these terms will be defined explicitly below.

The basic step of the GFMC method on a lattice is to define properly the matrix  $p_{x',x}$ , because it represents the term in the decomposition (2.27) allowing one to select statistically only *one* configuration among all the possible ones  $\{x'\}$  connected to  $x$ . Therefore  $p_{x',x}$  has to represent a probability and is restricted to be *i)* normalized  $\sum_{x'} p_{x',x} = 1$  and *ii)* with all positive matrix elements  $p_{x',x} \geq 0$ . This is just the definition of a stochastic matrix (see Appendix C). Since the matrix elements of  $\bar{G}$  are not restricted to be positive (sign problem)  $p_{x',x}$  is more clearly defined in terms of an appropriate Green function  $\bar{G}^{eff}$  with all positive matrix elements.  $\bar{G}_{x',x}^{eff}$  needs not to be normalized, as its normalization can be included in the definition of the positive constant

$$b_x = \sum_{x'} \bar{G}_{x',x}^{eff} \quad (2.28)$$

so that

$$\bar{G}_{x',x}^{eff} = p_{x',x} b_x. \quad (2.29)$$

The typical choice for  $\bar{G}^{eff}$  is given by the absolute value of the matrix elements of  $\bar{G}$ ,  $\bar{G}_{x',x}^{eff} = |\bar{G}_{x',x}|$ , but this is not the optimal choice for our purposes. Here we follow a recent development of the fixed-node (FN) technique on a lattice [15], and we choose for  $\bar{G}^{eff}$  the FN Green function (with importance sampling)

$$\bar{G}_{x',x}^{eff} = \Lambda \delta_{x',x} - \bar{H}_{x',x}^{eff}. \quad (2.30)$$

The constant shift  $\Lambda$  has to be large enough that all the diagonal elements of  $\bar{G}^{eff}$  are strictly positive. This is possible in general for the diagonal elements. If  $H^{eff}$  is appropriately defined [15], one can prove that its ground state *is a variational state of  $H$  with an energy better than the guiding wavefunction one*. Here we slightly modify this approach which neglects all the matrix elements of  $H$  crossing the nodes of the guiding wavefunction, namely the ones with  $\bar{H}_{x',x} > 0$ , by defining a matrix element  $\bar{H}_{x',x}^{eff} < 0$  even when  $\bar{H}_{x',x} > 0$  (see below). The generalization of the above ‘FN theorem’ to this case is straightforward, has been reported in the Appendix A of Ref. [17], and will not be repeated here.

More in detail, the definition of  $\bar{H}^{eff}$  is as follows. The off-diagonal matrix elements are given by

$$\bar{H}_{x',x}^{eff} = \begin{cases} \bar{H}_{x',x} & \text{if } \bar{H}_{x',x} \leq 0 \\ -\gamma \bar{H}_{x',x} & \text{if } \bar{H}_{x',x} > 0 \end{cases} \quad (2.31)$$

where  $\gamma$  is a positive constant, and the diagonal ones are

$$H_{x,x}^{eff} = H_{x,x} + (1 + \gamma)\mathcal{V}_{sf}(x), \quad (2.32)$$

where the diagonal *sign-flip* contribution is given by:

$$\mathcal{V}_{sf}(x) = \sum_{\{\bar{H}_{x',x} > 0, x' \neq x\}} \bar{H}_{x',x}. \quad (2.33)$$

Notice that there is no difference between the diagonal elements of the Hamiltonian  $H^{eff}$  ( $H$ ) and the ones of the transformed matrix  $\bar{H}^{eff}$  ( $\bar{H}$ ), as defined by Eq. (2.26).

With these definitions, the equality (2.27) holds if the factor  $s_{x',x}$  is given by:

$$s_{x',x} = \begin{cases} 1 & \text{if } \bar{G}_{x',x} \geq 0 \\ -1/\gamma & \text{if } \bar{G}_{x',x} < 0 \\ \frac{\Lambda - H_{x,x}}{\Lambda - H_{x,x}^{eff}} & \text{if } x' = x \end{cases}. \quad (2.34)$$

Then, the appropriate stochastic process relative to the Hamiltonian matrix  $H$  can be defined by introducing the basic element of the statistical approach: the *walker*. A walker is defined by an index  $x$  corresponding to a given element  $|x\rangle$  of the chosen basis and a weight factor,  $w$ , representing the amplitude of the sampled wavefunction on the element  $|x\rangle$  of the Hilbert space. In particular the Markov iteration implementing statistically the matrix multiplication (2.23) can be defined by the following three steps:

1. Given the walker  $(w, x)$ , change the weight by scaling it with  $b_x$ :

$$w \rightarrow b_x w.$$

2. Generate randomly a new configuration  $x'$  according to the stochastic matrix  $p_{x',x}$ .

3. Finally multiply the weight of the walker by  $s_{x',x}$ :

$$w' \rightarrow w s_{x',x}. \quad (2.35)$$

It is clear that, whenever the off-diagonal matrix elements of the importance sampled Green function (2.27) are non-positive, the walker's weight has no definite sign. This is the origin of the well-known sign problem, that will be discussed in detail in the following. Without the latter step, one is actually sampling the Hamiltonian  $H^{eff}$ , which we expect (or assume) to have a ground state close to the one of  $H$ , for suitably chosen guiding wavefunction. During the Markov iteration it is straightforward therefore to update both the weight  $w$  associated to the true Hamiltonian, and the *positive definite*

one  $w^{eff}$  associated to the approximate FN one,  $H^{eff}$ . Therefore, from now on the walker will be therefore characterized by the triad

$$(w, w^{eff}, x).$$

Of course, in absence of sign problem, i.e., whenever the off-diagonal matrix elements of  $\bar{G}_{x,x'}$  are positive definite,  $\bar{H}^{eff} = \bar{H}$  and  $s_{x,x'} \equiv 1$ , so that  $w^{eff} = w$ .

The previous Markov iteration allows one to define the evolution of the probability density for having the walker with weights  $w$  and  $w^{eff}$  in the configuration  $x$ , namely:

$$P_{n+1}(w', w^{eff'}, x') = \sum_x \frac{p_{x',x}}{b_x^2 |s_{x',x}|} P_n \left( \frac{w'}{b_x s_{x',x}}, \frac{w^{eff'}}{b_x}, x \right). \quad (2.36)$$

The first moments of the distribution  $P$  over  $w$  and  $w^{eff}$  give the state  $\psi_n(x)$  propagated with the exact Green function  $\bar{G}$  and the state  $\psi_n^{eff}(x)$  propagated with the FN Green function  $\bar{G}^{eff}$ , respectively. Indeed by defining the propagated wavefunctions as

$$\psi_n(x) = \int dw^{eff} \int dw w P_n(w, w^{eff}, x), \quad (2.37)$$

$$\psi_n^{eff}(x) = \int dw^{eff} \int dw w^{eff} P_n(w, w^{eff}, x), \quad (2.38)$$

one can be readily verify, using (2.36), that the above expressions for  $\psi_n$  and  $\psi_n^{eff}$ , satisfy the iteration condition (2.23) with  $\bar{G}$  and  $\bar{G}^{eff}$ , respectively. Therefore, after some equilibration (i.e., for large  $n$ ) the probability distribution  $P_n$  will reach its equilibrium form  $P_0$  so that  $\psi_n(x) \propto \psi_0(x) \psi_G(x)$ , and  $\psi_n^{eff}(x) \propto \psi_0^{eff}(x) \psi_G(x)$ , where  $\psi_0$  and  $\psi_0^{eff}$  are the ground states of  $H$  and  $H^{eff}$ .

As a result, the ground-state energy of  $H$  can be expressed as

$$E_0 = \frac{\langle \psi_G | \hat{\mathcal{H}} | \psi_0 \rangle}{\langle \psi_G | \psi_0 \rangle} = \frac{\sum_{x,x'} \bar{H}_{x',x} \int dw^{eff} \int dw w P_0(w, w^{eff}, x)}{\sum_x \int dw^{eff} \int dw w P_0(w, w^{eff}, x)}, \quad (2.39)$$

that is, remembering the definition (2.16) of the local energy,  $E_x = \sum_{x'} \bar{H}_{x',x}$ , it can be computed by means of the Monte Carlo sampling as

$$E_0 = \frac{\langle \psi_G | \hat{\mathcal{H}} | \psi_0 \rangle}{\langle \psi_G | \psi_0 \rangle} \simeq \frac{\sum_{(x,w) \in X} w E_x}{\sum_{(x,w) \in X} w}, \quad (2.40)$$

where  $\sum_{(x,w) \in X}$  means the sum over independent configurations of the walkers belonging to a sample  $X$ , generated according to the three steps of Eq. (2.35). Similarly, for the ground-state energy of  $H^{eff}$ ,  $E_0^{eff}$ , we have

$$E_0^{eff} \simeq \frac{\sum_{(x,w^{eff}) \in X} w^{eff} E_x}{\sum_{(x,w^{eff}) \in X} w^{eff}}. \quad (2.41)$$

In addition, within the same Monte Carlo sampling, it is also possible to calculate all the so-called *mixed averages* [14] of arbitrary linear operators  $\hat{O}^k$ ,

$$\frac{\langle \psi_G | O^k | 0 \rangle}{\langle \psi_G | 0 \rangle}, \quad (2.42)$$

where  $|0\rangle$  is the ground state of  $H$  or  $H^{eff}$ . In fact, such mixed averages can be calculated using Eq. (2.40) or Eq. (2.41) by substituting the local energy  $E_x$  with the local estimator associated to the operator  $\hat{O}^k$ , i.e.,

$$O_x^k = \sum_{x'} \bar{O}_{x',x}^k. \quad (2.43)$$

where  $\bar{O}_{x',x}^k$  are the operator matrix elements transformed according to the guiding wavefunction, as defined in Eq. (2.26). Of course the mixed average of a correlation function coincides with its ground-state expectation value only for operators commuting with the Hamiltonian.

If the guiding wavefunction  $\psi_G$  is exactly equal to the ground state of  $H$ , by definition  $E_x = E_0$ , independent of  $x$ , as  $\langle \psi_G | H = E_0 \langle \psi_G |$  in (2.16). This is the so-called *zero variance property* satisfied by the method. Namely if the guiding wavefunction approaches an exact eigenstate of  $H$ , the method is free of statistical fluctuations. Of course such a fortunate situation is not common at all. However, improving the guiding wavefunction the statistical fluctuations of the energy can be much reduced, leading to more efficient simulations. Moreover, since the most stable right eigenvector  $\psi_0^{eff}(x)\psi_G(x)$  of the positive definite Green function  $\bar{G}^{eff}$  can be chosen positive (see Appendix A), it is important to implement importance sampling with a guiding wavefunction with signs as similar as possible to the ones of the ground state of  $H$ , so that the Green function  $\bar{G}$  has its most stable right eigenvector  $\psi_0(x)\psi_G(x) > 0$  for most configurations  $x$ . In this case there are good chances that the latter state is well approximated by the positive vector  $\psi_0^{eff}(x)\psi_G(x)$ . As we will show later on, this is crucial for the efficiency of the method in presence of the sign problem.

In the practical implementation of the method, since the walker weights grow exponentially with the Markov iteration – simply as a result of the independent products in the steps (1) and (3) of Eq. (2.35) – the procedure for the statistical evaluation of the mixed averages is slightly different. The configurations  $x_n$  that are generated in the Markov process are distributed after many iterations according to the maximum right eigenstate of the matrix  $p_{x',x}$  [as, if we neglect the weights of the walkers, only the matrix  $p$  is effective in the matrix product (2.23)]. This state is in general different from the state  $\psi_G(x)\psi_0(x)$  we are interested in. So, after many iterations, the sampled configurations  $x_n$  are distributed according to an approximate state and we can consider this state

### 34 Numerical methods

as a trial state  $\psi_G$  for the initial iteration in the power method (2.23). At any Markov iteration  $n$ , we can compute the weight of the walker assuming that  $L$  iterations before its value was simply  $w = 1$ . In this way it is simple to compute the resulting weight of the walker with  $L$  power Green function  $\bar{G}$  applications:

$$G_n^L = \prod_{j=1}^L b_{x_{n-j}} s_{x_{n-j+1}, x_{n-j}}. \quad (2.44)$$

Therefore, for instance, in order to compute the ground-state energy of  $H$  with a single Markov chain of many iterations, the following quantity is usually sampled

$$E_0 = \frac{\sum_n E_{x_n} G_n^L}{\sum_n G_n^L}, \quad (2.45)$$

with  $L$  fixed, and as large as possible consistently with the necessity to keep the fluctuations under control [47].

At this stage the algorithm is exact and the Markov iteration allows one to sample the ground states of  $H$  and  $H^{eff}$  within statistical errors, that unfortunately may be very large, and increasing with the iteration number  $n$ , especially when there is sign problem. In fact, there are two important drawbacks for the single walker formulation that do not allow one to calculate the averages over the weight variable  $G_n^L$  in a stable and controlled manner. The first one arises because the weight  $G_n^L$  of the walker grows exponentially with  $L$  and can assume very large values, implying diverging variances in the above averages. This problem has a very well established solution by generalizing the GFMC to many walkers and introducing a scheme (*branching*) that enables to carry out walkers with reasonable values of the weights, by dropping the irrelevant walkers with small weights and splitting the ones with large weights. Recently a simple formulation of this scheme was defined at fixed number of walkers [47] in a way that allows one to control efficiently the residual bias related to the finite walker population. The second drawback is the more difficult one and is due to the sign problem. In fact, whenever the walkers' weights have no definite sign, the average sign  $\langle s_L \rangle = \sum_n G_n^L / \sum_n |G_n^L|$  vanishes exponentially with  $L$ , so that the walkers with positive weight cancel almost exactly the contribution of the walkers with negative weight, leaving an exponentially small quality to sample. In the formulation of Ref. [47] this problem looks quite similar to the first simple one. As we will see later on, some kind of remedy can be defined by a simple generalization of the Stochastic Reconfiguration (SR) which is useful in the case with no sign problem. This numerical technique is called Green function Monte Carlo with Stochastic Reconfiguration (GFMC SR) [16, 17].

## 2.4.2 The Stochastic Reconfiguration

Given  $M$  walkers we denote the corresponding configurations and weights with two vectors  $(\mathbf{w}, \mathbf{x})$ , where each vector component  $(w_i, w_i^{eff}, x_i)$  with  $i = 1, \dots, M$  corresponds to the  $i^{\text{th}}$  walker. Following Ref. [47], it is easy to generalize Eq. (2.36) to many walkers by introducing the corresponding probability  $P_n(\mathbf{w}, \mathbf{x})$  of having the  $M$  walkers with weights and configurations  $(\mathbf{w}, \mathbf{x})$  at the iteration  $n$ . Similarly to the single walker formulation, the propagated wavefunctions  $\psi_n(x)$  and  $\psi_n^{eff}(x)$  with the true Green function  $\bar{G}$  and the approximate one  $\bar{G}^{eff}$  read

$$\psi_n(x) = \int [d\mathbf{w}] \sum_{\mathbf{x}} \sum_j \frac{w_j \delta_{x, x_j}}{M} P_n(\mathbf{w}, \mathbf{x}), \quad (2.46)$$

$$\psi_n^{eff}(x) = \int [d\mathbf{w}] \sum_{\mathbf{x}} \sum_j \frac{w_j^{eff} \delta_{x, x_j}}{M} P_n(\mathbf{w}, \mathbf{x}), \quad (2.47)$$

where the symbol  $\int [d\mathbf{w}]$  indicates the  $2M$  multidimensional integral over the  $(w_i, w_i^{eff})$  variables  $i = 1, \dots, M$  ranging from  $-\infty$  to  $\infty$  and from  $0$  to  $\infty$ , respectively. Equations (2.46) and (2.47) show that the propagated quantum-mechanical states  $\psi_n$  and  $\psi_n^{eff}$ , which are sampled statistically, do not uniquely determine the walker probability function  $P_n(\mathbf{w}, \mathbf{x})$ . In particular, it is perfectly possible to define a statistical process, the SR, which changes the probability distribution  $P_n$  without changing the *exact* information content, i.e.,  $\psi_n$  and  $\psi_n^{eff}$ . In this way a linear transformation of  $P_n$ , described by a simple kernel  $X(\mathbf{w}', \mathbf{x}'; \mathbf{w}, \mathbf{x})$ , will be explicitly given:

$$P'_n(\mathbf{w}', \mathbf{x}') = \int [d\mathbf{w}] \sum_{\mathbf{x}} X(\mathbf{w}', \mathbf{x}'; \mathbf{w}, \mathbf{x}) P_n(\mathbf{w}, \mathbf{x}). \quad (2.48)$$

When there is no sign problem ( $w^{eff} = w$ ) it is possible to define the kernel  $X$  [47] by requiring that the weights  $w'_j$  are all equal to  $\sum_j w_j / M$  after the SR. In this case the algorithm is exact, and allows one to perform stable simulations by applying the SR each few  $k_p$  iterations. Furthermore, by increasing the number of walkers  $M$ , the exponential growth in the variance of the weights  $w_j$  can always be reduced and systematically controlled. In fact, for large enough  $M$ , it is possible to work with  $L$  sufficiently large ( $L \propto M$ ) obtaining results already converged in the power method iteration (2.23), and with small error bars.

In order to avoid the sign problem instability, at least in an approximate way, we can follow the previous scheme by using the following kernel  $X$  that defines the SR (2.48)

$$X(\mathbf{w}', \mathbf{x}'; \mathbf{w}, \mathbf{x}) = \prod_{i=1}^M \left( \frac{\sum_j |p_{x_j}| \delta_{x'_i, x_j}}{\sum_j |p_{x_j}|} \right)$$

$$\begin{aligned}
 & \times \delta \left( w'_i - \beta^{-1} \frac{\sum_j w_j}{M} \operatorname{sgn} p_{x'_i} \right) \\
 & \times \delta \left( w_i^{\text{eff}'} - |w'_i| \right), \tag{2.49}
 \end{aligned}$$

where the coefficients  $p_{x_j}$  will be defined in the following, and

$$\beta = \frac{\sum_j p_{x_j}}{\sum_j |p_{x_j}|}. \tag{2.50}$$

The kernel (2.49) has a particularly simple form since the outgoing variables  $x'_j$  and  $w'_j$  are completely independent for different values of  $j$ . In particular, it is possible to integrate easily each of the  $M$  factors of the kernel in the variables  $w'_j$ ,  $w_j^{\text{eff}'}$  and to sum over the configurations  $x'_j$ , the result being simply one, as it is required by the normalization condition of the probability density  $P'$  in Eq. (2.48). In general, the SR defines new states  $\psi'_n(x)$  and  $\psi_n^{\text{eff}}$  starting from the given states  $\psi_n(x)$  and  $\psi_n^{\text{eff}}$  at the given Markov iteration  $n$ . The new states  $\psi'_n(x)$  and  $\psi_n^{\text{eff}}$  are simply obtained by replacing  $P$  with  $P'$  in Eqs. (2.46) and (2.47). The SR will be exact if it does not affect the evolution of the state  $\psi_n(x)$  during the Markov chain, namely whenever

$$\psi'_n(x) = \psi_n(x). \tag{2.51}$$

In the SR, the new configurations  $x'_i$  are taken randomly among the old ones  $\{x_j\}$ , according to the probability  $|p_{x_i}| / \sum_j |p_{x_j}|$ , defined below in terms of the given weights  $\{w_j\}$ ,  $\{w_j^{\text{eff}}\}$  and configurations  $\{x_j\}$ . Moreover, the weights  $w'_i$  are changed consistently to Eq. (2.49) by  $w'_i = \beta^{-1} \sum_j w_j / M \operatorname{sgn} p_{x'_i}$  and the FN weights, restricted to be positive, are defined by taking their absolute values  $w_i^{\text{eff}'} = |w'_i|$ .

The coefficient  $\beta$ , given by Eq. (2.50), guarantees that the normalization is preserved by the SR, namely  $\sum_x \psi'_n(x) = \sum_x \psi_n(x)$  (see Appendix D). This coefficient  $\beta$  represents also the expected average walker sign  $\langle s \rangle' = \sum_j w'_j / \sum_j |w'_j|$  after the reconfiguration. It is supposed to be much higher than the average sign before the reconfiguration  $\langle s \rangle = \sum_j w_j / \sum_j |w_j|$ , so that a stable simulation with approximately constant average sign  $\langle s \rangle'$  can be obtained by iteratively applying the SR every few  $k_p$  steps of the power method iteration (2.23).

In the actual implementation of this algorithm (see Appendix E for the details) the weights are reset to unit values after the SR:  $w'_i = \operatorname{sgn} p_{x'_i}$  and  $w_i^{\text{eff}'} = 1$ , whereas only the overall constant  $\beta^{-1} \sum_j w_j / M$ , common to all the different walkers, is stored in a sequential file. As in the single walker formulation we can assume that, at any given iteration  $n$ ,  $L$  iterations before the trial state  $\psi_G$  is given by the equilibrium distribution of walkers with unit weights  $w_j = \operatorname{sgn} p_{x_j}$ . Therefore, in order to obtain the weights

predicted by the Eq. (2.49) for  $L$  power method iterations starting from  $\psi_G$  it is enough to multiply the previous  $L/k_p$  saved factors  $f_n = \beta^{-1} \sum_j w_j / M$ . This yields a natural extension of the factors  $G_n^L$  in Eq. (2.44) to the many walker case

$$G_n^L = \prod_{k=1}^{L/k_p} f_{n-k \times k_p} \quad (2.52)$$

and the corresponding mixed average correlation functions are obtained by averaging the local estimators over all the iterations  $n$  just before the SR (i.e.,  $n$  is a multiple of  $k_p$ )

$$\langle O^k \rangle = \frac{\sum_n G_n^L \sum_j w_j O_{x_j}^k}{\sum_n G_n^L \sum_j w_j}, \quad (2.53)$$

where, in the above equation, the weights  $w_j$  and the local estimators  $O_{x_j}^k$  are evaluated only before the SR.

### Choice of the coefficients $p_{x_j}$

The only left quantity in the kernel of Eq. (2.49), which we still need to define properly the whole algorithm, are the coefficients  $p_{x_j}$  which *have not* to be assumed positive. These coefficients may depend on all the weights  $w_j$ , the configurations  $x_j$  and the FN weights  $w_j^{eff}$ .

The choice  $p_{x_j} = w_j$  is exact in the sense that  $\psi'_n(x) = \psi_n(x)$ , and coincides with the one for the case without sign problem [47]. However this choice is obviously not convenient, because this reconfiguration will not improve the sign, which will decay exponentially in the same way.

Instead, in the case with sign problem, we can parameterize the coefficients  $p_{x_j}$  by assuming they are close enough to the positive definite weights  $\{w_j^{eff}\}$ , the ones obtained with the FN Green function  $G^{eff}$ . The rationale for this choice is that, though the weights  $w_j^{eff}$  may be occasionally very different from the exact weights  $w_j$  – namely their sign can be wrong – they sample a state  $\psi_n^{eff}(x)$  which is supposed to be quite close to the exact propagated state  $\psi_n(x)$ . This condition is clearly verified for an appropriate choice of the guiding wavefunction  $\psi_G$ , making the FN accurate. Then, we assume that small perturbations over the state  $\psi_n^{eff}(x)$  may lead to fulfill the equality (2.51) with an arbitrarily small error. This error will affect the equilibrium walker distribution  $P_n$  for large  $n$ , but there will be no problem if this error *i)* is small and *ii)* can be reduced within the desired accuracy.

In the simplest and most practical formulation we require that only the average energy before and after the SR coincide

$$\sum_{x',x} \bar{H}_{x',x} \psi_n(x) = \sum_{x',x} \bar{H}_{x',x} \psi'_n(x) \quad (2.54)$$

(the denominators in the mixed averages (2.42) are already equal by definition, as  $\sum_x \psi_n(x) = \sum_x \psi'_n(x)$  for the chosen  $\beta$  in Eq. (2.49)). Then, we define

$$p_{x_j} = w_j^{eff} (1 + \alpha(E_{x_j} - \bar{E}_{eff}))$$

and

$$\bar{E}_{eff} = \frac{\sum_j w_j^{eff} E_{x_j}}{\sum_j w_j^{eff}}, \quad \bar{E} = \frac{\sum_j w_j E_{x_j}}{\sum_j w_j}, \quad (2.55)$$

where  $E_{x_j}$  is the local energy (2.16) associated to the configuration  $x_j$ . Thus  $\bar{E}$  represents the estimate of the average energy correctly sampled with the sign, whereas  $\bar{E}_{eff}$  is the corresponding FN one. In order to satisfy the requirement (2.54) we just determine  $\alpha$  by

$$\alpha = \frac{\bar{E} - \bar{E}_{eff}}{\bar{E}_{eff}^2 - (\bar{E}_{eff})^2} \quad (2.56)$$

where  $\bar{E}_{eff}^2 = \sum_j w_j^{eff} E_{x_j}^2 / \sum_j w_j^{eff}$  is the average square energy over the positive weights  $w_j^{eff}$ .

A simple calculation shows that with this reconfiguration, that clearly improves the sign, the value of the energy (the mixed average energy) remains statistically the same before and after the SR (see Appendix D). It is clear, however, that this is not enough to guarantee convergence to the exact ground state, because fulfillment of Eq. (2.54) does not imply the exact equality (2.51). We can improve the definition of the constants  $p_{x_j}$  by including an arbitrary number  $p$  of parameters with,  $p \ll M$ ,

$$p_{x_j} = w_j^{eff} (1 + \alpha_1(O_{x_j}^1 - \bar{O}_{eff}^1) + \dots + \alpha_p(O_{x_j}^p - \bar{O}_{eff}^p)) \quad (2.57)$$

proportional to the fluctuations  $O_{x_j}^k - \bar{O}_{eff}^k$  of  $p$  different operators  $\hat{O}^k$  with corresponding local estimators  $O_{x_j}^k = \langle \psi_G | \hat{O}^k | x_j \rangle / \langle \psi_G | x_j \rangle$  ( $k = 1, \dots, p$ ), and average value over the positive weights  $\bar{O}_{eff}^k = \sum_j w_j^{eff} O_{x_j}^k / \sum_j w_j^{eff}$ . With the more general form (2.57) for the coefficients  $p_{x_j}$  it is possible to fulfill that all the mixed averages for the chosen  $p$  operators have the same value before and after the SR:

$$\sum_{x',x} \bar{O}_{x',x}^k \psi_n(x) = \sum_{x',x} \bar{O}_{x',x}^k \psi'_n(x). \quad (2.58)$$

In general, the reference weights  $w_j^{eff}$  in Eq. (2.57) may be also different from the ones generated by the FN Green function, the only restriction is that  $w_j^{eff} > 0$  for each walker  $j$  (see Appendix D).

It can be proven that, in order to fulfil exactly the SR conditions (2.58), it is *sufficient* that the coefficients  $p_{x_j}$  are chosen in a way that

$$\frac{\sum_j p_{x_j} O_{x_j}^k}{\sum_j p_{x_j}} = \frac{\sum_j w_j O_{x_j}^k}{\sum_j w_j}, \quad (2.59)$$

which can be fulfilled with a solution of a simple linear system for the unknown variables  $\alpha_k$ , for  $k = 1, \dots, p$ , as described in the Appendix D. The conditions (2.59) are much simpler to handle, because they can be satisfied at a given iteration of the Markov process. A theorem, proven in Appendix D, guarantees indeed that the exact conditions (2.58) are implied by the constraints (2.59) after the complete statistical average over the walker probability distribution  $P_n$ .

### Proof of the asymptotical convergence of the GFMCSR to the exact result

Asymptotically, by adding more and more parameters  $\{\alpha_j\}$ , we can achieve the exact SR conditions  $\psi'_n(x) = \psi_n(x)$  strictly, since the distribution  $\psi_n(x)$  is completely determined by its correlation functions. The proof of this important statement is very simple. Consider first the diagonal operators. All these operators may be written as linear combinations of the “elementary” ones  $O_{x',x}^{x_0} = \delta_{x',x} \delta_{x,x_0}$  acting on a single configuration  $x_0$ , plus at most some constants. If conditions (2.58) are satisfied for *all* the elementary operators  $O^{x_0}$  it immediately follows that  $\psi'_n(x_0) = \psi_n(x_0)$  for all  $x_0$ , which is the exact SR condition (2.51). Then it is simple to show that the coefficients  $p_{x_j}$ , determining  $P'_n$  and  $\psi'_n$ , are invariant for any constant shift of the operators  $O^k$ . Furthermore with a little algebra it turns out that these coefficients  $p_{x_j}$  do not change for any arbitrary linear transformation of the chosen operator set:  $O^{k'} = \sum_k L_{k',k} O^k$  (with real  $L$  and  $\det L \neq 0$ ) (see Appendix D). Thus the proven convergence of the GFMCSR is obtained for any sequence of diagonal operators, that, with increasing  $p$ , becomes complete. For non-diagonal operators  $O_{x',x}$  we simply note that they assume the same mixed average values of the equivalent diagonal ones  $O_{x',x}^{diag} = \delta_{x',x} \sum_{x'} O_{x',x}$ . Thus the proof that GFMCSR converges in principle to the exact solution is valid in general even when non-diagonal operators, such as the Hamiltonian itself, are included in the conditions (2.58).

### 2.4.3 The limit $\Lambda \rightarrow \infty$ for the power method: imaginary time evolution

The constant  $\Lambda$ , which defines the the Green function  $\bar{G}_{x',x} = \Lambda \delta_{x',x} - \bar{H}_{x',x}$  and the FN one  $\bar{G}^{eff}$  (2.30) has to be taken large enough to determine that all the diagonal elements of  $\bar{G}^{eff}$  are nonnegative (by definition the off-diagonal ones of  $\bar{G}^{eff}$  are always non-negative). This requirement often determines a very large constant shift which increases with larger size and is not known a priori. The trouble in the simulation may be quite tedious, as if for the chosen  $\Lambda$  a negative diagonal element is found for  $\bar{G}^{eff}$ , one needs to increase  $\Lambda$  and start again with a completely new simulation. The way out is to work with exceedingly large  $\Lambda$ , but this may slow down the efficiency of the algorithm as in the stochastic matrix  $p_{x',x}$  the probability to remain in the same configuration  $p_d$  may become very close to one

$$p_d = \frac{\Lambda - H_{x,x} - (1 + \gamma)\mathcal{V}_{sf}(x)}{\Lambda - E_x} \quad (2.60)$$

where  $\mathcal{V}_{sf}(x)$  is given in Eq. (2.33) and  $E_x$  is the local energy Eq. (2.16) that do not depend on  $\Lambda$  given the configuration  $x$ .

Following Ref. [14] the problem of working with large  $\Lambda$  can be easily solved with no loss of efficiency. We report this simple idea applied to our particular algorithm at fixed number of walkers. If  $\Lambda$  is large it is possible to take a large value of  $k_p$  (of order  $\Lambda$ ) iterations between two consecutive reconfigurations, because in most iterations the configuration  $x$  is not changed. The idea is that one can determine a priori, given  $p_d$ , what is the probability  $t(k)$  to make  $k$  diagonal moves before the first acceptance of a new configuration with  $x' \neq x$ . This is given by  $t(k) = p_d^k(1 - p_d)$  for  $k = 0, \dots, n_l - 1$  and  $t(n_l) = p_d^{n_l}$  if no off-diagonal moves are accepted during the  $n_l$  trials that are left to complete the loop without reconfigurations.

It is a simple exercise to show that, in order to sample  $t(k)$  one needs one random number  $0 < \xi < 1$ , so that the stochastic integer number  $k$  can be computed by the simple formula

$$k = \min \left( n_l, \left[ \frac{\ln \xi}{\ln p_d} \right] \right), \quad (2.61)$$

where the brackets indicate the integer part. During the  $k_p$  iterations one can iteratively apply this formula by bookkeeping the number of iterations  $n_l$  that are left to complete the loop without reconfigurations. At the first iteration  $n_l = k_p$ , then  $k$  is extracted using (2.61), and the weights  $(w, w^{eff})$  of the walker are updated according to  $k$  diagonal moves and if  $k < n_l$  a new configuration is extracted at random according to the off-diagonal matrix elements of  $p_{x',x}$ . The weights are correspondingly updated for this

off-diagonal move, and finally, if  $k < n_l$ ,  $n_l$  is changed to  $n_l - k - 1$ , so that one can continue to use Eq. (2.61) until all the  $k_p$  steps are executed for each walker.

The interesting thing of this method is that it can be readily generalized for  $\Lambda \rightarrow \infty$  by increasing  $k_p$  with  $\Lambda$ , namely  $k_p = [\Lambda \Delta\tau]$ , where  $\Delta\tau$  represents now exactly the imaginary time difference between two consecutive reconfigurations when the exact propagator  $e^{-H\Delta\tau}$  or  $e^{-H^{eff}\Delta\tau}$  is applied statistically (see also Appendix E).

## 2.5 Numerical tests

In this section some general properties of the GFMCSR technique are discussed and explicitly tested on the models under consideration in this work, namely the spin-half  $J_1-J_2$  and triangular Heisenberg antiferromagnets (see Introduction). In the following we will consider finite clusters of  $N$  sites with periodic boundary conditions. Details on the guiding wavefunctions used can be found in Chapters 3 and 4.

### 2.5.1 The limit of small $\Delta\tau$ and large number of walkers

We report here some test results useful to understand the crucial dependence of GFMCSR on the number of walkers  $M$  and the distance in imaginary time  $\Delta\tau$  between two consecutive SR. In fact, after the selection of a given number  $p$  of correlation functions in Eqs. (2.58), the results depend only on the number of walkers  $M$  and the frequency of reconfiguration  $\Delta\tau$ . In the limit of large number of walkers, at fixed  $p$ , the algorithm has the important property that the fluctuations of the coefficients  $\alpha_k$  and  $\bar{O}^k$  in Eq. (2.57) are obviously vanishing, because they depend on averages of a very large number of samples of many different walkers, implying that these fluctuations are decreasing with  $1/\sqrt{M}$ . In this limit it is possible to recover the important zero variance property of the FN: *if the guiding wavefunction is exact, the FN averages are also exact*. In fact suppose we begin to apply the propagator  $e^{-H\tau}$  starting at  $\tau = 0$  from the exact sampling of the ground state  $\psi_0$  determined by FN with the exact guiding wavefunction  $\psi_G = \psi_0$ . Then, at any Markov iteration  $n$ , before the SR is applied, both the mixed average correlation functions calculated with the FN weights  $w^{eff}$ ,  $\bar{O}_{eff}^k = \sum_j w_j^{eff} O_{x_j}^k / \sum_j w_j^{eff}$ , and the weights with arbitrary signs  $w$ ,  $\bar{O}^k = \sum_j w_j O_{x_j}^k / \sum_j w_j$ , sample statistically the true quantum average  $\langle \psi_0 | \hat{O}^k | \psi_0 \rangle / \langle \psi_0 | \psi_0 \rangle$ . If, for large  $M$ , we can neglect statistical fluctuations of these averages, then by Eq. (2.59)  $\alpha_k = 0$  and the SR algorithm just replace the weights  $w_j$  (with sign problem) with the FN weights  $w_j^{eff}$ , which also sample  $\psi_0$  exactly. This means that the SR approach does not affect this important property of the

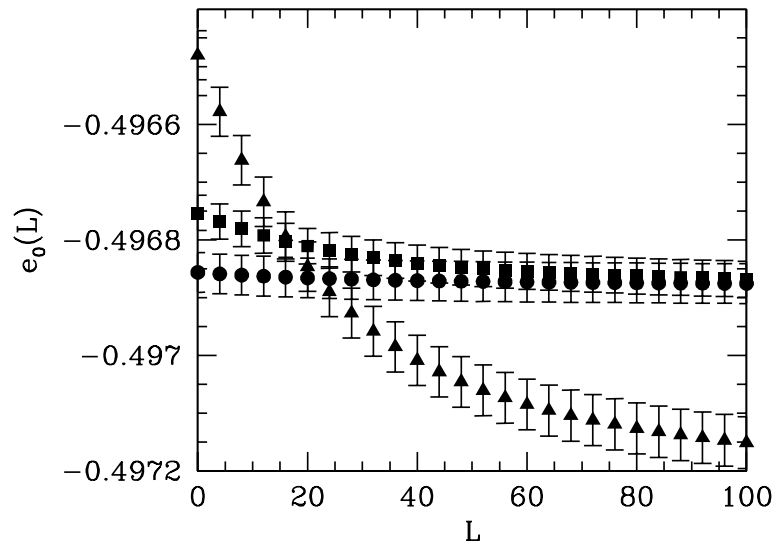


Figure 2.1: Dependence on the number  $L$  of correcting factors of the estimated ground-state energy per site of the  $J_1-J_2$  Heisenberg model for  $N = 64$  and  $J_2/J_1 = 0.5$  obtained with the GFMCSR technique ( $\Delta\tau = 0.01$ ) with  $M = 200$  (triangles), 1500 (squares) and 10000 (circles).

FN approach, at least in the limit  $M \rightarrow \infty$ .

Another reason to work in the limit  $M \rightarrow \infty$  is the following. In this limit it is not necessary to include in the SR conditions (2.59) operators  $O^k$  that vanish for some symmetry that is satisfied both by the true Hamiltonian  $\bar{H}$  and the FN one  $\bar{H}^{eff}$ . In fact, if the coefficients  $p_{x_j}$  are defined in terms of operators  $O^k$  that conserve the above mentioned symmetries (e.g., translation invariance, rotation by  $90^\circ$  degree of the lattice, etc.) by definition Eqs. (2.58) are satisfied for all the remaining non-symmetric operators which have vanishing expectation value due to symmetry constraints (such as, e.g., an operator that changes sign for a rotation operation which is a symmetry of  $\bar{H}$  and  $\bar{H}^{eff}$ ). In this case, both sides of Eqs. (2.58) are zero by such symmetry constraints. Moreover, for  $M \rightarrow \infty$  the statistical fluctuations are negligible and for the same reason Eqs. (2.59) are also automatically satisfied with vanishing  $\alpha_k$  for the above mentioned non-symmetric operators. In this limit, it is therefore useless to include non-symmetric operators in the SR (2.59).

The way the computed results depend on the number of walkers is shown in Fig. 2.1, as a function of the number of correcting factors. As shown in Ref. [47] these correcting factors allow one to eliminate the bias due to the finite population of walkers in the case there is no sign problem. In this case instead the finite population bias cannot be eliminated even by an infinite number of factors and a properly large number  $M$  of

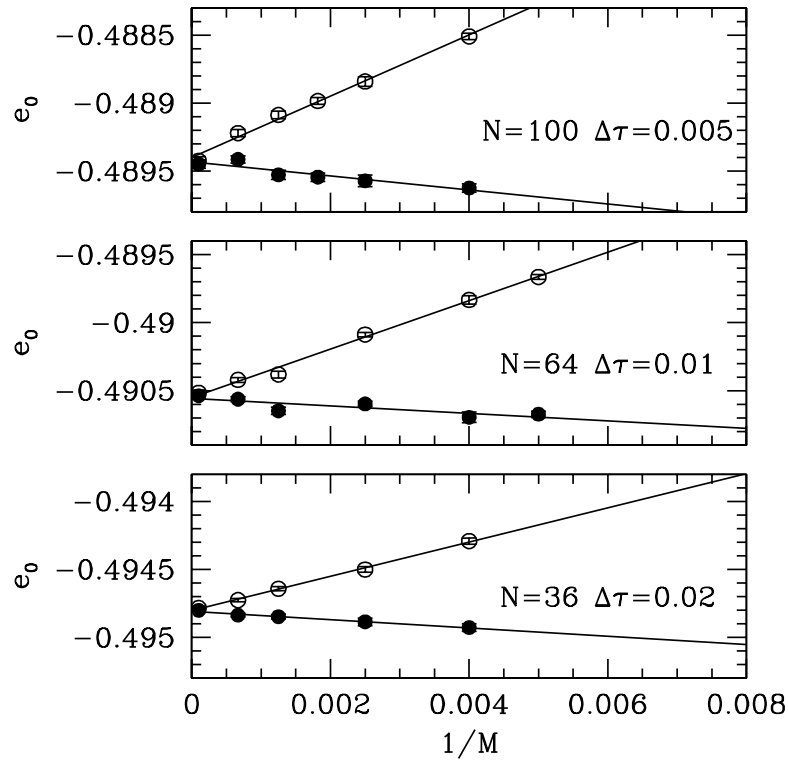


Figure 2.2: Ground-state energy per site of the  $J_1 - J_2$  Heisenberg model for  $J_2/J_1 = 0.5$  obtained for different clusters and different number of walkers. Empty dots are data obtained with zero correcting factors while full dots refer to converged values in  $L$ .

walkers has to be taken for unbiased simulations. In fact for  $M \rightarrow \infty$  the fluctuations of the  $G_n^L$  factors are bounded by the central limit theorem by  $O(\frac{1}{\sqrt{M}})$ . Therefore, for given  $L$  and large enough  $M$ , they do not play any role in the average quantities (2.53).

As it is evident, for large number of walkers ( $M \rightarrow \infty$ ) the correcting factors do not play any role and the estimate with minimum statistical error is obtained by simply ignoring the correcting factors. This is actually a common approach in GFMC, to consider a large number of walkers so that the bias of the finite walker population becomes negligible, and typically decreasing as  $1/M$  (see, e.g., Fig. 2.2). However from the picture it is also evident that, for large enough  $M$ , the predicted results obtained by including or by neglecting the correcting factors are both consistent. The convergence to the  $M \rightarrow \infty$  limit is however faster for the first method. Thus the inclusion of the correcting factors  $G_n^L$  in Eq. (2.53), though increasing the error bars, may be useful to reach the  $M \rightarrow \infty$  limit with a smaller number of walkers.

The other parameter affecting the accuracy of the SR approach is the imaginary time distance  $\Delta\tau$  between two consecutive SR. It is then natural to ask whether by increasing the frequency of the reconfigurations, one reaches a well defined dynamical limit for

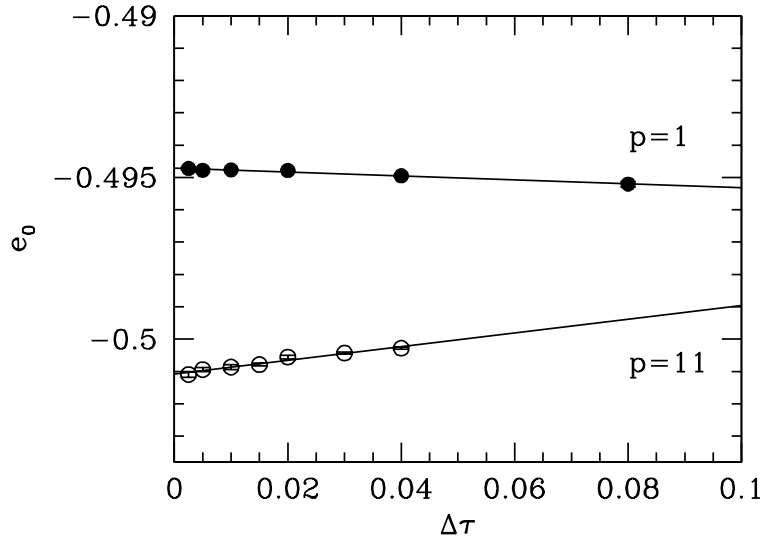


Figure 2.3: Dependence of the ground-state energy per site of the  $J_1-J_2$  Heisenberg model on the imaginary time step  $\Delta\tau$  obtained for  $J_2/J_1=0.5$  and  $N = 36$  with the GFMCSR technique by using in the SR the energy (full dots), all  $S^z(q)$ , the spin square and the order parameter  $m^{\dagger 2}$  (empty dots). The number of walkers was fixed to  $M = 10000$ , so that the finite- $M$  bias can be neglected on this scale. The lower horizontal axis coincides with the exact diagonalization result.

$\Delta\tau \rightarrow 0$ . This is important since, due to the sign problem, for large system size  $N$  the time interval  $\Delta\tau$  has to be decreased at least by a factor inversely proportional to  $N$ , because the average walker sign vanishes exponentially  $\sim e^{-\Delta_s\tau}$  with an exponent  $\Delta_s$  which diverges with  $N$ . Different calculations, performed for different sizes can be compared only when the finite  $\Delta\tau$  error (the difference between  $\Delta\tau \rightarrow 0$  and finite  $\Delta\tau$ ) is negligible.

As shown in Fig. 2.3, whenever the simulation is stable for  $\Delta\tau \rightarrow 0$ , the limit  $\Delta\tau \rightarrow 0$  can be reached with a linear extrapolation. This property can be easily understood since in the limit of a large number of walkers, the variation of the average correlation functions Eq. (2.53) both for the FN dynamics and the exact dynamics in a time interval between two consecutive SR differ clearly by  $O(\Delta\tau)$ .

In order to show more clearly how the method is working and systematically correcting the FN we have implemented a slightly different but more straightforward *release node* technique [48]. We first apply the standard FN [with  $\gamma = 0$ , see Eq. (2.31)] for a given number of walkers  $M$  and for long simulation time. We store the  $M$ -walkers configurations, after some equilibration at time interval large enough to allow uncorrelated and independent samples of the FN ground state. In a second step we recover each of these  $M$ -walker configurations and apply GFMCSR for a fixed imaginary time  $\tau$ , so

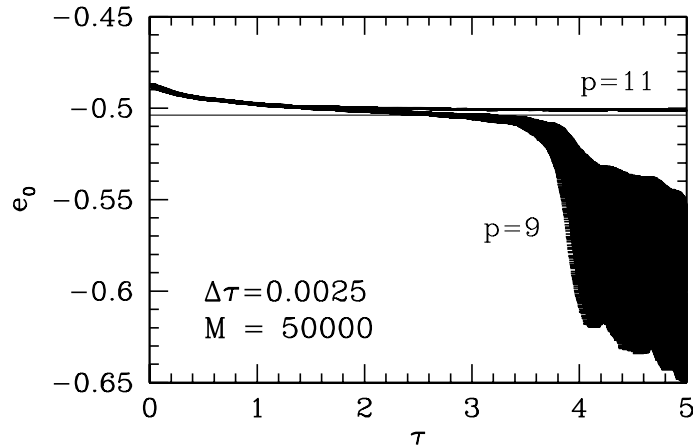


Figure 2.4: Stable (upper curve) and unstable (lower curve) imaginary time evolution of the GFMCSR estimates of the ground-state energy per site of the  $J_1-J_2$  Heisenberg model for  $J_2/J_1 = 0.5$  and the  $N = 36$  cluster. The horizontal line indicates the exact result.

that we can see how the energy expectation value evolves from the FN to a more accurate determination. Typically one obtains a reasonable behavior for these curves that always coincides with the exact dynamics in the initial part where an exact sampling of the sign is possible. However, for large imaginary time, exceedingly small  $\Delta\tau$  and large number of walkers, some instability may occur leading to results clearly off, as shown in Fig. 2.4. In this case, the instability is due to the fact that the correlation functions  $S^z(q) = 1/N^2 \sum_{i,j} S_i^z S_j^z e^{iq(i-j)}$  which we have used in the SR ( $p = 9$ ) [16], introduce some uncontrolled fluctuations for the momentum  $Q = (\pi, \pi)$  relevant for the antiferromagnetic order parameter. If we include in the SR technique also the spin isotropic operator corresponding to the order parameter  $m^{\dagger 2} = 1/N^2 \sum_{i,j} \vec{S}_i \cdot \vec{S}_j e^{iQ(i-j)}$  and the total spin square ( $p = 11$ ) this instability disappears (see Fig. 2.4, stable results, not shown in the picture, are obtained even without the total spin square, i.e., with  $p = 10$ ). This is a reasonable effect, since the order parameter has important fluctuations in all spin directions.

## 2.5.2 Convergence to the exact result and size consistency

In principle, within the GFMCSR method, convergence to the exact result can be achieved with an arbitrary accuracy if a sufficiently large number  $p$  of correlation functions are constrained to be equal before and after the SR. However this is only a theoretical limit

	N	VMC	FN	SR( $p = 2$ )	SR( $p = 7$ )	Exact
$e_0$	12	-0.5981	-0.6083(1)	-0.6085(1)	-0.6105(1)	-0.6103
	36	-0.5396	-0.5469(1)	-0.5534(1)	-0.5581(1)	-0.5604
	48	-0.5366(1)	-0.5426(1)	-0.5495(1)	-0.5541(1)	
	108	-0.5333(1)	-0.5387(1)	-0.5453(1)	-0.5482(1)	
$S_{tot}^2$	12	0.235	0.0111(2)	0.006(4)	-0.002(4)	0.00
	36	1.71	1.20(1)	0.65(1)	0.02(1)	0.00
	48	2.55(1)	2.12(2)	1.44(1)	0.23(3)	0.00
	108	6.36(4)	5.66(3)	4.35(4)	2.7(1)	0.00
$m^{\dagger 2}$	12	0.9241	0.9286(1)	0.9210(2)	0.9132(6)	0.9109
	36	0.7791	0.7701(4)	0.7659(2)	0.7512(3)	0.7394
	48	0.7496(3)	0.7243(5)	0.7177(2)	0.7080(5)	
	108	0.6338(7)	0.6182(4)	0.6040(3)	0.5836(5)	

Table 2.1: Variational estimate (VMC) and mixed averages (FN, SR and Exact) of the ground-state energy per site, the total spin square and the order parameter for the triangular Heisenberg antiferromagnet for various system sizes. SR data are obtained using the short-range correlation functions generated by  $\hat{\mathcal{H}}$  ( $p = 2$ ) and  $\hat{\mathcal{H}}^2$  ( $p = 7$ ) reported in Chap. 3. All the values reported in this table are obtained with large enough  $M$  and  $1/\Delta\tau$ , practically converged in the limit of  $\Delta\tau \rightarrow 0$  and  $M \rightarrow \infty$ . Exact results are obtained using the Lanczos technique.

because the number of correlation functions  $p$  required to obtain the exact result scales exponentially with the system size, yielding a computational effort similar to the exact diagonalization methods.

In order to minimize the number  $p$  of correlation functions used in the SR, one is limited to use an empirical approach, based on physical intuition, and/or by comparison with exact results obtained for small sizes with the exact diagonalization technique. Typically, the fundamental ingredient that we have found to be important for strongly correlated Hamiltonians is the locality. The most useful correlation functions are the short-ranged ones appearing in the Hamiltonian  $\hat{\mathcal{H}}$ . A successful example is the application of the method to the Heisenberg model on the triangular lattice [36] (see also Chap. 3) where a remarkable accuracy is obtained by including also the short-range correlation functions generated by the application of the square of the Hamiltonian. Table 2.1 reports all the values of the ground-state energy per site, the total spin square and the antiferromagnetic order parameter  $m^{\dagger 2}$  obtained with VMC, FN and GFMCSR (for

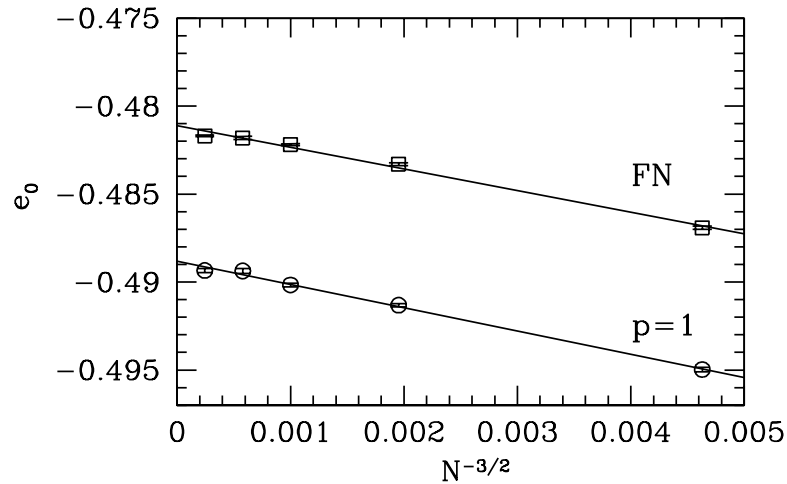


Figure 2.5: Finite-size scaling of the ground-state energy per site of the  $J_1 - J_2$  Heisenberg model for  $J_2/J_1 = 0.5$  obtained with the FN and GFMCSR technique applied reconfiguring the Hamiltonian ( $p = 1$ ).

two different  $p$ 's), up to  $N = 108$ . However, the method of increasing systematically  $p$ , by including in the SR the short-range correlation functions generated by  $\hat{\mathcal{H}}, \hat{\mathcal{H}}^2 \dots$ , does not seem general enough. For instance, it does not work for the  $J_1 - J_2$  Heisenberg model where the inclusion in the SR Eqs. (2.58) of long-range operators, such as the spin-spin correlation function  $S_i^z S_j^z$  at large distance  $|i - j|$ , is crucial to improve the accuracy of the method, whereas the short-range ones generated by  $\hat{\mathcal{H}}^2$  do not give any significant improvement.

Similarly to FN, the GFMCSR turns out to be size-consistent, in the sense that at fixed  $p$  the average correlation functions can be sizeably improved with respect to the variational guess, *even in the thermodynamic limit* (see Fig. 2.5). This is a nontrivial property because, whenever there is sign problem, it is basically impossible to improve the best variational FN guess by the conventional release node technique [48] since, for large sizes the variances become intractable even for a very short imaginary time propagation.

This kind of size consistency is a very important property of the present algorithm because the stability of the average sign at fixed  $p$  allows a *polynomial* complexity of the algorithm as a function of the system size.



## Chapter 3

# The triangular Heisenberg antiferromagnet

Historically the antiferromagnetic spin-1/2 Heisenberg model on the triangular lattice was the first proposed Hamiltonian for a microscopic realization of a non-magnetic ground state [30, 49]. This is due to the fact that in this system the usual antiferromagnetic alignment between spins is hindered by the geometry of the lattice so that the minimum energy configuration, the  $2\pi/3$  Néel state (Fig. 1), has an energy twice larger than that on the square lattice and therefore is far less stable.

However, after many years of intensive study, the question of whether the combined effect of frustration and quantum fluctuations in the ground state of the triangular Heisenberg antiferromagnet favors a disordered resonating valence bond (RVB) state (Sec. 1.4) or long-range Néel type order is still under debate. In fact, there has been considerable effort to elucidate the nature of the ground state and the results of numerical [12, 32, 50, 51, 52, 53, 54, 55, 56, 57, 58, 59, 60, 61], and analytical [62, 63, 64, 65, 22] works are controversial. In particular, the wide extension of exotic proposed ground states like spin-nematic [66], chiral [67], and spin liquid of the Kalmayer-Laughlin type [55, 59] gives an indication that the problem has not been theoretically resolved yet.

Spin-wave calculations [62, 63] predict an important reduction (by about one-half) of the sublattice magnetization by quantum fluctuations. In addition, perturbation theory [61], series expansions [57], and high-temperature calculations [58] suggest that the spin-wave calculations possibly underestimate the renormalization of the order parameter, but do not come to a definite conclusion about the nature of ground state. From the numerical point of view, exact diagonalizations (ED) results [50, 51, 52, 53, 54, 12], which are limited to small lattice sizes, have been interpreted both against [54] and in favor [12] of the presence of long-range Néel order in the thermodynamic ground state. In

any case, this approach, combined with the careful analysis of the symmetry properties of the low-energy excited states proposed by Bernu and co-workers [12], have provided very important evidence pointing towards a magnetic ground state: the spectra of the lowest energy levels order with increasing total spin, a reminiscence of the Lieb-Mattis theorem (see Sec. 1.1) for bipartite lattices, and are consistent with the symmetry of the classical order parameter. However, these very clear ED results cannot rule out that for large sizes quantum fluctuations could drive the system into a non-magnetic phase and therefore cannot be considered as conclusive. In addition, standard stochastic numerical methods, which usually allow one to handle large samples, clash with the sign problem numerical instability so that a definite answer on the ground-state properties of the triangular Heisenberg antiferromagnet is still lacking.

In this chapter we will tackle the problem of the existence of long-range Néel order in the ground state of the triangular Heisenberg antiferromagnet using the finite-size spin-wave theory [10], exact diagonalization, and several Monte Carlo methods among which the Green function Monte Carlo with Stochastic Reconfiguration (GFMC SR), recently developed to keep the sign problem (Sec. 2.4) under control. In the first part we apply the finite-size spin-wave theory to the triangular Heisenberg antiferromagnet, we then show how to construct within this framework the low-lying excited states, and finally derive a simple spin-wave variational wavefunction. The good agreement between the ED results and the finite-size spin-wave theory will support the reliability of the spin-wave expansion in describing not only the ground-state properties but also the low-energy spin excitations of the Heisenberg model even in presence of frustration. The second part will deal with the quantum Monte Carlo results. Data for the spin gap and for the antiferromagnetic order parameter will be presented for fairly large system sizes (up to 144 sites), providing a robust evidence for a gapless excitation spectrum and for the existence of long-range Néel order in the thermodynamic ground state of the model.

### 3.1 Finite-size spin-wave theory

Several attempts to generalize spin-wave theory to finite sizes can be found in the literature [10, 68, 69]. Here we will follow the method proposed by Zhong and Sorella in Ref. [10] which allows one to deal with finite clusters avoiding the spurious Goldstone modes divergences in a straightforward way, and, in particular, without imposing any *ad hoc* holonomic constraint on the sublattice magnetization [68, 69].

### 3.1.1 Application to the triangular antiferromagnet

Assuming the classical  $\mathbf{Q} = (4\pi/3, 0)$  magnetic structure lying in the  $xy$  plane, the first step of the derivation is to apply the unitary transformation given by Eq. (1.9), which defines a spatially varying coordinate system  $(x'y'z')$  in such a way that the  $x'$ -axis points on each site along the local Néel direction. The transformed Heisenberg Hamiltonian reads:

$$\begin{aligned} \hat{U}^\dagger \hat{\mathcal{H}} \hat{U} &= J \sum_{\langle i,j \rangle} \left[ \cos(\mathbf{Q} \cdot \mathbf{r}_{i,j}) (\hat{S}_i^{x'} \hat{S}_j^{x'} + \hat{S}_i^{y'} \hat{S}_j^{y'}) \right. \\ &\quad \left. + \sin(\mathbf{Q} \cdot \mathbf{r}_{i,j}) (\hat{S}_i^{x'} \hat{S}_j^{y'} - \hat{S}_i^{y'} \hat{S}_j^{x'}) + \hat{S}_i^{z'} \hat{S}_j^{z'} \right] \end{aligned} \quad (3.1)$$

where  $J$  is the (positive) exchange constant between nearest neighbors, the indices  $i, j$  label the points  $\mathbf{r}_i$  and  $\mathbf{r}_j$  on the  $N$ -site triangular lattice,  $\mathbf{r}_{i,j} = \mathbf{r}_i - \mathbf{r}_j$ , and the quantum spin operators satisfy  $|\hat{\mathbf{S}}_i|^2 = s(s+1)$ . In the new reference frame the spins in the classical configuration are *ferromagnetically* aligned so that, using Holstein-Primakoff transformation for spin operators to order  $1/s$ ,

$$\hat{S}_i^{x'} = s - \hat{a}_i^\dagger \hat{a}_i \quad \hat{S}_i^{y'} = \sqrt{\frac{s}{2}} (\hat{a}_i^\dagger + \hat{a}_i) \quad \hat{S}_i^{z'} = i \sqrt{\frac{s}{2}} (\hat{a}_i^\dagger - \hat{a}_i), \quad (3.2)$$

being  $\hat{a}$  and  $\hat{a}^\dagger$  the canonical creation and destruction Bose operators, after some algebra the Fourier transformed Hamiltonian results:

$$\hat{\mathcal{H}}_{\text{SW}} = E_{cl} + 3Js \sum_{\mathbf{k}} \left[ A_{\mathbf{k}} \hat{a}_{\mathbf{k}}^\dagger \hat{a}_{\mathbf{k}} + \frac{1}{2} B_{\mathbf{k}} (\hat{a}_{\mathbf{k}}^\dagger \hat{a}_{-\mathbf{k}}^\dagger + \hat{a}_{\mathbf{k}} \hat{a}_{-\mathbf{k}}) \right] \quad (3.3)$$

where  $E_{cl} = -3Js^2N/2$  is the classical ground-state energy,

$$A_{\mathbf{k}} = 1 + \gamma_{\mathbf{k}}/2, \quad B_{\mathbf{k}} = -3\gamma_{\mathbf{k}}/2, \quad (3.4)$$

$\gamma_{\mathbf{k}} = 2 [\cos(k_x) + 2 \cos(k_x/2) \cos(\sqrt{3}k_y/2)] / z$ ,  $\mathbf{k}$  is a vector varying in the first Brillouin zone of the lattice, and  $z = 6$  is the coordination number. The Hamiltonian  $\hat{\mathcal{H}}_{\text{SW}}$ , can be diagonalized for  $\mathbf{k} \neq 0, \pm\mathbf{Q}$  introducing the well-known Bogoliubov transformation,  $\hat{a}_{\mathbf{k}} = u_{\mathbf{k}} \hat{\alpha}_{\mathbf{k}} + v_{\mathbf{k}} \hat{\alpha}_{-\mathbf{k}}^\dagger$ , with

$$u_{\mathbf{k}} = \left( \frac{A_{\mathbf{k}} + \epsilon_{\mathbf{k}}}{2\epsilon_{\mathbf{k}}} \right)^{1/2}, \quad v_{\mathbf{k}} = -\text{sgn}(B_{\mathbf{k}}) \left( \frac{A_{\mathbf{k}} - \epsilon_{\mathbf{k}}}{2\epsilon_{\mathbf{k}}} \right)^{1/2}, \quad (3.5)$$

where  $\epsilon_{\mathbf{k}} = \sqrt{A_{\mathbf{k}}^2 - B_{\mathbf{k}}^2}$  is the spin-wave dispersion relation. This diagonalization leads to:

$$\mathcal{H}_{\text{SW}}^0 = E_{cl} + \frac{3Js}{2} \sum_{\mathbf{k} \neq 0, \pm\mathbf{Q}} (\epsilon_{\mathbf{k}} - A_{\mathbf{k}}) + \frac{3Js}{2} \sum_{\mathbf{k} \neq 0, \pm\mathbf{Q}} \epsilon_{\mathbf{k}} (\hat{\alpha}_{\mathbf{k}}^\dagger \hat{\alpha}_{\mathbf{k}} + \hat{\alpha}_{-\mathbf{k}}^\dagger \hat{\alpha}_{-\mathbf{k}}). \quad (3.6)$$

## 52 The triangular Heisenberg antiferromagnet

The Goldstone modes at  $\mathbf{k} = \mathbf{0}$  and  $\mathbf{k} = \pm\mathbf{Q}$  instead are singular, and cannot be diagonalized with a Bogoliubov transformation. For infinite systems such modes do not contribute to the integrals in Eq. (3.6), but in the finite-size case they are important and they must be treated separately. By defining the following Hermitian operators

$$\begin{aligned}\hat{Q}_x &= \frac{i}{2}(\hat{a}_{\mathbf{Q}}^\dagger + \hat{a}_{-\mathbf{Q}} - \hat{a}_{\mathbf{Q}} - \hat{a}_{-\mathbf{Q}}^\dagger), \\ \hat{Q}_y &= \frac{1}{2}(\hat{a}_{\mathbf{Q}}^\dagger + \hat{a}_{-\mathbf{Q}} + \hat{a}_{\mathbf{Q}} + \hat{a}_{-\mathbf{Q}}^\dagger), \\ \hat{Q}_z &= i(\hat{a}_0^\dagger - \hat{a}_0),\end{aligned}\tag{3.7}$$

such that,  $[\hat{Q}_\alpha, \hat{Q}_\beta] = 0$  and  $[\hat{Q}_\alpha, \hat{\mathcal{H}}_{\text{SW}}] = 0$  for  $\alpha, \beta = x, y, z$ , the contribution of the singular modes,  $\hat{\mathcal{H}}_{SM}$ , in Eq. (3.3) can be expressed in the form

$$\hat{\mathcal{H}}_{SM} = -3J_s A_0 + 3J_s \frac{A_0}{2} [\hat{Q}_x^2 + \hat{Q}_y^2 + \hat{Q}_z^2].\tag{3.8}$$

Then, taking into account the fact that to the leading order in  $1/s$ ,  $\hat{Q}_\alpha = \hat{S}^\alpha \sqrt{2/Ns}$ , where  $\hat{S}^\alpha$  are the components of the total spin,  $\hat{\mathcal{H}}_{SM}$  may be also rewritten in the more physical form

$$\hat{\mathcal{H}}_{SM} = -3J_s A_0 + 3J \frac{A_0}{N} [(\hat{S}^x)^2 + (\hat{S}^y)^2 + (\hat{S}^z)^2],\tag{3.9}$$

which clearly favors a singlet ( $S^2 = 0$ ) ground state (for an even number of sites) being  $A_0$  positive definite. This result is a reminiscence of the Lieb-Mattis property (see Sec. 1.1) which has not been demonstrated for non-bipartite lattices. Actually, a similar result is obtained by solving exactly the three Fourier components  $\mathbf{k} = \mathbf{0}, \pm\mathbf{Q}$  of the Heisenberg model [12]; however, our treatment allows us to construct a formal expression for the spin-wave ground state on finite triangular lattices which keeps the correct singlet behavior. In fact, starting from the usual spin-wave ground state, composed by the  $2\pi/3$  classical Néel order plus the zero point quantum fluctuations (i.e, zero Bogoliubov quasiparticles),

$$|0\rangle = \prod_{\mathbf{k} \neq \mathbf{0}, \pm\mathbf{Q}} u_{\mathbf{k}}^{-1} \exp\left[\frac{1}{2} \frac{v_{\mathbf{k}}}{u_{\mathbf{k}}} \hat{a}_{\mathbf{k}}^\dagger \hat{a}_{-\mathbf{k}}^\dagger\right] |F\rangle\tag{3.10}$$

with  $|F\rangle = \prod_i |S_i^{x'} = s\rangle$ , the corresponding singlet wavefunction is obtained by projecting  $|0\rangle$  onto the subspace  $S = 0$ :

$$|\psi_{\text{SW}}\rangle = \int_{-\infty}^{\infty} d\alpha \int_{-\infty}^{\infty} d\beta \int_{-\infty}^{\infty} d\gamma e^{i\alpha Q_x + i\beta Q_y + i\gamma Q_z} |0\rangle\tag{3.11}$$

and reads  $|\psi_{\text{SW}}\rangle \sim e^{(-\hat{a}_{\mathbf{Q}}^\dagger \hat{a}_{-\mathbf{Q}}^\dagger + \frac{1}{2} \hat{a}_0^\dagger \hat{a}_0^\dagger)} |0\rangle$ . In particular the singular modes have no contribution to the ground-state energy which reads

$$E_{\text{SW}} = E_{cl} + \frac{3Js}{2} \sum_{\mathbf{k}} (\epsilon_{\mathbf{k}} - 1), \quad (3.12)$$

while the computation of the order parameter requires their removal:

$$\hat{m}^\dagger = \sqrt{\langle (\hat{S}_i^{x'})^2 \rangle} = s - \frac{1}{N} \sum_{\mathbf{k} \neq \mathbf{0}, \pm \mathbf{Q}} v_{\mathbf{k}}^2. \quad (3.13)$$

For  $s = 1/2$ , the previous spin-wave calculation predicts a very good quantitative agreement with exact results on small clusters ( $N \leq 36$ ) of both ground-state energy and sublattice magnetization [70]. The agreement is even more remarkable as far as the low-lying excited states are concerned, as it will be shown in the following section.

### 3.1.2 Low-energy spin-wave spectrum

In this section, we show how to construct the low-lying energy spectra  $E(S)$  for finite systems where  $S$  represents the total spin. So far, we have performed a standard spin-wave expansion whose relevant quantum number is  $s$ . Thus, computing  $E(S)$  is not straightforward and requires a little more involved calculation. Following Lavalle, Sorella and Parola [28], a magnetic field in the  $z$ -direction is added to stabilize the desired total spin excitation  $S$ :

$$\hat{\mathcal{H}}_{\text{SW}}^h = \hat{\mathcal{H}}_{\text{SW}} - hs \sum_i \hat{S}_i^z. \quad (3.14)$$

Classically, for magnetic fields not large enough to induce a spin-flop transition, the new solution is the  $2\pi/3$  Néel order canted by an angle  $\theta$  along the direction of the field  $h$ . In order to develop a spin-wave calculation, a new rotation around  $y'$ -axis is performed on the spin operators and it can be proven that  $\mathcal{H}_{\text{SW}}^h$  takes the same form of Eq. (3.3) with renormalized coefficients  $A_{\mathbf{k}}$  and  $B_{\mathbf{k}}$ :

$$A_{\mathbf{k}}^h = 1 + \gamma_{\mathbf{k}} \left[ \frac{1}{2} - \frac{3}{2} \left( \frac{2h}{z3J} \right)^2 \right], \quad B_{\mathbf{k}}^h = -\frac{3}{2} \gamma_{\mathbf{k}} \left[ 1 - \left( \frac{2h}{z3J} \right)^2 \right], \quad (3.15)$$

being  $2h/z3J = \sin \theta$ . For  $h \neq 0$  the only singular mode is  $\mathbf{k} = 0$  (associated to the rotation invariance in the  $xy$  plane) and its contribution is given by

$$\mathcal{H}_{SM} = -\frac{3Js}{2} A_{\mathbf{0}}^h + 3J \frac{A_{\mathbf{0}}^h}{N} (S^z - Ns \sin \theta)^2, \quad (3.16)$$

which now favors a value of  $S^z$  consistent with the applied field, at the classical level.

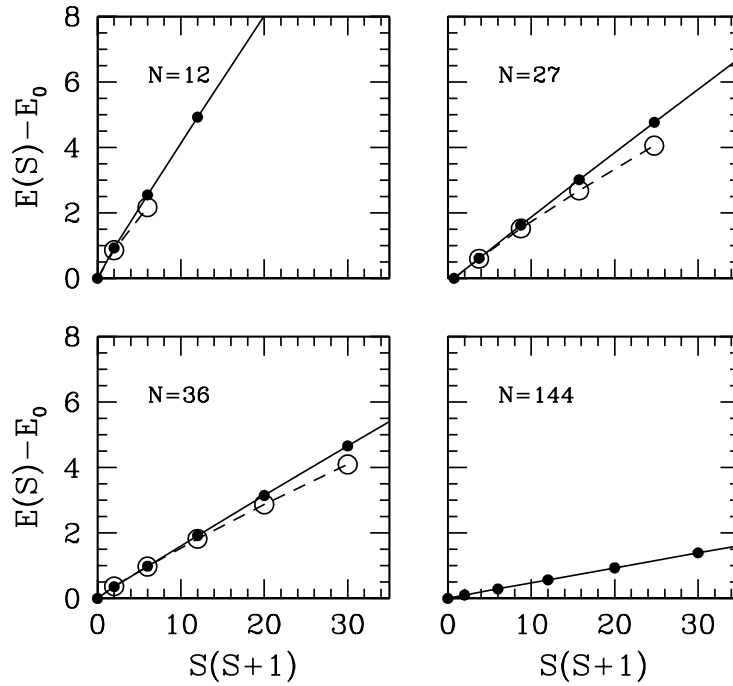


Figure 3.1: Spin-wave (full dots and continuous line) and exact (empty dots and dashed lines) low-energy spectra as a function of  $|\mathbf{S}^2| = S(S+1)$  for  $N = 12, 27, 36, 144$  and  $s = 1/2$ .

The Hellmann-Feynman theorem relates the total spin  $S = N\langle S_i^z \rangle$  of the excitation to the magnetic field  $h$  as it follows:

$$\langle S_i^z \rangle = -\frac{1}{Ns} \frac{\partial}{\partial h} E(h) = s \frac{2h}{z3J} \left[ 1 + \frac{1}{2Ns} \sum_{\mathbf{k} \neq 0} \gamma_{\mathbf{k}} \sqrt{\frac{A_{\mathbf{k}}^h + B_{\mathbf{k}}^h}{A_{\mathbf{k}}^h - B_{\mathbf{k}}^h}} \right] \quad (3.17)$$

where

$$E(h) = E_{cl} - \frac{1}{2} (sh)^2 \frac{2N}{3zJ} - 3Js \frac{N}{2} + \frac{3Js}{2} \sum_{\mathbf{k}} \epsilon_{\mathbf{k}}^h. \quad (3.18)$$

is the spin-wave energy in presence of the field and  $\epsilon_{\mathbf{k}}^h = \sqrt{(A_{\mathbf{k}}^h)^2 - (B_{\mathbf{k}}^h)^2}$ . In particular, the first term in  $(sh)^2$  in Eq. (3.18) gives the classical uniform spin susceptibility (Appendix B)  $\chi_{cl} = 1/9J$ , while taking the whole expression the known spin-wave result [64]  $\chi_{sw}/\chi_{cl} = 1 - 0.449/2s$  is recovered. Finally, as suggested by Lavalle and co-workers [28], given the value  $S$ , the corresponding values of  $h$  and of  $E(h)$  can be found with Eqs. (3.17) and (3.18), and the energy of the spin excitation  $E(S)$  can be calculated, at fixed  $s$ , with a Legendre transformation  $E(S) = E(h) + hsS$  (see Appendix B).

As explained in Sec. 1.3, the occurrence of a symmetry breaking in the ground state

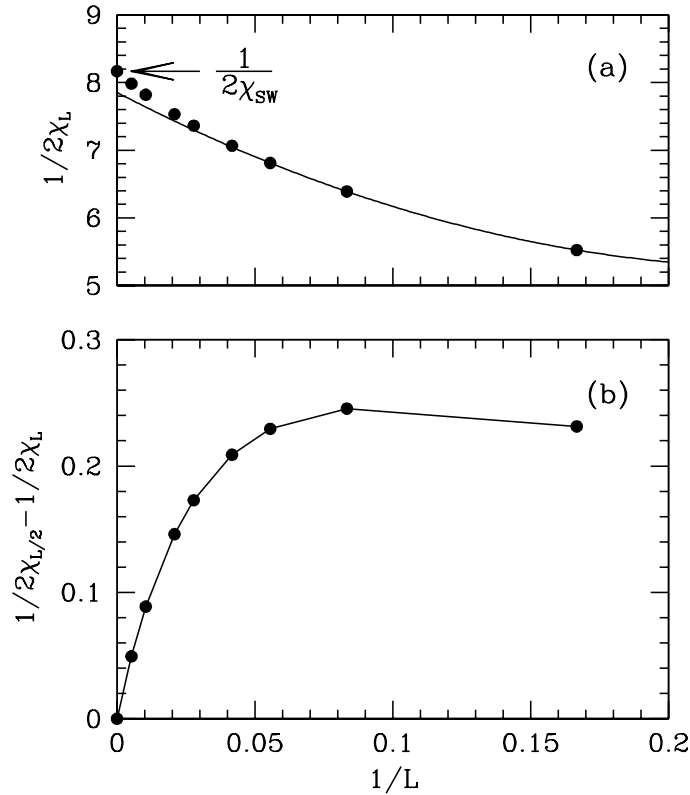


Figure 3.2: Size dependence of  $1/2\chi_L$  (a) and of  $1/2\chi_{L/2} - 1/2\chi_L$  (b) obtained according to Eq. (3.19) using the ( $s = 1/2$ ) spin-wave excitation spectra. The continuous line is a quadratic fit for  $L < 18$  in (a) and a guide for the eye in (b).

for  $N \rightarrow \infty$  can be evidenced from the structure of the finite-size energy spectra. In particular, when long-range order is present in the thermodynamic limit, the low-lying excited states of energy  $E(S)$  and spin  $S$  are predicted to behave as the spectrum of a free quantum rotator (1.28) as long as  $S \ll \sqrt{N}$ . Actually, on the triangular lattice the quantum-top effective Hamiltonian displays a correction due to the anisotropy of the susceptibility tensor [12]. However, in the following we will consider only the leading contribution (1.28) which depends on the perpendicular susceptibility. Fig. 3.1 shows  $E(S)$  vs  $S(S+1)$  calculated within the spin-wave theory compared with the exact diagonalization results of Bernu and co-workers [12]. Remarkably the spin-wave theory turns out to be accurate in reproducing the low-energy spectrum in the whole range of sizes. Furthermore, we can extend our calculation to the thermodynamic limit and observe easily the collapse of a macroscopic number of states with different  $S$  to the ground state as  $N \rightarrow \infty$ . This clearly gives rise to a broken  $SU(2)$  symmetry ground state (Sec. 1.3), as expected within the spin-wave framework.

## 56 The triangular Heisenberg antiferromagnet

In addition, as explained in Sec. 1.3, whenever the quantum top law (1.28) is verified, the quantity

$$[2\chi_S]^{-1} = NE(S) [S(S+1)]^{-1}, \quad (3.19)$$

should approach the physical inverse susceptibility  $1/2\chi_{\text{SW}}$  for infinite size and for any spin excitation  $S \ll N$ . This feature is clearly present in the spin-wave theory and it is shown in Fig. 3.2 (a) where the  $1/2\chi_S$  is plotted for  $S = L \equiv \sqrt{N}$  and approaches the predicted value ( $1/2\chi_{\text{SW}} = 8.167$ ), even if the correct asymptotic scaling  $1/2\chi_L \simeq 1/2\chi_{\text{SW}} + a/L + b/L^2$  turns out to be satisfied only for very large sizes ( $L \geq 36$ ). Such feature is also shared by the Heisenberg antiferromagnet on the square lattice where a similar spin-wave analysis has allowed the authors of Ref. [28] to account for the anomalous finite-size spectrum resulting from an accurate quantum Monte Carlo calculation. Furthermore, similarly to the latter case, a non-monotonic behavior of  $1/2\chi_{L/2} - 1/2\chi_L$  [Fig. 3.2 (b)], which should extrapolate to 0 as  $1/L$  according to the quantum top law, persists also in presence of the frustration within the spin-wave approximation and is likely to be a genuine feature of the Heisenberg model.

### 3.1.3 Spin-wave variational wavefunctions

As explained in Sec. 2.4, in a Green function Monte Carlo (GFMC) calculation it is in general important to start from an accurate variational guess of the ground-state wavefunction. So far, many wavefunctions have been proposed in the literature [32, 55, 56, 59] and the lowest ground-state energy estimation was obtained with the long-range ordered type [32, 56].

The simplest starting point for constructing a long-range ordered wavefunction is of course the classical Néel state. Since on finite-size the ground state is expected to be rotationally invariant, the Néel state should be projected onto the  $\mathfrak{S} = 0$  subspace. However it is in general numerically very difficult to perform the projection onto a total spin subspace so that only the projection onto the subspace with  $S^z = 0$  (a quantum number of the states of the chosen basis) is usually performed. Quantum correction to this classical wavefunction can be introduced by means of a Jastrow factor containing all the two-spin correlations

$$|\psi_G\rangle = \hat{P}_0 \exp\left(\frac{\eta}{2} \sum_{i,j} v(i-j) \hat{S}_i^z \hat{S}_j^z\right) |N\rangle, \quad (3.20)$$

where  $\hat{P}_0$  is the projector onto the  $S^z = 0$  subspace. Starting from the spin-wave ground state (3.11) it is possible to derive [71] a simple variational wavefunction which is both

accurate and easily computable also when used for importance sampling (Sec. 2.4). Such wavefunction is defined for any  $s$  in the correct Hilbert space of the spin operators and reduces for  $s \rightarrow \infty$  to the spin wave form (3.11).

To this purpose let us consider the following variational wavefunction

$$|\tilde{\psi}_G\rangle = \hat{P}_0 \exp \left[ \frac{1}{s} \sum_{\mathbf{k} \neq 0} g_{\mathbf{k}} \hat{S}_{\mathbf{k}}^z \hat{S}_{-\mathbf{k}}^z \right] |F\rangle, \quad (3.21)$$

where  $\hat{S}_{\mathbf{k}}^z = N^{-1/2} \sum_j e^{-i\mathbf{k}\cdot\mathbf{r}_j} \hat{S}_j^z$ . The spin-wave  $s \rightarrow \infty$  limit of the wavefunction (3.21) can be easily carried out by means of a Hubbard-Stratonovich transformation [71] and leads to (neglecting an unessential normalization)

$$|\tilde{\psi}_G\rangle = \hat{P}_0 \exp \left[ -\frac{1}{2} \sum_{\mathbf{k} \neq 0} \frac{g_{\mathbf{k}}}{1 - g_{\mathbf{k}}} \hat{a}_{\mathbf{k}}^\dagger \hat{a}_{-\mathbf{k}}^\dagger \right] |F\rangle. \quad (3.22)$$

By requiring that  $|\psi_G\rangle$  reduces to the spin-wave wavefunction (3.11) for  $s \rightarrow \infty$  one obtains for  $g_{\mathbf{k}}$

$$g_{\mathbf{k}} = \frac{v_{\mathbf{k}}}{v_{\mathbf{k}} - u_{\mathbf{k}}} = 1 - \sqrt{\frac{1 + 2\gamma_{\mathbf{k}}}{1 - \gamma_{\mathbf{k}}}} \quad (3.23)$$

which is singular only for  $\mathbf{k} = 0$ . This analysis, for the more general XXZ Hamiltonian with an exchange easy-plane anisotropy  $\alpha$  [72], gives

$$g_{\mathbf{k}} = 1 - \sqrt{\frac{1 + 2\alpha\gamma_{\mathbf{k}}}{1 - \gamma_{\mathbf{k}}}}. \quad (3.24)$$

In the original (unrotated) reference frame, the Néel state  $|N\rangle$  can be written in terms of  $|F\rangle = \prod_i |S_i^x = s\rangle$  by applying the inverse of the unitary transformation (1.9)

$$|N\rangle = \hat{\mathcal{U}}|F\rangle = \sum_x \mathcal{U}(x)|x\rangle = \sum_x \exp \left[ +\frac{2\pi i}{3} \left( \sum_{i \in B} S_i^z - \sum_{i \in C} S_i^z \right) \right] |x\rangle, \quad (3.25)$$

where  $|x\rangle$  is an Ising spin configuration specified by assigning the value of  $\mathcal{S}$  (or equivalently of  $S_i^z$ ) for each site, and  $\mathcal{U}(x) = \langle x|\hat{\mathcal{U}}|x\rangle$ . Then, introducing a variational parameter  $\eta$  scaling the latter potential, for  $s = 1/2$  and in the original spin representation,  $|\psi_G\rangle$  assumes the very simple form of Eq. (3.20), i.e.,

$$|\psi_G\rangle = \hat{\mathcal{U}}|\tilde{\psi}_G\rangle = \sum_x \mathcal{U}(x) \exp \left[ \frac{\eta}{2} \sum_{i,j} v(i-j) S_i^z S_j^z \right] |x\rangle, \quad (3.26)$$

where  $v(r) = 1/N \sum_{\mathbf{q} \neq 0} e^{-i\mathbf{q}\cdot\mathbf{r}} g_{\mathbf{q}}$  and the summation is restricted only to the Ising configurations with  $\sum_i S_i^z = 0$  to enforce the projection onto the  $S^z = 0$  subspace. In contrast to the linear spin-wave ground state (3.11), which does not satisfy the constraint  $\langle \hat{a}_i^\dagger \hat{a}_i \rangle \leq 2s$ , the present variational wavefunction is defined in the correct Hilbert space of the spin operators.

## 3.2 Quantum Monte Carlo calculation

### 3.2.1 From Marshall-Peierls to Huse-Elser sign rule

According to the Marshall theorem (see Sec. 1.1), for the Heisenberg antiferromagnet on the square lattice, as well as on any other bipartite lattice, the classical part of the wavefunction by itself determines exactly the phases of the ground state in the chosen basis. For the triangular case, instead, the exact phases are unknown and the classical part is not enough to fix them correctly. In particular, starting from a long-range ordered wavefunction of the form (3.20), Huse and Elser [56] introduced important three-spin correlation factors in the wavefunction

$$\hat{T} = \exp \left( i \beta \sum_{\langle i,j,k \rangle} \gamma_{ijk} \hat{S}_i^z \hat{S}_j^z \hat{S}_k^z \right), \quad (3.27)$$

defined by the coefficients  $\gamma_{ijk} = 0, \pm 1$ , appropriately chosen so as to preserve the symmetries of the classical Néel state, and by an overall factor  $\beta$ . In particular the sum in Eq. (3.27) runs over all distinct triplets of sites  $i, j, k$  where both  $i$  and  $k$  are nearest neighbors of  $j$ , and  $i$  and  $k$  are next-nearest neighbors to one another. The sign factor  $\gamma_{ijk} = \gamma_{kji} = \pm 1$  is invariant under rigid translations and rotations in real space by an angle of  $2\pi/3$  of the three-spin cluster  $i, j, k$ , but changes sign under rotations by  $\pi/3$  or  $\pi$ . The resulting wavefunction reads therefore:

$$|\psi_G\rangle = \sum_x \Omega(x) \exp \left( \frac{\gamma}{2} \sum_{i,j} v(i-j) S_i^z S_j^z \right) |x\rangle, \quad (3.28)$$

with a phase factor given by

$$\Omega(x) = T(x) \exp \left[ + \frac{2\pi i}{3} \left( \sum_{i \in B} S_i^z - \sum_{i \in C} S_i^z \right) \right] \quad (3.29)$$

where  $T(x) = \langle x | \hat{T} | x \rangle$ . Finally, since the Hamiltonian is real, a better variational wavefunction on a finite size is obtained by taking the real part of Eq. (3.28).

Although the three-body correlations of Eq. (3.27) do not provide the exact answer, they allow us to adjust the signs of the wavefunction in a nontrivial way without changing the underlying classical Néel order. In this respect it is useful to define an average sign of the variational wavefunction relative to the normalized exact ground state  $|\psi_0\rangle$  as

$$\langle s \rangle = \sum_x |\psi_0(x)|^2 \text{sgn}[\psi_G(x)\psi_0(x)], \quad (3.30)$$

with  $\psi(x) = \langle x | \psi \rangle$ . We have compared the variational calculation with the exact ground state obtained by ED on the  $N = 36$  cluster. For completeness we have considered the

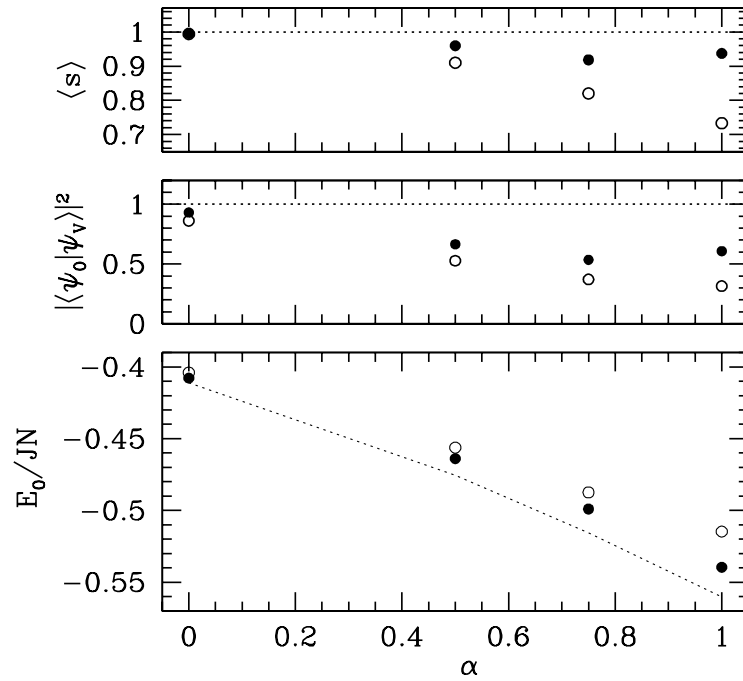


Figure 3.3: Average sign, overlap square and ground-state energy per site obtained for  $N = 36$  using the variational wavefunction of Eq. (3.28), with (full dots) and without (empty dots) the triplet term of Eq. (3.27), as a function of the easy-plane anisotropy  $\alpha$ . The calculations were performed by summing exactly over all the configurations and the dotted line connects the exact results.

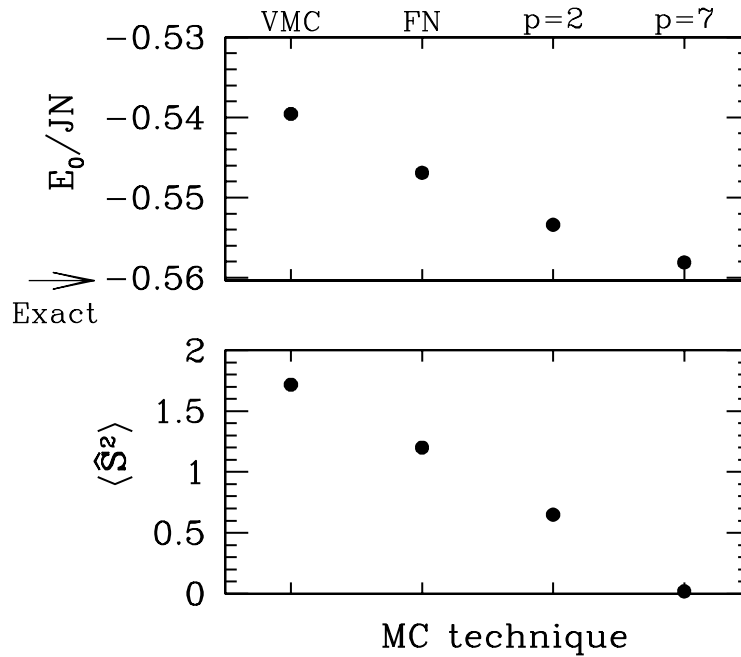


Figure 3.4: Variational estimate (VMC) and mixed averages (FN, GFMCSR) of the ground-state energy per site  $E_0/JN$  and of the total spin square  $\langle \hat{S}^2 \rangle$  for  $N = 36$ . GFMCSR data are obtained using the short-range correlation functions generated by  $\hat{\mathcal{H}}$  ( $p = 2$ ), and  $\hat{\mathcal{H}}^2$  ( $p = 7$ ) as explained in the text.

more general XXZ Hamiltonian with the exchange easy-plane anisotropy  $\alpha$ , ranging from the XY case ( $\alpha = 0$ ) to the standard spin-isotropic case ( $\alpha = 1$ ). As shown in Fig. 3.3, the introduction of the three-body correlations of Eq. (3.27), although not providing the exact answer, improves the overlap square of the variational wavefunction on the true ground state and the accuracy of the variational estimate of the ground-state energy as well. In particular the average sign  $\langle s \rangle$  is very much improved by the triplet term, particularly in the spin-isotropic limit  $\alpha \rightarrow 1$ . This is crucial when the variational wavefunction is used for importance sampling within the modifications of the GFMC technique developed to handle the sign problem instability (Sec. 2.4). In the following the wavefunction (3.28) will be used as the guiding wavefunction in our quantum Monte Carlo calculations.

### 3.2.2 The reconfiguration scheme

In order to study the ground-state properties we have used the GFMCSR quantum Monte Carlo technique, which allows one to release the fixed-node (FN) approximation (see

Sec. 2.4), in a controlled but approximate way. This systematic improvement introduced by the GFMCSR on the accuracy of the ground-state properties, is illustrated in Fig. 3.4, where we display a comparison between the estimates of the ground-state energy per site and of total spin square, for the  $N = 36$ , obtained with the stochastic sampling of the variational wavefunction (3.28), the FN and the GFMCSR techniques. As explained in Sec. 2.5, in the appropriate limit of large number of walkers and high frequency of stochastic reconfiguration (SR), the residual bias introduced by the GFMCSR depends only on the number  $p$  of operators used to constrain the GFMC Markov process, allowing simulations without numerical instabilities. In principle the exact answer can be obtained, within statistical errors, provided  $p$  equals the huge Hilbert space dimension. In practice it is necessary to work with small  $p$  and an accurate selection of physically relevant operators is therefore crucial. As can be easily expected, the short-range correlation functions  $\hat{S}_i^z \hat{S}_j^z$  and  $(\hat{S}_i^+ \hat{S}_j^- + \hat{S}_i^- \hat{S}_j^+)$  contained in the Hamiltonian ( $p = 2$ ) give a sizable improvement of the FN ground-state energy when they are included in the SR procedure. In order to be systematic, we have included in the SR also the short-range correlations generated by  $\hat{\mathcal{H}}^2$  ( $p = 7$ ), averaged over all spatial symmetries commuting with the Hamiltonian. These local correlations (see Fig. 3.5) are particularly important to obtain quite accurate and reliable estimates not only of the ground-state energy but also of the mixed average [Eq. (2.42)] of the total spin square  $\hat{S}^2$ . In particular it is interesting that, starting from a variational wavefunction with no definite spin, the spin rotational invariance of the finite-size ground state is systematically recovered by means of the GFMCSR technique (see lower panel of Fig. 3.4).

Having obtained an estimate for the ground-state energy, at least an order of magnitude more accurate than our best variational guess, it appears possible to obtain physical features, such as a gap in the spin spectrum, that are not present at the variational level. For instance in the frustrated  $J_1 - J_2$  Heisenberg model (see Chap. 4), with the same technique and a similar accuracy, a gap in the spin spectrum is found in the thermodynamic limit, starting with a similar ordered and therefore gapless variational wavefunction.

### 3.2.3 Ground-state energy and spin gap

In presence of Néel long-range order, being the magnon dispersion relation linear in the wavevector  $\mathbf{k}$ , the leading finite-size correction to the ground-state energy per site is  $\mathcal{O}(N^{-3/2})$  [12]: this is clearly shown by the behavior of the finite-size spin-wave results in Fig. 3.6. In the same figure the size scaling of the estimates of the ground-state energy per site obtained with the VMC, the FN and the GFMCSR ( $p = 7$ ) tech-

## 62 The triangular Heisenberg antiferromagnet

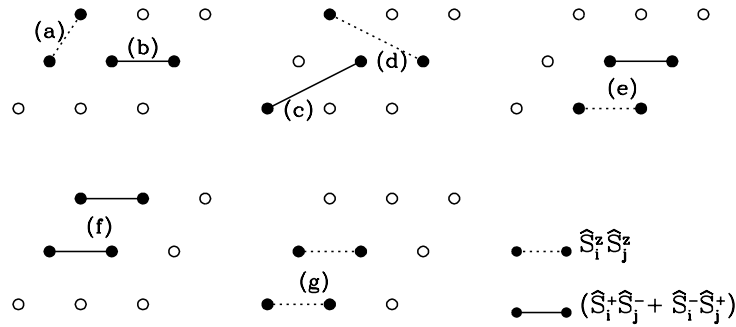


Figure 3.5: Short range spin correlation functions generated by  $\hat{\mathcal{H}}$  (a,b) and  $\hat{\mathcal{H}}^2$  (c-g).

niques is also reported. The predicted size scaling, fulfilled of course by the variational wavefunction (3.28), is also preserved within the FN and the more accurate GFMCSR technique, thus providing a first clue on the existence of long-range Néel order in the thermodynamic ground state of the model. The quality of our results is similar to the variational one obtained by Sindzingre and co-workers [32], using a long-range ordered RVB wavefunction (Sec. 1.4). The latter approach is almost exact for small lattices, but the sign problem is already present at the variational level, and the calculation has not been extended to high statistical accuracy or to  $N > 48$ . Our best estimate is that in the thermodynamic limit the ground-state energy per site is  $e_0 = -0.5458 \pm 0.0001$  in unit of the exchange coupling.

In the isotropic triangular antiferromagnet, the gap to the first spin excitation is rather small. Furthermore, for the particular choice of the guiding wavefunction (3.28), the translational symmetry of the Hamiltonian is preserved only if projected onto subspaces with total  $S^z$  multiple of three. Then, we have studied the gap to the spin  $S = 3$  excitation as a function of the system size. Technically, within our numerical framework, such a spin gap can be evaluated by performing two simulations in the  $S^z = 0$  and  $S^z = 3$  subspaces. This can be easily done by restricting the sampling to the configurations  $|x\rangle$  in Eq. (3.28) with the desired value of  $S^z$ . In this case the potential  $v(r)$  used was the same in both subspaces and the variational parameter  $\eta$  was found by optimizing the energy in the  $S^z = 0$  subspace.

As it is shown in Fig. 3.7, for the lattice sizes for which a comparison with ED data is possible, the spin gap estimated with the GFMCSR technique is nearly exact. The importance of extending the numerical investigation to clusters large enough to allow a more reliable extrapolation is particularly evident in the same figure, in which the  $N = 12$  and  $36$  exact data extrapolate linearly to a large finite value. This behavior, is certainly a finite-size effect and it is corrected by the GFMCSR data for  $N \geq 48$ ,

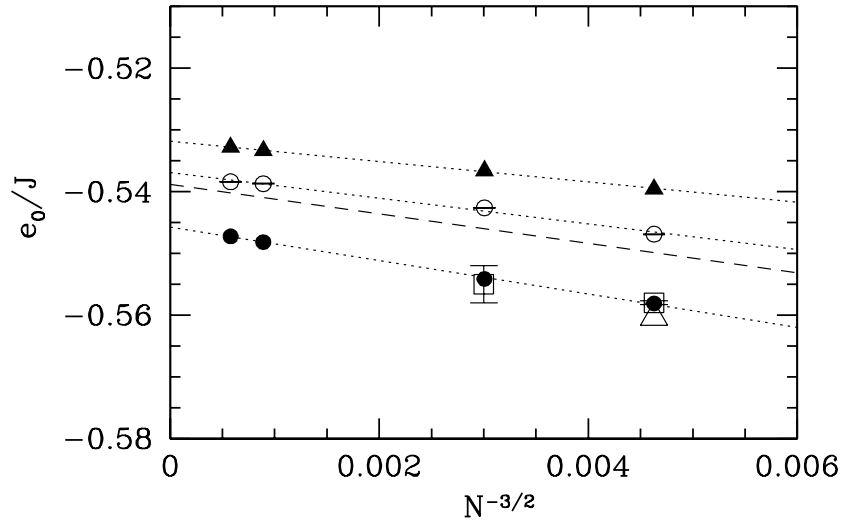


Figure 3.6: Ground-state energy per site  $e_0 = E_0/N$ , in unit of  $J$ , as a function of the system size, obtained with VMC (full triangles), FN (empty dots) and GFMCSR with  $p = 7$  (full dots) techniques. Spin-wave size scaling is assumed and short-dashed lines are linear fits against  $1/N^{3/2}$ . The long-dashed line is the linear spin-wave prediction (Sec. 3.1), the empty triangle is the  $N = 36$  ED result and the empty squares are data taken from Ref. [32].

suggesting, strongly, a gapless excitation spectrum  $[(E_3 - E_0)/J = 0.002 \pm 0.01]$ .

### 3.2.4 Staggered magnetization

As seen in Sec. 2.4, the GFMC allows us to obtain a very high statistical accuracy on the ground-state energy, but does not allow us to compute directly ground-state expectation values  $\langle \psi_0 | \hat{O} | \psi_0 \rangle$ . A straightforward way to calculate such expectation values is to use the Hellmann-Feynman theorem. In fact, if the Hamiltonian is perturbed with a term  $-\lambda \hat{O}$  the first order correction to the ground-state energy is, by standard perturbation theory,

$$E(\lambda) = E_0 - \lambda \langle \psi_0 | \hat{O} | \psi_0 \rangle. \quad (3.31)$$

As a consequence it is possible to evaluate the ground-state expectation value  $\langle \psi_0 | \hat{O} | \psi_0 \rangle = -dE(\lambda)/d\lambda|_{\lambda=0}$  estimating the limit

$$\langle \psi_0 | \hat{O} | \psi_0 \rangle = -\lim_{\lambda \rightarrow 0} \frac{E(\lambda) - E_0}{\lambda} \quad (3.32)$$

with few computations at different *small*  $\lambda$ 's.

A further complication for nonexact calculations like the FN or GFMCSR, is that if the off-diagonal matrix elements  $O_{x',x}$  of the operator  $\hat{O}$  (in the chosen basis) have signs

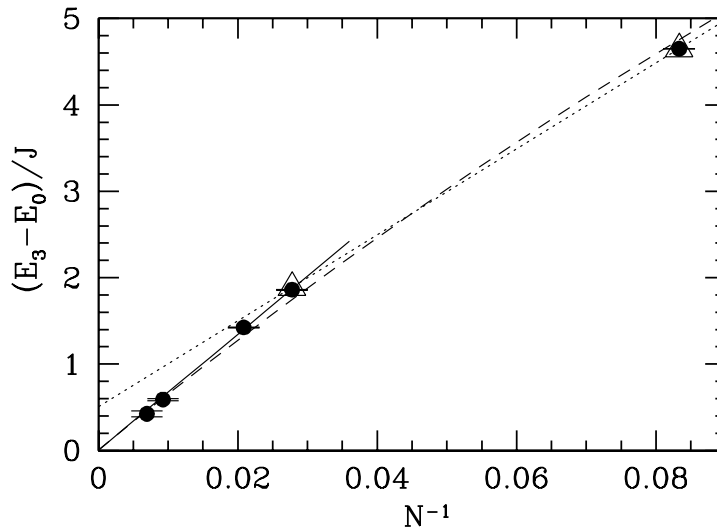


Figure 3.7: Size scaling of the spin gap to the  $S = 3$  excitation obtained with the GFMCSR ( $p = 7$ ) technique (full dots). Empty triangles are the ED results, the long-dashed line is the linear spin-wave prediction (Sec. 3.1), the dotted line is the linear extrapolation of the  $N = 12, 36$  exact results and the solid line is the least-squares fit of the GFMCSR data for  $N \geq 36$ .

which are opposite to those of the product  $\psi_G(x')\psi_G(x)$  (so that the importance-sampled matrix elements  $\bar{O}_{x',x}$  are not all negative), they cannot be handled exactly within the FN because the addition of such a perturbation to the Hamiltonian changes the nodal surface of the guiding wavefunction (see Sec. 2.4). In that case, in fact, the effective FN Hamiltonian associated to the unperturbed Hamiltonian is also affected by the presence of the field and this leads naturally to the breakdown of Eq. (3.31). A way out of this difficulty is to split the operator  $\hat{O}$  into three contributions:  $\hat{O} = \hat{D} + \hat{O}^+ + \hat{O}^-$ , where  $\hat{O}^+$  ( $\hat{O}^-$ ) is the operator with the same off-diagonal matrix elements of  $\hat{O}$  when they have the same (opposite) signs of  $\psi_G(x')\psi_G(x)$ , and zero otherwise, whereas  $\hat{D}$  is the diagonal part of  $\hat{O}$ . Then, we can add to the Hamiltonian a contribution that does not change the nodes:  $\hat{\mathcal{H}}(\lambda) = \hat{\mathcal{H}} - \lambda(\hat{D} + 2\hat{O}^+)$  for  $\lambda > 0$  and  $\hat{\mathcal{H}}(\lambda) = \hat{\mathcal{H}} - \lambda(\hat{D} + 2\hat{O}^-)$  for  $\lambda < 0$ . Then the expectation value of the operator  $\hat{O}$  can be written as

$$\langle \psi_0 | \hat{O} | \psi_0 \rangle = \lim_{\lambda \rightarrow 0} \frac{E(-\lambda) - E(\lambda)}{2\lambda}. \quad (3.33)$$

With this method, using the FN and GFMCSR techniques, we have calculated the order parameter

$$m^{\dagger 2} = 36 \frac{\mathcal{M}^2}{N(N+6)}, \quad (3.34)$$

where  $\mathcal{M}^2$  is the sublattice magnetization squared [12]. Our results are plotted in Fig. 3.8. For the order parameter the inclusion of many short-range correlations in the

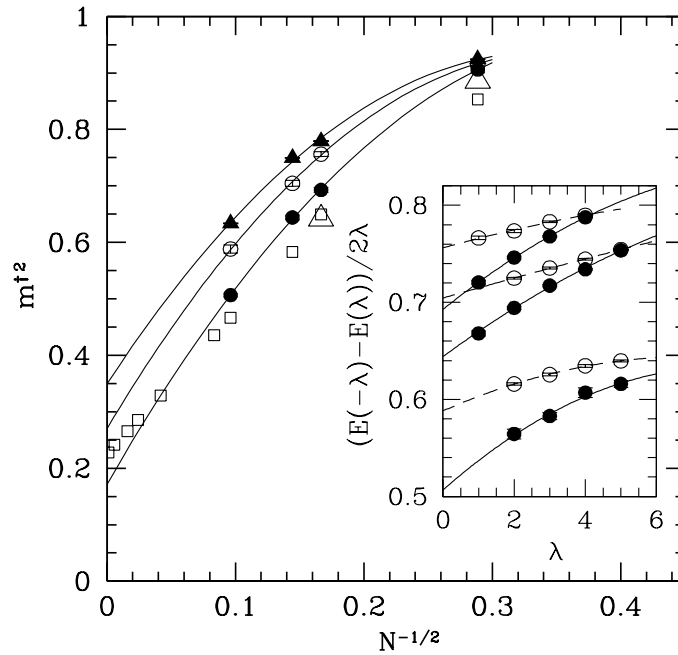


Figure 3.8: Size scaling of the order parameter: VMC (full triangles), FN (empty dots), GFMCSR (full dots), exact data (empty triangles) and finite-size linear spin wave theory [70] (empty squares). The inset displays the  $\lambda \rightarrow 0$  extrapolation for  $N > 12$ . Lines are quadratic fits in all the plots.

SR is not very important. Then, in order to minimize the numerical effort, we have chosen to put in the SR conditions the first four correlation functions shown in Fig. 3.6, the order parameter itself and  $\hat{S}^2$ . While the FN data extrapolate to a value not much lower than the variational result, the GFMCSR calculation provides a much more reliable estimate of the order parameter with no apparent loss of accuracy with increasing sizes. In this way we obtain for  $\hat{m}^\dagger$  a value well below the linear and the second order (which has actually a *positive* correction [63]) spin-wave predictions. Our best estimate is that in the thermodynamic limit the order parameter  $m^\dagger = 0.41 \pm 0.02$  is reduced by about 59% from its classical value. This is partially in agreement with the conclusions of the finite-temperature calculations [58] suggesting a ground state with a small but nonzero long-range antiferromagnetic order and with series expansions [57] indicating the triangular antiferromagnet to be likely ordered but close to a critical point. In our simulation, however, which to our knowledge represents a first attempt to perform a systematic size-scaling analysis of the order parameter, the value of  $\hat{m}^\dagger$  remains sizable and finite, consistent with a gapless spectrum.

### 3.3 Conclusions

We have presented analytical and numerical results on the ground-state properties of the spin-1/2 Heisenberg antiferromagnet on the triangular lattice. The accuracy of the finite-size spin-wave results indicates that the spin-wave theory is a reliable analytical approximation to describe the ground-state properties of the present model. In particular, the effectiveness of the spin-wave theory in reproducing on finite sizes the low-energy part of the excitation spectrum provides support to the existence of long-range Néel order in the ground state, suggesting also that the value of the spin susceptibility should be very close to the spin-wave prediction. On the other hand, our quantum Monte Carlo numerical simulations provide robust evidences for a gapless spectrum and a sizable value of the order parameter in the thermodynamic limit, in remarkable *quantitative* agreement with the spin-wave results. In addition, our numerical simulations have also allowed us to identify the ground-state correlations that are important at short distances. Both the VMC and the SR approach show the crucial role of ground-state correlations defined on the smallest four spin clusters: in the variational calculation they are important to determine the correct relative phases of the ground-state wavefunction whereas in the latter more accurate approach this correlations allow one to obtain very accurate results for the energy and the spin gap and to restore the spin rotational invariance of the finite-size ground state.

In conclusion all our results, point toward the existence of long-range Néel order in the thermodynamic ground state of the spin-1/2 Heisenberg antiferromagnet on the triangular lattice. Our best estimate for the antiferromagnetic order parameter in the thermodynamic limit  $m^\dagger = 0.41 \pm 0.02$  is reduced by about 59% from its classical value. This prediction could be also verified experimentally on the K/Si(111):B interface [6] which has turned out recently to be the first realization of a really two-dimensional triangular antiferromagnet [6].

# Chapter 4

## The $J_1 - J_2$ Heisenberg model

In Chap. 3 we have studied the ground-state properties of a frustrated spin system, the triangular Heisenberg antiferromagnet, in which frustration is induced by the geometry of the lattice. The other possible origin of the frustration comes from competing interactions as in the so-called  $J_1 - J_2$  Heisenberg model on the square lattice defined in Eq. (2) of the Introduction.

In the last few years several studies – including exact diagonalizations of small clusters [23, 73], spin-wave [10, 74, 75] and Schwinger-boson [76] calculations, series [77, 78, 79] and large- $N$  [80] expansions – have provided some evidence for the absence of Néel order in the ground state of the spin-1/2  $J_1 - J_2$  Heisenberg model for  $0.38 \lesssim J_2/J_1 \lesssim 0.6$ . However, a systematic size-scaling of the spin gap is still lacking and no definite conclusion on the nature of the non-magnetic phase has been drawn yet. In particular, an open question is whether the ground state in the quantum disordered phase is a resonating valence bond (RVB) spin liquid with no broken symmetry [81], or if it breaks some *crystal* symmetries by dimerizing in some special pattern (Sec. 1.4).

In this chapter, we will address the problem of the quantum phase-transition to a non-magnetic ground state driven by frustration in the spin-1/2  $J_1 - J_2$  Heisenberg model by means of the finite-size spin-wave theory, exact diagonalization (ED) and Green function Monte Carlo (GFMC) techniques. We will demonstrate the reliability of the spin-wave theory as an analytical tool to describe the Néel ordered phase and we will provide robust evidence indicating the so-called *plaquette* RVB – a dimerized state with spontaneously broken translation symmetry but no broken rotation symmetry – as the most plausible ground state in the quantum disordered regime.

## 4.1 Finite-size spin-wave results

The finite-size spin-wave theory for the spin- $s$   $J_1-J_2$  Heisenberg model can be derived along the same lines followed for the triangular Heisenberg antiferromagnet in Sec. 3.1. In this section we will only show the main results for  $J_2/J_1 < 0.5$ , assuming the two sublattice classical Néel order [Fig. 2 (a)] in the  $xy$ -plane.

Applying the unitary transformation (1.4) which rotates the spin quantization axis by a angle  $\pi$  about the  $z$ -axis on one of the two sublattices, setting the order parameter along the  $x$ -axis, and using the Holstein-Primakoff transformation for spin operators at the leading order in  $1/s$  (Sec. 3.1), the Fourier transformed spin-wave Hamiltonian results as in Eq. (3.3) with  $E_{cl} = -zJs^2N(1-\beta)/2$ ,  $z = 4$ ,  $\beta = J_2/J_1$ ,

$$A_{\mathbf{k}} = 1 + \beta(\delta_{\mathbf{k}} - 1), \quad B_{\mathbf{k}} = -\gamma_{\mathbf{k}}, \quad (4.1)$$

$\gamma_{\mathbf{k}} = (\cos k_x + \cos k_y)/2$ , and  $\delta_{\mathbf{k}} = \cos k_x \cos k_y$ .

Similarly to the triangular lattice case, the singular Goldstone modes [ $\mathbf{k} = \mathbf{0}$  and  $\mathbf{k} = (\pi, \pi)$ ] cannot be diagonalized by means of the Bogoliubov transformation but can be recombined to give the total spin squared  $\hat{\mathbf{S}}^2$  at the leading order in  $1/s$ :

$$\hat{\mathcal{H}}_{SM} = -J_1szA_0 + J_1z\frac{A_0}{N} [(S^x)^2 + (S^y)^2 + (S^z)^2]. \quad (4.2)$$

As seen in Sec. 3.1 this term, being  $A_0$  positive definite, favors a singlet ground state and implies the Lieb-Mattis property, which has been demonstrated only for bipartite Hamiltonians, but nonetheless can be verified numerically on finite sizes for the  $J_1-J_2$  Heisenberg model (see Sec. 1.1).

As in the triangular case, the above analysis allows one to derive a variational wavefunction which is both accurate and easily computable in a quantum Monte Carlo algorithm. Here we will not repeat the derivation, which follows very closely the one for the triangular antiferromagnet, and leads to the following result for  $s = 1/2$ :

$$|\psi_G\rangle = \sum_x S_M(x) \exp \left[ \frac{\eta}{2} \sum_{i,j} v(i-j) S_i^z S_j^z \right] |x\rangle, \quad (4.3)$$

where  $v(r) = 1/N \sum_{\mathbf{q} \neq 0} e^{-i\mathbf{k}\cdot\mathbf{r}} g_{\mathbf{k}}$  with

$$g_{\mathbf{k}} = \frac{v_{\mathbf{k}}}{v_{\mathbf{k}} - u_{\mathbf{k}}} = 1 - \sqrt{\frac{1 - \beta(1 - \delta_{\mathbf{k}}) + \gamma_{\mathbf{k}}}{1 - \beta(1 - \delta_{\mathbf{k}}) - \gamma_{\mathbf{k}}}}; \quad (4.4)$$

$|x\rangle$  is an Ising spin configuration specified by assigning the value of  $\mathcal{S}$  for each site and  $S_M(x) = (-1)^{N_{\uparrow}(x)}$  represents the so-called *Marshall sign* (Sec. 1.1.1), depending on

$J_2/J_1$	VMC	VMCLS	SRLS	Exact
0.0	-0.6695 (1.4%)	-0.6756 (0.5%)	-0.6789 (0.00%)	-0.67887
0.1	-0.6287 (1.5%)	-0.6352 (0.5%)	-0.6379 (0.03%)	-0.63810
0.2	-0.5898 (1.5%)	-0.5963 (0.5%)	-0.5988 (0.04%)	-0.59905
0.3	-0.5526 (1.8%)	-0.5599 (0.5%)	-0.5619 (0.10%)	-0.56246
0.4	-0.5112 (3.5%)	-0.5260 (0.7%)	-0.5289 (0.16%)	-0.52974
0.5	-0.4798 (4.8%)	-0.4957 (1.6%)	-0.5022 (0.32%)	-0.50381

Table 4.1: Estimates of the ground-state energy per site and their relative accuracy (in brackets) for  $N = 36$  and various values of the  $J_2/J_1$  ratio. VMC: variational Monte Carlo. VMCLS: variational Monte Carlo with LS wavefunction. SRLS: GFMCSR with LS wavefunction and  $p = 8$  (see text).

the number  $N_\uparrow(x)$  of spin up on one of the two sublattices. The summation is restricted only to the Ising configurations with  $\sum_i S_i^z = 0$  in order to enforce the projection onto the  $S^z = 0$  subspace. In the following we will use the latter variational wavefunction as the starting point for more refined quantum Monte Carlo calculations. In particular for  $J_2/J_1 = 0.5$  we have chosen to work with  $\beta = 0.4$  in Eq. (4.4). The possibility to restrict to any total spin projection  $S^z = \sum_i S_i^z$  allows one to evaluate the spin gap by performing two simulations for  $S^z = 0$  and  $S^z = 1$ . As in the triangular case, the potential  $v(r)$  used was the same in both subspaces and the variational parameter  $\eta$  was found by optimizing the energy in the  $S^z = 0$  subspace. The latter spin-wave variational wavefunction (see Tab. 4.1) provides a rather good estimate of the ground-state energy for  $J_2/J_1 \leq 0.3$ . Instead such accuracy abruptly decreases instead in the regime of strong frustration, suggesting a change in the nature of the ground state.

Within the finite-size spin-wave theory, we can also gain information about the low-lying excited states. As shown in Sec. 3.1.2, in order to stabilize a low-energy total spin excitation  $S$  a magnetic field  $h$  in the  $z$ -direction must be added to the spin Hamiltonian. Keeping into account that, for small fields, the classical minimum energy configuration is the Néel order canted by an angle  $\theta$  along the direction of  $h$  (with  $\sin \theta = h/2J_1z$ ), the finite-size spin-wave expansion is straightforward and leads to a linearized Hamiltonian as in Eq. (3.3) with the following field-dependent coefficients

$$A_{\mathbf{k}}^h = 1 + \beta(\delta_{\mathbf{k}} - 1) + \gamma_{\mathbf{k}} \left( \frac{h}{2J_1z} \right)^2, \quad B_{\mathbf{k}}^h = -\gamma_{\mathbf{k}} \left[ 1 - \left( \frac{h}{2J_1z} \right)^2 \right], \quad (4.5)$$

and with a singular part given by

$$\mathcal{H}_{SM} = -\frac{J_1sz}{2} A_{\mathbf{0}}^h + \frac{J_1z}{N} (S^z - Ns \sin \theta)^2, \quad (4.6)$$

## 70 The $J_1$ - $J_2$ Heisenberg model

favoring a value of  $S^z$  (in the original spin representation) consistent with the applied field, at the classical level.

The total spin  $S = N\langle S_i^z \rangle$  of the excitation can be related to the magnetic field  $h$  by means of the Hellmann-Feynman theorem

$$\langle S_i^z \rangle = -\frac{1}{Ns} \frac{\partial}{\partial h} E(h) = s \frac{h}{2J_1 z} \left[ 1 + \frac{1}{2Ns} \sum_{\mathbf{k} \neq 0} \gamma_{\mathbf{k}} \sqrt{\frac{A_{\mathbf{k}}^h + B_{\mathbf{k}}^h}{A_{\mathbf{k}}^h - B_{\mathbf{k}}^h}} \right] \quad (4.7)$$

where

$$E(h) = E_{cl} - (sh)^2 \frac{N}{4J_1 z} - \frac{J_1 s z}{2} \left[ N(1 - \beta) - \sum_{\mathbf{k}} \epsilon_{\mathbf{k}}^h \right] \quad (4.8)$$

and  $\epsilon_{\mathbf{k}}^h = \sqrt{(A_{\mathbf{k}}^h)^2 - (B_{\mathbf{k}}^h)^2}$ . The final step in order to evaluate the energy spectrum  $E(S)$  is to perform a Legendre transformation  $E(S) = E(h) + hS$  (see Appendix B).

Finally, the spin-wave uniform susceptibility (Sec. 1.3),

$$\chi_{sw} = -1/N \partial^2 E(h) / \partial h^2 |_{h=0},$$

is, at the leading order in  $1/s$ ,

$$\chi_{sw} / \chi_{cl} = 1 + \frac{1}{2Ns} \sum_{\mathbf{k} \neq 0} \gamma_{\mathbf{k}} \sqrt{\frac{A_{\mathbf{k}} + B_{\mathbf{k}}}{A_{\mathbf{k}} - B_{\mathbf{k}}}}. \quad (4.9)$$

where  $\chi_{cl} = 1/2J_1 z$ .

## 4.2 Transition to a quantum disordered state induced by frustration

### 4.2.1 Spin-wave susceptibilities and low-energy spectra

For the unfrustrated Heisenberg model, even for  $s = 1/2$ , the spin-wave predictions are very accurate as far as the energy, the order parameter and the spin uniform susceptibility are concerned [10, 28]. Turning on  $J_2$  the model is increasingly frustrated and one can expect the spin-wave theory to remain accurate only in the region where the nature of the order parameter is the same as in the classical case ( $S \rightarrow \infty$ ). Within this analytical approach we can therefore detect a non-magnetic phase by looking for the breakdown of the spin-wave expansion.

As pointed out by Zhong and Sorella [10], for moderate frustration ( $J_2/J_1 < 0.2$ ) the linear spin-wave predictions on finite sizes are quite accurate for both the energy

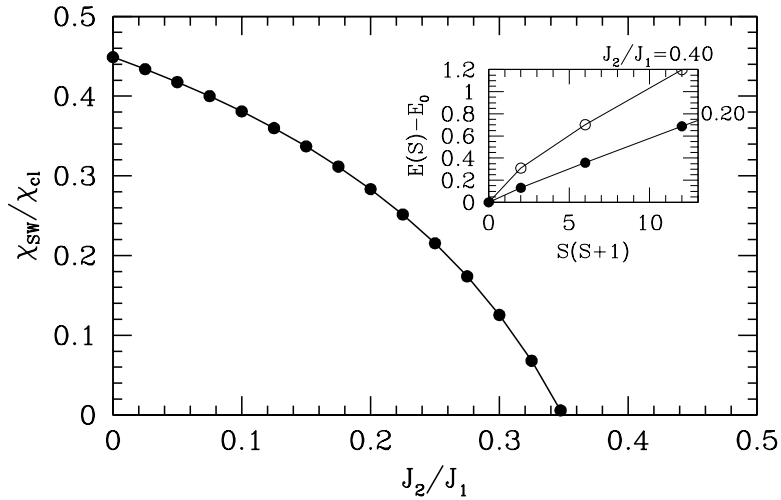


Figure 4.1: Spin-wave uniform susceptibility as a function of  $J_2/J_1$  for  $s = 1/2$ . The inset displays the low-energy spin-wave spectrum for  $N = 144$  for two values of the  $J_2/J_1$  ratio as a function of  $|\mathbf{S}|^2 = S(S + 1)$ .

and the antiferromagnetic order parameter. Moreover, in this regime, the second order correction [10] leads to an almost exact result. For large  $J_2/J_1$ , instead, the second order term does not improve the first order estimate and a possible breakdown of the spin-wave expansion may occur even well below the classical transition point  $J_2/J_1 = 0.5$ . In particular at the leading order in  $1/s$ , and for  $s = 1/2$  the order parameter vanishes at a critical value  $(J_2/J_1)_c = 0.38$  [10, 74].

Analogously, a breakdown of the spin-wave expansion can be evidenced from the vanishing of the uniform susceptibility, which is always finite when there is long-range Néel order in the thermodynamic limit and vanishes instead in presence of a finite triplet gap (see Sec. 1.3). As it is shown in Fig. 4.1, the classical uniform susceptibility is strongly renormalized by the quantum fluctuations for  $s = 1/2$  at the spin-wave level (4.9). As expected, increasing the frustration such reduction is enhanced and leads eventually to the vanishing of the susceptibility for  $J_2/J_1 \simeq 0.35$ . The structure of the finite-size spin-wave excitation spectrum below and above this critical point is very different (see the inset of Fig. 4.1) with an evident breakdown of the quantum top law (1.28), as well as of the spin-wave approximation scheme, in the non-magnetic phase. Below the critical point, instead, the spin-wave theory reproduces remarkably well the exact and Green function Monte Carlo with Stochastic Reconfiguration (GFMC/SR) results for the low-energy part of the spectrum in the whole range of sizes (see Fig. 4.2). Furthermore, as already observed for the triangular antiferromagnet (Sec. 3.1.2), increasing the size, the slope of  $E(S)$  vs  $S(S + 1)$  decreases and gives rise to the collapse of a macroscopic

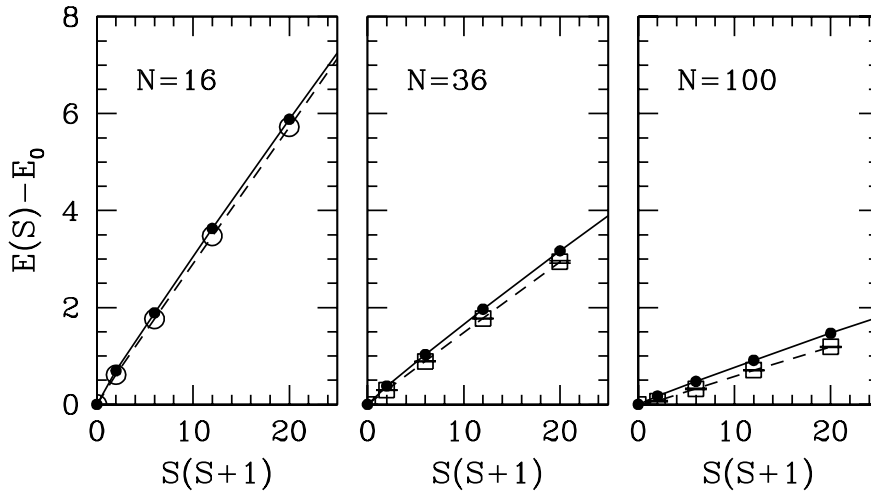


Figure 4.2: Low-energy excitation spectra as a function of  $|\mathbf{S}|^2 = S(S+1)$  for  $J_2/J_1 = 0.2$ ,  $s = 1/2$  and  $N = 16, 36, 100$ : spin-wave (full circles and continuous line), exact (empty circles and dashed lines), GFMCSR with  $p = 8$  [see Sec. 4.3.2] (empty squares and dashed lines).

number of states with different  $S$  on the ground state as  $N \rightarrow \infty$ : i.e., a ground state with a broken  $SU(2)$  symmetry.

## 4.2.2 Size-scaling of the spin gap

The spin-wave prediction for the occurrence of a non-magnetic region in the phase diagram of the  $J_1 - J_2$  Heisenberg model is confirmed by our results for the spin triplet gap obtained using the GFMCSR. The latter calculation, which extends the recent one by Sorella [16], has been performed using (4.3) as guiding wavefunction and including in the SR conditions the energy, all  $\hat{S}_i^z \hat{S}_j^z$  independent by symmetry, and the antiferromagnetic order parameter. The latter, as discussed in Sec. 2.5, though not improving the accuracy of the calculation, allows a very stable and reliable simulation for large  $p$ . The new results, extended up to  $N = 144$ , confirm the previous findings [16] of a finite spin gap in the thermodynamic limit for  $J_2/J_1 \gtrsim 0.40$  (Fig. 4.3). Remarkably, these results are not an artifact of the chosen guiding wavefunction: in fact, unlike the FN approximation, the GFMCSR is able to detect a finite gap in the thermodynamic limit by starting from a spin-wave like wavefunction (4.3) which is Néel ordered and therefore gapless. This behavior is very different from the one observed in the case of the  $s = 1/2$  Heisenberg antiferromagnet on the triangular lattice (see Fig. 3.7) where, with the same numerical scheme, a similar guiding wavefunction and a comparable accuracy we obtained a gapless excitation spectrum. Therefore the existence of a gapped phase in

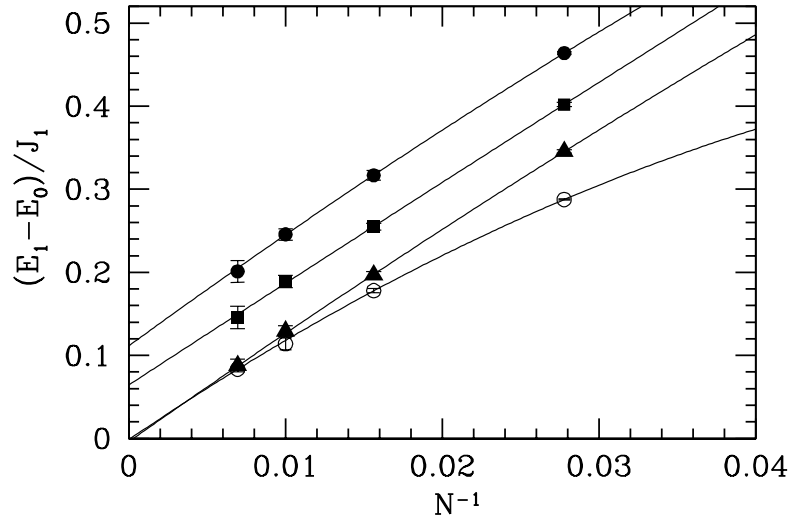


Figure 4.3: Size scaling of the energy gap to the first  $S = 1$  spin excitation obtained with the GFMCSR technique for  $J_2/J_1 = 0.38$  (full triangles),  $0.45$  (full squares) and  $0.50$  (full circles). Data for the unfrustrated ( $J_2 = 0$ ) Heisenberg model taken from Ref. [47], are also shown for comparison (empty circles). Lines are weighted quadratic fits of the data.

the regime of strong frustration is likely to be a genuine feature of the  $J_1 - J_2$  Heisenberg model.

### 4.3 The nature of the non-magnetic phase

In principle either a RVB crystal, with some broken spatial symmetry, or a homogeneous spin liquid is compatible with a triplet gap in the excitation spectrum. Among the dimerized phases proposed in the literature, the so-called *columnar* and *plaquette* RVB are the states which are the most likely candidates. These kind of states can be thought of as a collection of valence bond states  $|\bullet\text{---}\bullet\rangle = |\uparrow\downarrow\rangle - |\downarrow\uparrow\rangle$  between neighboring sites arranged in the patterns shown in Fig. 4.4, where the plaquettes in (b) are the following rotationally invariant superpositions:

$$|\square\rangle = |\begin{array}{cc} \bullet & \bullet \\ \text{---} & \text{---} \\ \bullet & \bullet \end{array}\rangle + |\begin{array}{cc} \bullet & \bullet \\ \text{---} & \text{---} \\ \bullet & \bullet \end{array}\rangle.$$

Both the columnar and the plaquette states break the translation invariance along the  $x$  and  $y$  directions, but only the latter preserves the symmetry of interchange of the two axes. In both cases, however, the resulting ground state is fourfold degenerate in the thermodynamic limit, in agreement with Haldane's hedgehog argument described in

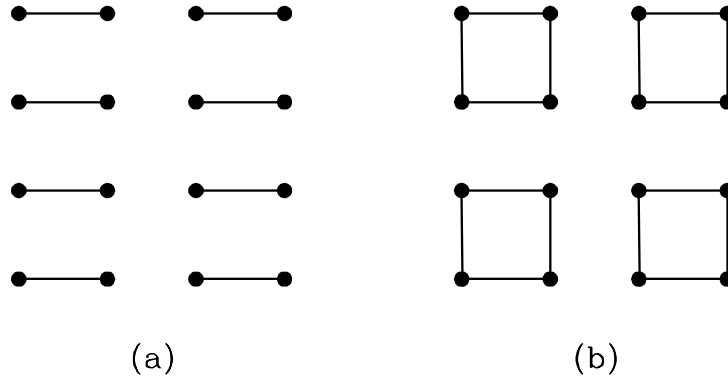


Figure 4.4: Columnar (a) and plaquette (b) RVB states.

Ref. [82] and with a suggested, but yet not proven, generalization of the Lieb-Schultz-Mattis theorem to the two-dimensional case [83].

Read and Sachdev [80] with a field-theoretic large- $N$  expansion, were the first to conjecture that quantum fluctuations and a next-nearest-neighbor frustrating interaction could drive the ground state of the square lattice antiferromagnet into a columnar RVB state and series expansion studies [77, 78] have supported over the years this prediction. Recently, Kotov and co-workers [84] with a study that combines an analytic effective Hamiltonian approach, extended dimer expansions and exact diagonalizations have presented a body of evidences that has been interpreted as supporting the columnar scenario. Finally, using the Green function Monte Carlo (GFMC) with Stochastic Reconfiguration (SR) (Sec. 2.4), du Croo de Jongh and co-workers [85] have proposed a ground state with intermediate properties between the plaquette and columnar RVB.

### 4.3.1 The method of generalized susceptibilities

In order to better characterize the nature of the ground state in the gapped phase, we have checked the occurrence of some kind of crystalline order, by calculating the response of the system to operators breaking the most important lattice symmetries. As suggested in Refs. [78, 79, 86], and also shown in Sec. 1.2, the occurrence of some kind of crystalline order in the thermodynamic ground state can be checked by adding to the Hamiltonian (2) a term  $-\delta\hat{O}$ , where  $\hat{O}$  is an operator that breaks some symmetry of  $\hat{\mathcal{H}}$ . In fact, if true long-range order exists in the thermodynamic ground state, the finite-size susceptibility  $\chi_O = \langle \hat{O} \rangle_\delta / N\delta$  has to diverge with the system size and, in particular, it is bounded from below by the system volume squared [Eq. (1.25)]. Thus susceptibilities are a very sensitive tool – much more than the square of the order parameter – for detecting the

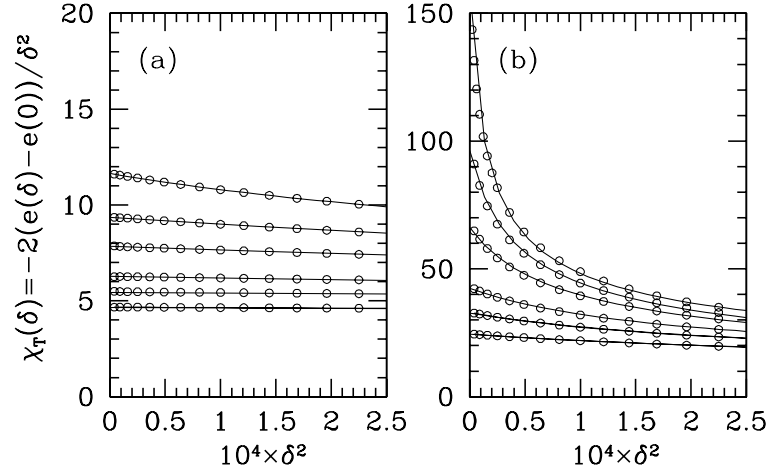


Figure 4.5: Exact results for the  $J_1 - J_2$  chain:  $\chi_T(\delta)$  associated to the operator  $\hat{O}_T$  (breaking the translational invariance) for  $J_2/J_1 = 0.2$  (a) and  $J_2/J_1 = 0.4$  (b). Data are shown for  $N = 12, 14, 16, 20, 24, 30$  for increasing values of  $\chi_T(\delta)$ . Lines are guides for the eye.

occurrence of long-range order.

Within a numerical technique, the susceptibility  $\chi_O = d^2 e(\delta)/d\delta^2|_{\delta=0}$  can be calculated with only energy measurements by computing the ground-state energy per site in presence of the perturbation for few values of  $\delta$  and by estimating numerically the limit

$$\chi_O = \lim_{\delta \rightarrow 0} \chi_O(\delta) = -\frac{2(e(\delta) - e_0)}{\delta^2}. \quad (4.10)$$

As we have tested in the one dimensional  $J_1 - J_2$  model, the numerical study of long-range order by means of  $\chi(\delta)$  is very effective and reliable. Here a quantum critical point at  $J_2/J_1 \simeq 0.2412$  separating a gapless spin-fluid phase from a gapped dimerized ground state (which is two-fold degenerate and adiabatically connected to the Majumdar-Ghosh exact solution for  $J_2/J_1 = 0.5$ ) is rather well accepted [87, 88, 89]. As shown in Fig. 4.5, the response of the system to the perturbation  $\delta \hat{O}_T$ , with

$$\hat{O}_T = \sum_j e^{ikj} \hat{\mathbf{S}}_j \cdot \hat{\mathbf{S}}_{j+x}, \quad (4.11)$$

breaking the translation invariance with momentum  $k = \pi$ , is very different below and above the dimer-fluid transition point. However it is extremely important to perform very accurate calculations at small  $\delta$  to detect the divergence of the susceptibilities for large system sizes.

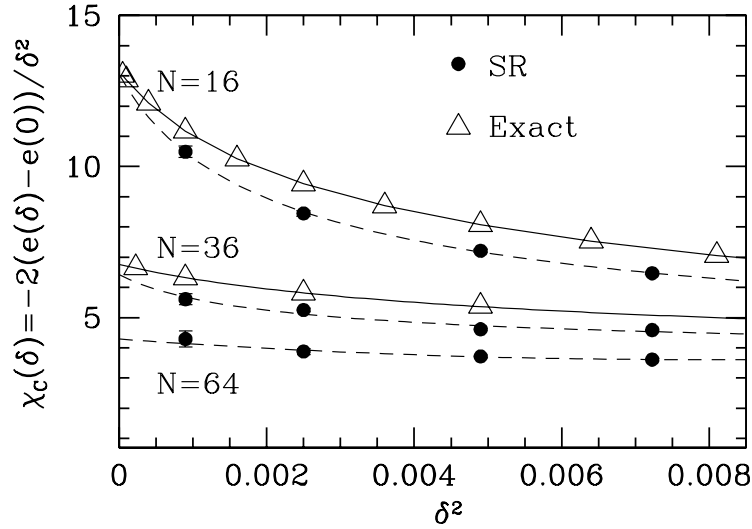


Figure 4.6: Exact and GFMCSR calculation of  $\chi_C(\delta)$  associated to  $\hat{O}_C$  (columnar dimerization) for  $J_2/J_1 = 0.5$ . Lines are guides for the eye.

### 4.3.2 Stability of Plaquette vs Columnar RVB

As also suggested in a recent paper by Singh and co-workers [78], the appearance of a columnar state can be probed by using as order parameter the operator

$$\hat{O}_C = \sum_i (\hat{\mathbf{S}}_i \cdot \hat{\mathbf{S}}_{i+x} - \hat{\mathbf{S}}_i \cdot \hat{\mathbf{S}}_{i+y}), \quad (4.12)$$

where  $x = (1, 0)$ ,  $y = (0, 1)$ . As shown in Fig. 4.6, the exact diagonalization results for  $N = 16$  and  $N = 36$  indicate that the susceptibility associated with this kind of symmetry breaking,  $\chi_C$ , decreases with the system size. In order to exclude an anomalous size scaling, with the SR scheme described in Sec. 4.2.2, we have extended the calculation up to  $N = 64$ . Our quantum Monte Carlo results, which reproduce quite well the ED data, rule out clearly the columnar dimerization.

The above result is in disagreement with the conclusions of several series expansion studies [77, 78]. However, as stated in Ref. [78], the series for  $\chi_C$  are very irregular and do not allow a meaningful extrapolation to the exact result. In our calculation instead, even the ED results for  $N \leq 36$ , are already conclusive.

Having established that the columnar susceptibility is bounded, it is now important to study the response of the  $J_1 - J_2$  model to a small field coupled to the perturbation

$$\hat{O}_T = \sum_i e^{i\mathbf{Q}_0 \cdot \mathbf{r}_i} \hat{\mathbf{S}}_i \cdot \hat{\mathbf{S}}_{i+x}, \quad (4.13)$$

with  $\mathbf{Q}_0 = (\pi, 0)$ , explicitly breaking the translation invariance of the Hamiltonian. The evaluation of  $\chi_T$ , with a reasonable accuracy, is a much more difficult task. In fact in

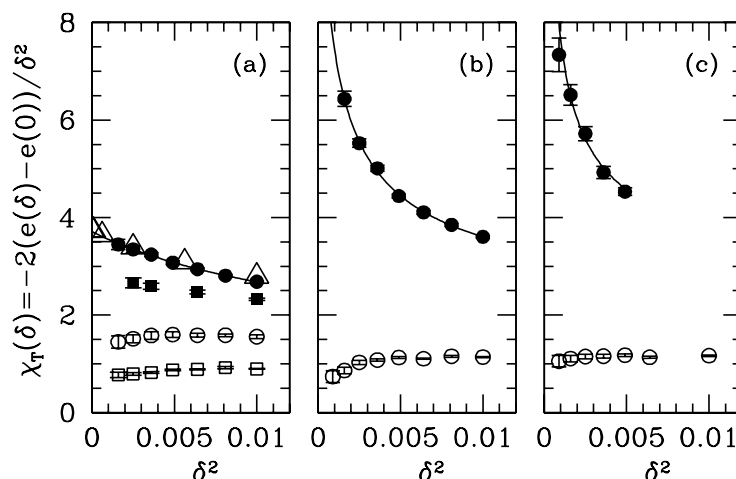


Figure 4.7:  $\chi_T(\delta)$  associated to  $\hat{O}_T$  for  $J_2/J_1 = 0.5$ ,  $N = 32$  (a),  $N = 64$  (b) and  $N = 100$  (c): FN (empty squares), GFMCSR (full squares), FN with LS (empty circles), GFMCSR with LS (full circles), exact (empty triangles).

this case the ED values of the susceptibility for  $N = 16$  and  $N = 32$  increase with the size and much more effort is then required to distinguish if this behavior corresponds to a spontaneous symmetry breaking in the thermodynamic limit. As it is shown in Fig. 4.7 (a), the FN technique, starting from a guiding wavefunction without dimer order, is not able to reproduce the actual response of the system to  $\hat{O}_T$ , even on small sizes. The GFMCSR technique allows us to get an estimate of the susceptibility which is a factor of three more accurate, but not satisfactory enough. In order to improve on this estimate, we have attempted to include in the SR conditions many other, reasonably simple, correlation functions (such as the spin-spin correlation functions  $\hat{S}_i \cdot \hat{S}_j$  for  $|r_i - r_j| > \sqrt{2}$ ), but without obtaining a sizable change of the estimate of  $\chi_T$ . In fact, the most effective SR conditions are those obtained with operators more directly related to the Hamiltonian [17, 36].

After many unsuccessful attempts, we have realized that it is much simpler and straightforward to improve the accuracy of the guiding wavefunction itself. As discussed in Sec. 2.3.1, this can be obtained by applying a generalized Lanczos operator  $(1 + \alpha \hat{\mathcal{H}})$  to the variational wavefunction  $|\psi_G\rangle$ , where  $\alpha$  is a variational parameter. This defines the so-called one Lanczos step (LS) wavefunction, described also in Appendix F. In the present model by using the LS wavefunction, a clear improvement (by about a factor of 3) on the variational estimate of the ground-state energy is obtained at all strengths of frustration (see Tab. 4.1). With this starting point the GFMCSR provides an estimate of the ground-state energy which is basically exact for moderate frustration and remarkable accurate for  $J_2/J_1 = 0.4$  and  $0.5$ . More importantly, as shown in Fig. 4.7 (a),

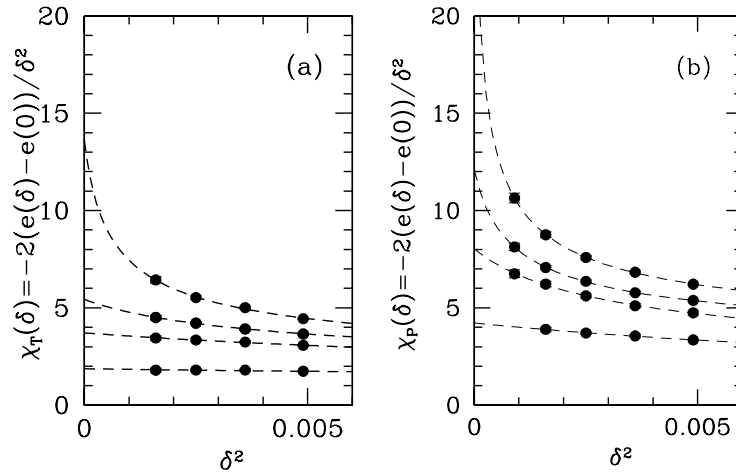


Figure 4.8: GFMCSR calculation of  $\chi_T(\delta)$  (left panel) and  $\chi_P(\delta)$  (right panel) for  $J_2/J_1 = 0.5$  and (from the bottom)  $N = 16, 32, 36, 64$ . Lines are guides for the eye.

the LS wavefunction allows a much better estimate of the susceptibility. Remarkably, on all the finite sizes where ED is possible, the GFMCSR estimate of this important quantity is basically exact within few error bars. This calculation was obtained by including in the SR conditions the energy, the spin-spin correlation functions up to next-nearest-neighbors, distinguishing also  $\hat{S}_i^z \hat{S}_j^z$  and  $(\hat{S}_i^x \hat{S}_j^x + \hat{S}_i^y \hat{S}_j^y)$  ( $p = 4$ ). The mixed averages of these correlation functions can be computed over both the wavefunction  $|\psi_G\rangle$  and the LS wavefunction  $(1 + \alpha \hat{\mathcal{H}})|\psi_G\rangle$  during the same Monte Carlo simulation. Thus with a LS wavefunction one can also easily double the number of constraints that are effective to improve the accuracy of the method ( $p = 8$ ). In this case, we have tested that it is irrelevant to add further long-range correlation functions in the SR conditions even for large size.

By increasing the size [see Figs. 4.7, 4.8 (a)], the response of the system is very strongly enhanced, in very close analogy with the one dimensional model in the dimerized phase [see Fig. 4.5 (b)]. This is obtained only with the GFMCSR technique, since as shown in Fig. 4.7, the combination of FN and Lanczos step alone, is not capable of detecting these strongly enhanced correlations. For  $N = 100$  the GFMCSR increases by more than one order of magnitude the response of the system to the dimerizing field. This effect is particularly striking, considering that the guiding wavefunction (4.3) is spin-wave like, i.e., gapless, Néel ordered and without any dimer long-range order. This suggests that all our systematic approximations are able to remove almost completely even a very strong bias present at the variational level. Of course, for a definite conclusion, one should check whether the susceptibility diverges as the volume squared,

as implied by Eq. (1.25). However, in order to obtain quantitatively reliable zero-field extrapolations (4.10), the limit of very small fields has to be reached. This is in general possible within exact diagonalization (see Fig. 4.5) but it is rather difficult within a stochastic technique like the GFMC which is always affected by a statistical error.

The plaquette state is not the only rotationally invariant RVB crystal having a finite value of the order parameter  $\hat{O}_T$ , even if perhaps it is the most plausible one. In order to corroborate our previous conclusions, we have calculated the generalized susceptibility associated to the order parameter tailored on the plaquette state, namely

$$\hat{O}_P = \sum_{n.n.} h_{i,j} \hat{\mathbf{S}}_i \cdot \hat{\mathbf{S}}_j, \quad (4.14)$$

where  $h_{i,j} = 1$  on the solid bonds forming the plaquettes in Fig. 4.4-(b) and -1 otherwise<sup>1</sup>. As shown in Fig. 4.8, our GFMC results indicate that the response of the system to the plaquette order parameter  $\hat{O}_P$  is a factor of two larger than to the one observed for  $\hat{O}_T$ , breaking generically the translation symmetry. Therefore these new results provide a robust indication for a plaquette RVB ground state in the non-magnetic phase of the  $J_1 - J_2$  Heisenberg model.

Recently du Croo de Jongh and co-workers [85], using the GFMC technique with a density matrix renormalization group guiding wavefunction, have observed a pattern of the spin correlations in the gapped phase which is in-between the columnar and the plaquette dimerization, with a stronger dimerization on one of the two coordinate axes (see Fig. 5 of Ref. [85]). However, this conclusion seems to be ruled out by our results for the susceptibility associated to  $\hat{O}_C$  since the latter order parameter should be finite on this kind of state. The *plaquette-columnar hybrid* is therefore likely to be an artifact of the chosen guiding wavefunction. Indeed, by construction the latter wavefunction is not invariant under rotations of the crystal. Instead our guiding wavefunction is both rotationally and translationally invariant so that the observed broken translation symmetry is likely to be a genuine feature of the model.

## 4.4 Conclusions

In conclusion we have studied the ground-state properties of the spin-half  $J_1 - J_2$  Heisenberg model on the square lattice by means of the finite-size spin-wave theory, exact diagonalization and quantum Monte Carlo techniques. We have found that the combined effect of frustration and quantum fluctuations is enough to melt the antiferromagnetic Néel long-range order, driving the ground state into a quantum disordered phase at

---

<sup>1</sup>I am grateful to R. R. P. Singh for suggesting this susceptibility.

## 80 The $J_1$ – $J_2$ Heisenberg model

$J_2/J_1 \simeq 0.4$ . In order to characterize the nature of the latter phase we have studied the susceptibilities for the most important crystal symmetry breaking operators. Our results, while ruling out clearly the occurrence of a columnar RVB, indicate the plaquette RVB as the most plausible ground-state in the nonmagnetic phase. Moreover, the comparison between the low-energy part of the spin-wave excitation spectrum and the exact and quantum Monte Carlo results indicates a remarkable agreement in the ordered phase, suggesting strongly that the value of the spin susceptibility should be very close to the spin-wave prediction for  $J_2/J_1 \lesssim 0.30$ .

Our predictions could be verified experimentally in the recently synthesized compound  $\text{Li}_2\text{VOGeO}_4$  which has been shown recently [8] to be well described by a spin-half  $J_1$ – $J_2$  Heisenberg model on the square lattice with  $J_2/J_1 \simeq 0.30$ . Forthcoming measurements under pressure [9] could also allow one to tune the  $J_2/J_1$  ratio and to investigate experimentally also the gapped regime.

# Conclusions

In this thesis we have studied the interplay between frustration and zero-point quantum fluctuations in the ground state of the triangular and  $J_1 - J_2$  Heisenberg antiferromagnets. These frustrated systems are the simplest examples of two-dimensional spin models in which quantum effects may be strong enough to destroy the classical Néel order, thus stabilizing a ground state with symmetries and correlations different from their classical counterparts. For this reason, in the last few years, they have attracted much theoretical interest even if a general consensus on the nature of their ground state has not yet been achieved. With this work, by using several techniques including the Green function Monte Carlo with Stochastic Reconfiguration [16, 17], a quantum Monte Carlo method recently developed to keep under control the sign problem, we have put on firmer grounds the conclusions on the ground-state properties of these frustrated models.

Despite the fact that the spin-half Heisenberg antiferromagnet on the triangular lattice was the first historical candidate for a non-magnetic ground state [30, 49], all our results point toward the existence of zero-temperature long-range Néel order. In fact, our quantum Monte Carlo simulations provide robust evidences for a gapless spectrum and for a value of the order parameter that, although reduced (by about 59%) with respect to the classical case, remains finite in the thermodynamic limit. This is partially in agreement with the conclusions of finite-temperature calculations [58] suggesting a ground state with a small but nonzero long-range antiferromagnetic order and with series expansions studies [57] indicating the triangular antiferromagnet to be likely ordered but close to a critical point. However, in our simulation, which to our knowledge represents the first attempt to perform a systematic finite-size scaling analysis, the value of the thermodynamic order parameter is sizeable, indicating the presence of stable long-range order. Moreover, the accuracy of the finite-size spin-wave predictions indicates that the spin-wave theory is a reliable analytical approximation to describe the ground-state properties of the present model. In particular, the effectiveness of the spin-wave theory in reproducing on finite sizes the low-energy excitation spectrum provides further support to the existence of long-range Néel order in the ground state, suggesting also that the value of

the uniform spin susceptibility should be very close to the spin-wave result. We believe that our results, together with the clear indications recently provided by Bernu and co-workers [12] with a symmetry analysis of the low-energy excitation spectra, finally solve the issue of the ordered nature of the ground state of the Heisenberg antiferromagnet on the triangular lattice.

The effects of quantum fluctuations are more remarkable in the  $J_1 - J_2$  Heisenberg model, where the combined effect of frustration and zero-point motion interferes with the mechanism of spontaneously broken symmetry, giving rise to a non-magnetic ground state of purely quantum-mechanical nature. In fact, our spin-wave, exact diagonalization, and quantum Monte Carlo results indicate that quantum fluctuations are able to melt the antiferromagnetic long-range order in the regime of strong frustration, driving the ground state into a quantum disordered phase at  $J_2/J_1 \simeq 0.4$ . In addition, our Lanczos and quantum Monte Carlo calculations of the susceptibilities for the most important crystal symmetry breaking operators have allowed us to characterize the nature of the latter phase and have brought us to a novel interpretation of the disordered ground state of this frustrated model. Our results, in fact, while casting serious doubt on the conclusions of series expansion studies [78, 84], indicate the *plaquette* RVB, with spontaneously broken translation symmetry and no broken rotation symmetry, as the most plausible ground state in the non-magnetic phase. In the ordered phase, instead, similarly to the triangular case, we find a remarkable agreement between the spin-wave low-energy excitation spectrum and the exact and quantum Monte Carlo results. This suggests that the value of the uniform spin susceptibility should be very close to the spin-wave prediction up to  $J_2/J_1 \simeq 0.30$ .

Our results could be also verified experimentally on the novel realizations of these frustrated models, like the triangular K/Si(111):B interface [6], and the  $\text{Li}_2\text{VO}_2\text{SiO}_4$ ,  $\text{Li}_2\text{VOGeO}_4$  compounds [8], quite recently argued to be well described by a spin-half  $J_1 - J_2$  Heisenberg model on the square lattice. Forthcoming measurements under pressure [9] could also allow one to tune the  $J_2/J_1$  ratio and to investigate the properties of these systems in various regimes of frustration.

## **Acknowledgments**

It is a pleasure to acknowledge the stimulating collaboration with S. Sorella, A. Parola, G. Santoro, and A. Trumper. Special thanks to F. Becca, M. Calandra, M. Capone, and S. Caprara. Thanks also to V. Tognetti, A. Rigamonti, P. Carretta and C. Lhuillier for suggestions, stimulating discussions and their warm hospitality in Firenze, Pavia and Paris.



## (Further) Acknowledgments and Greetings

Ed eccoci infine alle pagine più tormentate – e di gran lunga più lette – di una tesi di dottorato: i ringraziamenti e i saluti.

Il primo pensiero va senz'altro a Sandro, cui va tutta la mia riconoscenza per la dedizione con cui mi ha seguito, guidato, sostenuto e aiutato nel mio lavoro. Lavorare con Sandro è un'esperienza incredibile: è prima di tutto un gioco, in cui si parla un gergo allusivo fatto di 'tabpip' e 'rsign', di suscettività che si 'arrapano' e Monte Carli che 'planano' in un surreale alternarsi di gioia, depressione, esaltazione, e imprecazioni, sull'onda degli ultimi risultati. Un caloroso ringraziamento pure ad Alberto, persona di straordinaria e delicata competenza, nonché di humor impagabile, capace di portare con le sue incursioni triestine stimoli per la ricerca e il buon umore. A Giuseppe, per la sua disponibilità e l'attenta lettura di questa tesi e a Valerio per i numerosi consigli e l'attenzione che ha dedicato al mio lavoro. Un grazie anche all'amico Adolfo, a cui sono unito dalla travolgente passione per i triangoli, e un pensiero speciale per Matteo, Massimo e Federico con i quali ho avuto la fortuna di condividere in allegria lavoro, amicizia e l'ufficio; dove i nonsense del primo, il ricercato gossip del secondo e le colorite esclamazioni del terzo sono stati preziosissimi per alleviare la fatica e stemperare le tensioni che – sembra impossibile – abbondano anche a fare questo mestiere. Ciao anche al quarto compagno di stanza: il sagace Tromba, incolpevole testimone della nostra rumorosa attività di ricerca. E grazie pure allo splendido Fabio che ha passato con tutti noi indimenticabili momenti a sventolare e a spalmare la crema sulle nostre accaldate CPU (sì: avete capito bene!). E naturalmente grazie anche a Luisa per l'estrema disponibilità e per aver sopportato con pazienza che gli 'amanti' di suo marito non solo glielo sequestrassero per ore e ore ma gli dedicassero pure amorose telefonate notturne.

Un posto d'onore in questi ringraziamenti spetta poi senza dubbio a Michele. Porto nel cuore i viaggi sull'*Ippolito Nievo* in compagnia sua e del poetico Zimone, con le soste a Mestre, il primino 'alle botti' e la volata giù dal treno per l'hamburger da Mc Donald's; l'incontro con Belzebù, le belle serate dell'ineffabile terzetto ad intrattenere 'le villeggianti' (Giulia e Michela, che saluto con simpatia), il concorsone nella splendida Livorno col cacciucchino e il '5-e-5', il jogging, le serate E.R., l'aerobica e lo step (programma GAG). Michelone ha senza dubbio migliorato molto la qualità della mia vita triestina e la sua amicizia è una delle cose più belle che riporto a casa da Trieste.

Un saluto specialissimo anche a Zimone non solo per essere stato il compagno delle già citate scorribande ma anche per i preziosi insegnamenti di vita che da lui ho ricevuto. Conserverò tra le cose più care i fini tatticismi nell'arte della seduzione che ho avuto la fortuna di imparare dal suo esempio: la tecnica del triste-ma-sensibile con la testa sotto il letto, quella del Re Magio che reca preziosi doni nel suggestivo scenario dello *spazio-porto* (il bar ICTP), oppure quella dello scienziato-poeta che indirizza eleganti versi telematici alla concupita (anche se in questo caso forse non era proprio tutta farina del suo sacco).

Gabriele è poi il migliore compagno di casa che si possa desiderare. Più di un caro amico

e un riservato confidente: una sposa quasi<sup>1</sup>. Di indiscusse doti culinarie, vero virtuoso dell'arte di cucinare il pollo, premuroso e paziente: sempre pronto a preparare un pranzetto coi focchi (a base di pollo, in genere) anche quando rincasavo all'improvviso, mai una scenata o un broncio se una sera rientravo a notte fonda o non rientravo affatto. Un rapporto senza vincoli, intenso e gioioso. Sono felice di avere trovato Gabriele. Grazie Ciccio! (a lui gli piace tanto quando, nell'intimità, lo chiamo così).

Mi sa che in futuro sarà parecchio difficile che io torni così contento da un congresso come lo ero il marzo scorso al ritorno da Fai della Paganella. Da quel giorno infatti e per tre mesi intensissimi, la vitalità partenopea di Francesca ha sconvolto piacevolmente i ritmi della mia vita triestina, trascinandomi in entusiasmanti maratone automobilistiche, aeree e ferroviarie su e giù per la penisola, facendomi immergere nell'incredibile universo di Napoli, che ignoravo completamente e di cui mi sono innamorato a prima vista, e partecipare da vicino (ma proprio vicino vicino) alla incredibile gioia della promozione della 'sua' squadra. Ma come faccio a non volere bene alla ragazza che mi ha fatto scoprire il signor Malaussène gustando i babà di 'Scaturchio'? E infatti gliene voglio. Un bacio.

Ciao e grazie a Mario, mai abbastanza salutato, impareggiabile vicino di stanza con la sua amabile conversazione e le ottime merende a base di caffè e crostatine. La più grande simpatia e i migliori auguri ad Andrea e Janet. Ciao ad Anna (sembra quasi impossibile che una ragazza così bella e simpatica venga da Pisa) e a Biri; ciao a Lorenzo (sorprendente ballerino e mio pusher personale di psichedelici packages  $\LaTeX$ ) e al prestigioso Luigi. Ciao alle due belle Paole e al trasformista Latitanzi (quando sono triste ti penso in versione ultras sugli spalti ad urlare 'orgoglio SISSA' e subito recupero il buon umore). Ciao a Gianluca l'impavido alpinista e ciao a Filippo, col suo fascino irresistibile del 'bello e dannato' e il suo gran gusto per le donne: peccato per Wanda. Ciao alle sue tre 'zie' (beato lui!): Cristina, Valeria e Laura. Ciao a Silvia e Giovanni (e Andrea), e al grande Antonio (vittima privilegiata delle mie gag telefoniche). Ciao ad Andrea (col quale ultimamente ho scoperto di condividere la passione per quel cinema di qualità che va da 'Airforce One' a 'Final Destination') e a Guido. Ciao a Sara e Fabio (che mi stanno troppo simpatici), e un bacetto alla cara Sonia che per me ha sempre una parolina buona. Ciao a Mleone (dalle funamboliche esperienze a Hyde Park), e alla bella Sandrine (*l'un des plus beaux sourires disponibles sur le marchè*). Ciao a Gianni e a Lore, al nobile Stefano e a quel sorprendente incrocio tra Messner e Topo Gigio che è Leonardo. Ciao e grazie anche a Paul che, vittima in questi anni del mio improbabile toscano-english, non se l'è sentita di lasciare che facessi scempio della sua lingua anche nella tesi.

Un grazie affettuoso a Franca, Luigi e Giorgio che con la loro presenza solida ma discreta mi sono stati di grande, grande aiuto. E grazie alla Lella, per essere riuscita – in un modo o nell'altro – a tirarmi fuori dallo stato di alienazione in cui ero sprofondata dopo un anno di dottorato, facendomi recuperare il senso della misura e la capacità di distinguere le cose che

---

<sup>1</sup>Lato erotico a parte.

sono più importanti per una vita completa da quelle che lo sono decisamente meno.

E infine la dedica. Non sapete quanto ho aspettato questo momento. Lo so che è poca cosa, ma per me ha un significato speciale perché non capita spesso l'occasione giusta per mostrare ad una persona o ad un gruppo di persone quanto sono importanti per te. E quale migliore opportunità della dedica di un lavoro che, bello o brutto che sia, ti è comunque costato la fatica di tre anni? Nessuna, appunto. E allora non la perdo di certo questa occasione e senza indugi dedico la mia tesi di dottorato al Bete, al Bonzo, al Butco, al Cipo, al Lubos, al Maffo, al Paro, a Pippio, al Pulce, e al Santo. A loro sono legato da una bellissima amicizia, nata sulla strada (anzi più precisamente in Piazza S. Gervasio), che ci unisce fin da quando eravamo poco più che bambini. Un'amicizia difficile da descrivere, tra persone che l'una con l'altra ci incastrano poco o nulla. Un legame inspiegabile fatto di un sentire comune, della stessa voglia e dello stesso modo di divertirsi, dello stesso gusto di sfottersi a vicenda, magari anche in modo un po' crudele ma mai con malizia, tanto per non prendersi troppo sul serio. Per me sono un punto di riferimento importante e la loro amicizia mi fa sentire ricco e fortunato.

Per questo voglio dedicare la mia tesi al 'Gruppaccio'.

Luca (detto Il Caprio)  
Trieste, 22 Settembre 2000



# Appendix A

## An important property of non-positive Hamiltonian matrices

Let us consider an Hamiltonian  $\hat{\mathcal{H}}$  and a basis  $|\alpha\rangle$  of the Hilbert space such that  $H_{\alpha\beta} = \langle\alpha|\hat{\mathcal{H}}|\beta\rangle \leq 0$  for  $\alpha \neq \beta$ . In this hypothesis, if every state of the basis is connected to all the others by successive application of the Hamiltonian, then it is possible to demonstrate [18] that the (normalized) ground state of  $\hat{\mathcal{H}}$ ,  $|\psi_0\rangle = \sum_{\alpha} f_{\alpha}|\alpha\rangle$ , *i*) has positive-definite components on the chosen basis (i.e.,  $f_{\alpha} > 0$ ) and therefore *ii*) is *non-degenerate*.

The proof of this result, which can be also viewed as a direct consequence of the Perron-Frobenius theorem [20] for *irreducible*<sup>1</sup> nonnegative matrices, is the following. The matrix  $H_{\alpha\beta}$  can be written as the sum of a diagonal and of an off-diagonal contribution  $H_{\alpha\beta} = K_{\alpha\beta} + D_{\alpha\beta}$  such that  $K_{\alpha\beta} = -|K_{\alpha\beta}|$ ,  $K_{\alpha\alpha} = 0$  and  $D_{\alpha\beta} = \delta_{\alpha\beta} e_{\alpha}$ . In these notations, the Schrödinger equation for the ground state  $|\psi_0\rangle$  reads

$$-\sum_{\beta} |K_{\alpha\beta}|f_{\beta} + e_{\alpha}f_{\alpha} = E_0f_{\alpha}, \quad (\text{A.1})$$

where  $E_0$  is the ground-state energy. According to the variational principle (Sec. 2.3), the variational energy on any trial wavefunction exceeds  $E_0$ , unless it is also a ground-state eigenfunction. This implies that the state  $|\psi_T\rangle = \sum_{\alpha} |f_{\alpha}||\alpha\rangle$  is a ground-state eigenfunction. In fact:

$$\begin{aligned} \langle\psi_T|\hat{\mathcal{H}}|\psi_T\rangle &= \sum_{\alpha} e_{\alpha}|f_{\alpha}|^2 - \sum_{\alpha,\beta} |K_{\alpha\beta}||f_{\alpha}||f_{\beta}| \\ &\leq \sum_{\alpha} e_{\alpha}|f_{\alpha}|^2 - \sum_{\alpha,\beta} |K_{\alpha\beta}|f_{\alpha}f_{\beta} = E_0. \end{aligned} \quad (\text{A.2})$$

---

<sup>1</sup>See the footnote of Sec. 1.1.1 .

## 90 An important property of non-positive Hamiltonian matrices

Then, being  $|\psi_T\rangle$  a ground-state eigenfunction, it must satisfy the eigenvalue equation

$$-\sum_{\beta} |K_{\alpha\beta}| |f_{\beta}| + e_{\alpha} |f_{\alpha}| = E_0 |f_{\alpha}|. \quad (\text{A.3})$$

Moreover,

$$e_{\alpha} - E_0 > 0 \quad \text{for all } \alpha, \quad (\text{A.4})$$

otherwise one state of the basis  $|\alpha\rangle$  would be the ground state, which is in general impossible. Therefore, taking the absolute value of  $(e_{\alpha} - E_0)f_{\alpha}$  in Eq. (A.1) and combining with Eq. (A.3), we obtain

$$\left| \sum_{\beta} |K_{\alpha\beta}| |f_{\beta}| \right| = \sum_{\beta} |K_{\alpha\beta}| |f_{\beta}|, \quad (\text{A.5})$$

implying in turn  $f_{\alpha} \geq 0$  for all  $\alpha$ . This result has followed from the non-positive definition of the off-diagonal matrix elements of the Hamiltonian. In the additional hypothesis that every state of the basis is connected to all the others by successive application of the Hamiltonian, it is possible to prove the stronger result:  $f_{\alpha} > 0$  for all  $\alpha$ . In fact, if some  $f_{\alpha}$  vanished, then Eq. (A.3) would read

$$\sum_{\beta} K_{\alpha\beta} |f_{\beta}| = 0, \quad (\text{A.6})$$

implying  $f_{\beta} = 0$  for all  $\beta$  such that  $K_{\alpha\beta} \neq 0$ . Then, by succeeding applications of the Hamiltonian, one could establish that all the amplitudes vanished. Therefore, all the amplitudes  $f_{\alpha}$  of the ground-state expansion  $|\psi_0\rangle = \sum_{\alpha} f_{\alpha} |\alpha\rangle$  are positive and non-vanishing. Since there cannot be an other state orthogonal to  $|\psi_0\rangle$  with only positive-definite coefficients,  $E_0$  is non-degenerate.

# Appendix B

## The uniform spin susceptibility

The uniform spin susceptibility represents the response of the system to a uniform magnetic field. Following the general indications sketched in Sec. 1.2 this quantity can be calculated for the Heisenberg antiferromagnet by adding to the unperturbed Hamiltonian  $\hat{\mathcal{H}}$  a Zeeman operator favoring the alignment of the spins along the quantization axis:

$$\hat{\mathcal{H}}_h = \hat{\mathcal{H}} - h \sum_i \hat{S}_i^z . \quad (\text{B.1})$$

By standard perturbation theory, on any finite size  $N$ , the corrections to the ground-state energy per site are proportional to  $h^2$

$$e(h) \simeq e_0 - \frac{1}{2} \chi h^2 , \quad (\text{B.2})$$

where  $\chi$  is the uniform spin susceptibility on that size. The magnetization induced by the ordering field can be calculated in the thermodynamic limit using the Hellman-Feynman theorem:

$$m(h) \equiv \langle \psi_0 | \hat{S}_i^z | \psi_0 \rangle = -de(h)/dh , \quad (\text{B.3})$$

so that, taking the limit for  $N \rightarrow \infty$  of Eq. (B.2), the usual definition of thermodynamic susceptibility  $m(h) \simeq \chi h$  is recovered.

On a finite size, since the Zeeman term is diagonal, the eigenstates of  $\hat{\mathcal{H}}$  are also eigenstates of  $\hat{\mathcal{H}}_h$ , even if with a different ordering of the energy levels. Hence, the ground-state energy per site in presence of the field is given by

$$e(h) = \min_{\{S, S^z\}} \left[ e(S) - h \frac{S^z}{N} \right] \quad (\text{B.4})$$

where  $S$  and  $S^z$  are the total spin and its projection on the quantization axis, and  $e(S)$  is the ground-state energy per site of  $\hat{\mathcal{H}}$  in the subspace with total spin equal to  $S$ . This relation implies  $S^z = S$ . Therefore, if  $S$  is the value of the spin excitation stabilized by the

## 92 The uniform spin susceptibility

ordering field according to Eq. (B.4), the magnetization reads  $m(h) \equiv S^z/N = S/N$ . Moreover, the expectation value of the Heisenberg Hamiltonian  $\hat{\mathcal{H}}$  on an eigenstate with magnetization  $m = S/N$  is given by the following Legendre transformation:

$$e(m) = e(h) + hm. \quad (\text{B.5})$$

In the thermodynamic limit, the second derivative of the latter expression with respect to  $m$ , calculated for  $m = h = 0$ , reads:

$$\left. \frac{d^2 e(m)}{dm^2} \right|_{m=0} = \left[ \frac{d^2 e(h)}{dh^2} \left( \frac{dh}{dm} \right)^2 + 2 \frac{dh}{dm} \right] \Big|_{h=0}. \quad (\text{B.6})$$

Therefore, using the relation  $m(h) = -de(h)/dh$  and the definition of the spin susceptibility in the thermodynamic limit,  $\chi = \lim_{h \rightarrow 0} \lim_{N \rightarrow \infty} -d^2 e(h)/dh^2$ , the following expansion of  $e(m)$ , for small  $m$ , is readily obtained:

$$e(m) \simeq e_0 + \frac{m^2}{2\chi}. \quad (\text{B.7})$$

Hence, the spin susceptibility can be equivalently calculated, by taking *first* the infinite-volume limit of the energy per site  $e(m) = E(S)/N$  at fixed magnetization  $m = S/N$  and then letting  $m \rightarrow 0$  in Eq. (B.7).

# Appendix C

## Properties of a stochastic matrix

In this Appendix we remind some properties of a stochastic matrix  $p_{x',x}$ . The stochastic matrices are square matrices that have all nonnegative matrix elements  $p_{x',x}$  and satisfy the normalization condition

$$\sum_{x'} p_{x',x} = 1, \quad (\text{C.1})$$

for each column matrix index  $x$ . We assume also that the number of row and column indices is finite and that each index  $x$  is connected to any other  $x'$  by at least one sequence  $p_{x',x_1} p_{x_1,x_2} \cdots p_{x_N,x}$  of nonzero matrix elements of  $p$ <sup>1</sup>.

The stochastic matrices are generally non-symmetric and their eigenvalues may be also complex. For each eigenvalue there exist a left  $\sum_{x'} \psi_L(x') p_{x',x} = \lambda \psi_L(x)$  and a corresponding right eigenvector  $\sum_x p_{x',x} \psi_R(x) = \lambda \psi_R(x')$ . A very simple left eigenvector is the constant one  $\psi_L(x) = 1$ , that by property (C.1) has eigenvalue  $\lambda = 1$ . We will show in the following that this is actually the maximum eigenvalue because: *i) to each right eigenvector  $\psi_R(x)$  of  $p$  corresponds an eigenvalue  $\lambda$ , which is bounded by one  $|\lambda| < 1$ .*

In fact, be  $\psi_R(x)$  a generic (complex or real) right eigenvector of  $p$

$$\lambda \psi_R(x') = \sum_x p_{x',x} \psi_R(x),$$

by taking the complex modulus of both sides of the previous equation and summing over  $x'$  we obtain

$$|\lambda| \sum_{x'} |\psi_R(x')| = \sum_{x'} \left| \sum_x p_{x',x} \psi_R(x) \right| \leq \sum_x \sum_{x'} p_{x',x} |\psi_R(x)| = \sum_x |\psi_R(x)|,$$

---

<sup>1</sup>A matrix satisfying this property is also called *irreducible* [20].

## 94 Properties of a stochastic matrix

where in the above inequality we have interchanged the summation indices and used the elementary bound for the complex modulus  $|\sum_x z_x| \leq \sum_x |z_x|$  for arbitrary numbers  $z_x = p_{x',x}\psi_R(x)$ . This immediately gives:

$$|\lambda| \leq 1 .$$

Obviously the equality sign holds if, for each  $x$ ,  $|\sum_x z_x| = \sum_x |z_x|$ , which implies that, given a right eigenvector with maximum eigenvalue  $\lambda = 1$ , the real positive definite vector  $|\psi_R(x)|$  is also a right eigenvector with maximum eigenvalue.

Now we will show that: *ii) the maximum right eigenvector is unique*. In fact suppose that there are two right eigenvectors  $\psi_1$  and  $\psi_2$  with  $\lambda = 1$ , then by linearity also  $\psi_1 - \alpha\psi_2$  is a right eigenvector with  $\lambda = 1$  and the complex constant  $\alpha$  can be chosen to give  $\psi_1 - \alpha\psi_2 = 0$  for a given index  $x_0$ . On the other hand using the property derived previously also  $|\psi_1(x) - \alpha\psi_2(x)|$  is a right maximum eigenvector that vanishes for  $x = x_0$ . Using iteratively the definition of a right eigenvector

$$\sum_x p_{x',x} |\psi_1(x) - \alpha\psi_2(x)| = |\psi_1(x') - \alpha\psi_2(x')| ,$$

starting from  $x' = x_0$ , we arrive easily to derive that for all the index  $x$  connected to  $x_0$  by nonzero sequence of matrix elements  $p_{x_0,x_1}p_{x_1,x_2} \cdots p_{x_N,x}$

$$|\psi_1(x) - \alpha\psi_2(x)| = 0 .$$

Since by hypothesis all the possible indices are connected to  $x_0$  by at least one such a sequence, we derive  $\psi_1 = \alpha\psi_2$ , which means that  $\psi_1$  and  $\psi_2$  are the same eigenvector, which contradicts the initial hypothesis. Thus the maximum right eigenvector is unique. This result can also be seen as an application of the Perron-Frobenius theorem for nonnegative matrices [20].

Collecting the above properties, *the maximum right eigenvector of a stochastic matrix, has eigenvalue equal to 1, is unique and can be chosen real and positive*. Then it is simple to show [see e.g., Eq. (2.2)] that the iterated application of a stochastic matrix to a trial state  $\psi_T$ ,

$$p^n \psi_T ,$$

converges for large  $n$  to its maximum right eigenvector with an exponentially decreasing error  $\propto \gamma^n$ ,  $\gamma < 1$  being the modulus of largest eigenvalue of  $p$  different from the maximum one <sup>2</sup>.

---

<sup>2</sup>Of course, the initial state  $\psi_T$  must be non-orthogonal to the maximum right eigenvector of  $p$ .

# Appendix D

## Stochastic Reconfiguration conditions

### D.1 Formal proof of the SR conditions

As stated in Sec. 2.4.2, in order to fulfil exactly the SR conditions (2.58),

$$\sum_{x',x} \bar{O}_{x',x}^k \psi_n(x) = \sum_{x',x} \bar{O}_{x',x}^k \psi'_n(x), \quad (\text{D.1})$$

for  $k = 1, \dots, p$ , plus the normalization one  $\sum_x \psi'_n(x) = \sum_x \psi_n(x)$ , it is *sufficient* that the coefficients  $p_{x_j}$  are chosen in a way that

$$\frac{\sum_j p_{x_j} O_{x_j}^k}{\sum_j p_{x_j}} = \frac{\sum_j w_j O_{x_j}^k}{\sum_j w_j}. \quad (\text{D.2})$$

The wavefunction  $\psi'_n(x)$  after the SR defined by (2.49) can be explicitly written in terms of the original walker probability distribution. To this purpose we single out in the definition of  $\psi'_n(x)$ ,

$$\psi'_n(x) = \int [d\mathbf{w}'] \sum_{\mathbf{x}'} P'_n(\mathbf{w}', \mathbf{x}') \frac{\sum_j \delta_{x,x'_j} w'_j}{M}, \quad (\text{D.3})$$

a term  $k$  in the above summation over  $j$  which gives an additive contribution to  $\psi'_n$ , namely  $\psi'_n = \sum_k \{\psi'_n\}_k / M$  with

$$\{\psi'_n(x)\}_k = \int [d\mathbf{w}'] \sum_{\mathbf{x}'} \int [d\mathbf{w}] \sum_{\mathbf{x}} X(\mathbf{w}', \mathbf{x}'; \mathbf{w}, \mathbf{x}) P_n(\mathbf{w}, \mathbf{x}) \delta_{x,x'_k} w'_k, \quad (\text{D.4})$$

where in the above equation we have substituted the definition of  $P'$  in terms of  $P$  given by Eqs. (2.48) and (2.49). In the latter equation it is easy to integrate over all variables  $w'_j, w_j^{eff}, x'_j$  for  $j \neq k$  using the fact that the kernel  $X$  is particularly simple as discussed

in Sec. (2.4.2). Then, the remaining three integrals and summations over  $w'_k, w_k^{eff}, x'_k$  can be easily performed using the simple  $\delta$  functions that appear in the kernel  $X$  and the definition of  $\beta = \sum_j p_{x_j} / \sum_j |p_{x_j}|$ , so that one easily obtains

$$\{\psi'_n(x)\}_k = \int [d\mathbf{w}] \sum_{\mathbf{x}} P_n(\mathbf{w}, \mathbf{x}) \frac{\sum_j w_j}{M} \operatorname{sgn} p_x \frac{\sum_j |p_{x_j}| \delta_{x, x_j}}{\sum_j p_{x_j}}. \quad (\text{D.5})$$

We can replace in general  $\operatorname{sgn} p_x \sum_j |p_{x_j}| \delta_{x, x_j} / \sum_j p_{x_j} = \sum_j p_{x_j} \delta_{x, x_j} / \sum_j p_{x_j}$  even when, occasionally, more configurations satisfy  $x_j = x$ <sup>1</sup>. Thus, we obtain a closed expression for  $\psi'_n(x)$  after the simple summation on the index  $k$ :

$$\psi'_n(x) = \int [d\mathbf{w}] \sum_{\mathbf{x}} P_n(\mathbf{w}, \mathbf{x}) \left( \frac{\sum_j w_j}{M} \right) \sum_j p_{x_j} \delta_{x, x_j} / \sum_j p_{x_j}. \quad (\text{D.6})$$

Then the normalization condition,

$$\sum_x \psi'_n(x) = \int [d\mathbf{w}] \sum_{\mathbf{x}} P_n(\mathbf{w}, \mathbf{x}) \left( \frac{\sum_j w_j}{M} \right) = \sum_x \psi_n(x), \quad (\text{D.7})$$

easily follows. On the other hand the left-hand side of Eqs. (D.1) can be also computed easily, yielding

$$\sum_{x', x} \bar{O}_{x', x}^k \psi'_n(x) = \int [d\mathbf{w}] \sum_{\mathbf{x}} P_n(\mathbf{w}, \mathbf{x}) \left( \frac{\sum_j w_j}{M} \right) \frac{\sum_j p_{x_j} O_{x_j}^k}{\sum_j p_{x_j}}, \quad (\text{D.8})$$

where  $O_{x_j}^k = \sum_{x'} \bar{O}_{x', x_j}$  is the mixed estimator of the operator  $\hat{O}^k$ .

Finally, by substituting the conditions (D.2) into the previous equation, one obtains

$$\sum_{x', x} \bar{O}_{x', x}^k \psi'_n(x) = \int [d\mathbf{w}] \sum_{\mathbf{x}} P_n(\mathbf{w}, \mathbf{x}) \frac{\sum_j w_j O_{x_j}^k}{M} = \sum_{x', x} \bar{O}_{x', x}^k \psi_n(x), \quad (\text{D.9})$$

which proves the statement at the beginning of this section.

The latter conditions can be fulfilled with a solution of a simple linear system for the unknown variables  $\alpha_k$  ( $k = 1, \dots, p$ ) in the definition (2.57) of the coefficients  $p_j$ , as described in the following section.

## D.2 Existence and uniqueness of a solution for the SR

In this section we prove that given the  $p + 1$  SR conditions (D.2) the elements of the table  $p_{x_j}$  in Eq. (2.49) are uniquely determined for each walker configuration  $(\mathbf{w}, \mathbf{x})$ .

---

<sup>1</sup>In fact  $\operatorname{sgn} p_x$  is the same for all the corresponding indices matching  $x_j = x$ , as implied by the definition (2.57) of  $p_{x_j}$  and the condition  $w_j^{eff} > 0$  valid for all  $j$ .

We define here the quantity

$$v_j^k = (O_{x_j}^k - \bar{O}_f^k), \quad (\text{D.10})$$

for each configuration  $j$ , where  $\bar{O}_f^k = \sum_j w_j^f O_{x_j}^k / \sum_j w_j^f$  is the average value over the reference weights,  $w_j^f$ , of the operator considered, labeled by the number  $k$ . The reference weights  $w_j^f$  are restricted to be strictly positive but can be in general arbitrary functions of all the FN weights  $\{w_j^{eff}\}$ , the exact weights  $\{w_j\}$ , and the configurations  $\{x_j\}$ . It is easy to show that, in order that

$$p_{x_j} = w_j^f \left( 1 + \sum_k \alpha_k v_j^k \right) \quad (\text{D.11})$$

satisfy the SR conditions (D.2), it is sufficient that  $\alpha_k$  are determined by the simple linear equation

$$\sum_{k'} s_{k,k'} \alpha_{k'} = \frac{\sum_j w_j^f v_j^k}{\sum_j w_j^f}, \quad (\text{D.12})$$

where

$$s_{k,k'} = \frac{\sum_j w_j^f v_j^k v_j^{k'}}{\sum_j w_j^f} \quad (\text{D.13})$$

is the covariance matrix of the operators  $\hat{O}^k$  over the reference weights  $w_j^f$ . The solution to (D.12) is possible if the determinant of  $s_{k,k'}$  is non-vanishing. Since  $s$  represents an overlap matrix defined with a nonsingular scalar product,

$$\langle v^k | v^{k'} \rangle = \frac{\sum_j w_j^f v_j^k v_j^{k'}}{\sum_j w_j^f}, \quad (\text{D.14})$$

as  $w_j^f$  are positive, its determinant is always nonzero provided the vectors  $v^k$  are linearly independent. Thus, in the latter case, the solution to (D.12) exists and is unique.

On the other hand suppose that among the  $p$  vectors  $v^k$  only  $p' < p$  are linearly independent. Thus the remaining  $p - p'$  vectors can be written as linear combination of  $p'$  linearly independent ones (henceforth we assume that these linearly independent vectors are labeled by the consecutive indices  $k = 1, \dots, p'$ )

$$v_j^{k'} = \sum_{k=1}^{p'} x_k^{k'} v_j^k, \quad (\text{D.15})$$

for  $k' > p'$ , where  $x_k^{k'}$  are suitable coefficients. The same previous considerations allow one to satisfy the first  $p'$  SR conditions as for Eq. (D.12) a unique solution exists if we

## 98 Stochastic Reconfiguration conditions

restrict all the sums for  $k, k \leq p'$ , and  $p_{x_j}$  is determined only by the first  $p'$  linearly independent vectors in (D.11). With the determined  $p_{x_j}$  it is obvious that

$$\frac{\sum_j p_{x_j} v_j^k}{\sum_j p_{x_j}} = \frac{\sum_j w_j v_j^k}{\sum_j w_j} \quad (\text{D.16})$$

is verified for  $k = 1, \dots, p'$ .

On the other hand we can easily show that all the remaining SR conditions (D.16) for  $k' > p'$  are identically satisfied. In fact, in this case the left-hand side of Eq. (D.16) can be manipulated as follows, using definition (D.15)

$$\frac{\sum_j p_{x_j} v_j^{k'}}{\sum_j p_{x_j}} = \sum_{k=1}^{p'} x_k^{k'} \left( \frac{\sum_j v_j^k p_{x_j}}{\sum_j p_{x_j}} \right) = \sum_{k=1}^{p'} x_k^{k'} \left( \frac{\sum_j v_j^k w_j}{\sum_j w_j} \right) = \frac{\sum_j v_j^{k'} w_j}{\sum_j w_j}, \quad (\text{D.17})$$

where in the intermediate steps we have used Eq. (D.16) for  $k \leq p'$ . Thus the SR conditions determine uniquely the table  $p_{x_j}$ .

### Invariance of the SR conditions under linear transformations of the set of reconfigured operators

With the above definitions it is also possible to show that  $p_{x_j}$  remains unchanged for any linear transformation of the operator set. Namely, suppose we consider the new operators

$$\tilde{O}^{k'} = \sum_k L_{k',k} O^k + \beta_{k'} \quad (\text{D.18})$$

in the SR conditions, where the real matrix  $L$  is assumed to have non-vanishing determinant. Within this assumption it is simple to show that  $p_{x_j}$  will remain unchanged.

In fact, the new set of operators will define a new covariance matrix between the new vectors

$$\tilde{v}_j^{k'} = \sum_k L_{k',k} v_j^k, \quad (\text{D.19})$$

i.e.,  $\tilde{v} = Lv$ ,  $\tilde{s} = LsL^T$ , where  $L^T$  is the transposed of  $L$  and the set of new equations

$$\sum_{k'} \tilde{s}_{k,k'} \tilde{\alpha}_{k'} = \frac{\sum_j w_j \tilde{v}_j^k}{\sum_j w_j}$$

is obviously satisfied by

$$\tilde{\alpha} = (L^{-1})^T \alpha, \quad (\text{D.20})$$

where  $\alpha$  is the solution of the SR conditions before the transformation (D.18). Whenever the number  $p'$  of linearly independent  $v^k$  is less than  $p$ , also the number of linearly

independent  $\tilde{v}^k$  will be  $p'$  as  $L$  is nonsingular. The solutions  $\alpha$  and  $\tilde{\alpha}$ , as described previously, refer therefore to the first  $p'$  components, and all the matrix involved, such as  $\tilde{L}$  and  $\tilde{s}$  are in this case restricted to this subspace.

Then, by Eq. (D.20) and Eq. (D.19), it easily follows that the new coefficients  $\tilde{p}_{x_j} = w_j^f (1 + \sum_k \tilde{\alpha}_k \tilde{v}_j^k) = w_j^f (1 + \sum_k \alpha_k v_j^k) = p_{x_j}$ , which finally proves the invariance of the SR conditions under linear transformations of the set of reconfigured operators.

### Optimization of the weights

The definition of the weights  $p_{x_j}$  that satisfy the SR conditions (D.1) is highly arbitrary because as we have mentioned before the probabilities  $P_n$  and  $P'_n$  do not uniquely determine the quantum states  $\psi_n$  and  $\psi'_n$  that are subject to the conditions (D.1). In this sense there may be different definitions of the weights  $p_{x_j}$  that may behave differently at finite  $p$  with less or more accuracy. Though Eqs. (D.1) are equally satisfied for different choices of the coefficients  $p_{x_j}$  the two states  $\psi_n$  and  $\psi'_n$  may be much closer (less bias) for an optimal choice. The optimal choice that minimizes the distance  $|\psi_n - \psi'_n|$ , at fixed number  $p$  of correlation functions included in the SR, probably has not been found yet. We have attempted several choices for the reference weights  $w_j^f$  of Eq. (D.11) but until now no significant improvement of the simplest FN ones has been obtained.



# Appendix E

## Details of the GFMCSR algorithm

In this Appendix the flow chart of the GFMCSR algorithm is briefly sketched. As described in Sec. 2.4.3, it is possible to work without the extra constant shift  $\Lambda$  and apply directly  $e^{-H\tau}$ , the usual imaginary time propagator, to filter out the ground state from the chosen trial wavefunction  $\psi_T$ .

For practical purposes, the algorithm can be divided into three steps: 1) the Green function (GF) evolution, 2) the SR and 3) the measurements of physical mixed average correlation functions. These three steps are iterated until a satisfactory statistical accuracy is obtained for the latter quantities.

The algorithm works with a finite number  $M$  of walkers which is kept fixed. Starting from the first walker ( $j = 1$ ), the basic steps of the algorithm are described below:

1. In the GF evolution, the exact propagator  $e^{-H\Delta\tau}$  and the FN one  $e^{-H^{eff}\Delta\tau}$  are applied statistically for a given imaginary time interval  $\Delta\tau$ . In practice this can be done by setting initially  $\Delta\tau_l = \Delta\tau$  and repeating the following steps until  $\Delta\tau_l > 0$ :
  - (a) Given the configuration of the walker,  $x_j$ , the quantities  $E_{x_j}$ ,  $\mathcal{V}_{sf}(x_j)$  and  $H_{x_j, x_j}^{eff}$  Eqs. (2.16), (2.33), and (2.32) are evaluated. Then the interval  $\Delta\tau_d$  during which the walker is expected to perform only diagonal moves (see Sec. 2.4.3) is computed using the relation  $\Delta\tau_d = \min(\Delta\tau_l, \ln \xi / \pi_d)$ , where  $\xi$  is a random number between 0 and 1 and  $\pi_d = \lim_{\Lambda \rightarrow \infty} \Lambda \ln p_d = E_{x_j} - H_{x_j, x_j}^{eff}$  according to Eq. (2.60).
  - (b)  $\Delta\tau_l$  is updated  $\Delta\tau_l \rightarrow \Delta\tau_l - \Delta\tau_d$  and the walker weights  $(w_j, w_j^{eff})$  are multiplied respectively by

$$e^{(-E_{x_j} + (1+\gamma)V_{sf}(x_j))\Delta\tau_d} \text{ and } e^{-E_{x_j}\Delta\tau_d} .$$

Then if  $\Delta\tau_l > 0$  a new configuration  $x'_j \neq x_j$  is chosen according to the probability table defined only by the normalized off-diagonal matrix elements of  $p_{x',x_j}$ ,

$$\frac{p_{x',x_j}}{\sum_{x' \neq x_j} p_{x',x_j}},$$

and the weight  $w_j$  is multiplied by  $s_{x'_j,x_j}$  (2.34). The GF evolution then restarts from (a). Otherwise, if  $\Delta\tau_l = 0$  the GF evolution for the walker  $j$  terminates and the algorithm proceeds for the next walker starting from step (1).

2. After all the walkers  $(w_j, w_j^{eff}, x_j)$  have been propagated for the total imaginary time interval  $\Delta\tau$ , the SR can be applied. The mixed averages

$$O_{x_j}^k = \langle \psi_G | O | x_j \rangle / \langle \psi_G | x_j \rangle$$

are computed at the end of such propagation for the chosen set of operators  $\hat{O}^k$ . With these quantities both

$$\bar{O}_{eff}^k = \frac{\sum_j w_j^{eff} O_{x_j}^k}{\sum_j w_j^{eff}}$$

and the covariance matrix  $s_{k,k'}$  in Eq. (D.13) are evaluated. By using the latter quantities in the linear system (D.12), the coefficients  $\alpha_k$  are computed and the table  $p_{x_j}$  is determined according to Eq. (D.11). At this stage the reconfiguration procedure for the walkers can finally be performed, i.e., the new  $M$  configurations of the walkers are chosen among the old ones according to the probability  $|p_{x_j}| / \sum_k |p_{x_k}|$ .

3. The mixed averages of the physical observables  $O_j^k$  and the quantity

$$\frac{\sum_k w_k}{M} \frac{\sum_k |p_{x_k}|}{\sum_k p_{x_k}},$$

needed for the calculation of the statistical averages, are stored. The walker weights are set to  $w_j = \text{sgn } p_{x_j}$  and  $w_j^{eff} = 1$ , and the GF evolution can continue from step (1), starting again from the first walker.

In the practical implementation of the algorithm the FN dynamic can be worked out at fixed  $\gamma$ , where  $\gamma$  has to be a nonzero number otherwise the exact GF would not be sampled [see Eqs. (2.31), and (2.32)]. On the other hand the FN is more accurate for  $\gamma = 0$ . A good compromise is to work with  $\gamma = 0.5$  fixed. An alternative choice is to

perform a few runs with different nonzero  $\gamma$ , and to extrapolate the results for  $\gamma \rightarrow 0$ , which should represent the most accurate calculation. Typically, this extra effort is not necessary because there is a very weak dependence of the results upon  $\gamma$  [90].



# Appendix F

## Optimization of the one Lanczos step variational parameter

In this Appendix we describe an efficient way to find the optimal one Lanczos step wavefunction  $|\psi_\alpha\rangle = (1 + \alpha\hat{\mathcal{H}})|\psi\rangle$  (Sec. 2.3.1), starting from a chosen variational guess  $|\psi\rangle$ , *i.e.*, to calculate the value of  $\alpha$  for which the energy

$$E(\alpha) = \frac{\langle\psi|(1 + \alpha\hat{\mathcal{H}})\hat{\mathcal{H}}(1 + \alpha\hat{\mathcal{H}})|\psi\rangle}{\langle\psi|(1 + \alpha\hat{\mathcal{H}})^2|\psi\rangle} \quad (\text{F.1})$$

has a minimum. It is easy to show that

$$E(\alpha) = \frac{h_1 + 2\alpha h_2 + \alpha^2 h_3}{1 + 2\alpha h_1 + \alpha^2 h_2}, \quad (\text{F.2})$$

with  $h_n = \langle\psi|\hat{\mathcal{H}}^n|\psi\rangle/\langle\psi|\psi\rangle$ , and that the condition  $dE(\alpha)/d\alpha = 0$  leads to the solutions:

$$\alpha = (h_1 h_2 - h_3 \pm \sqrt{\Delta})/2(h_1 h_3 - h_2^2) \quad (\text{F.3})$$

with  $\Delta = (h_1 h_2 - h_3)^2 - 4(h_2^2 - h_1 h_3)(h_1^2 - h_2)$ . The existence of a minimum  $\alpha_0$  among them is guaranteed by the variational principle.

Then, in order to find  $\alpha_0$ , a standard method is to calculate statistically the various powers of the Hamiltonian  $h_n$  using the configurations  $x$  generated by the Metropolis algorithm according to the weight  $\psi(x)^2$ . This method is however inefficient since much better importance sampling is obtained when configurations are instead generated according to the optimal Lanczos wavefunction  $\psi_{\alpha_0}(x) = (1 + \alpha_0 E_\psi(x)) \psi(x)$ , where  $E_\psi(x) = \langle\psi|\hat{\mathcal{H}}|x\rangle/\langle\psi|x\rangle$  is the local energy. This wavefunction maybe much better leading to much lower variances especially for the higher moments  $h_2$  and  $h_3$ .

Then, in order to calculate  $\alpha_0$ , given an arbitrary value of  $\alpha$ , it is convenient first to compute the energy expectation value  $h_1$  with the standard statistical method and then,

in place of the direct calculation of the remaining Hamiltonian higher moments  $h_2$  and  $h_3$ , generate statistically configurations according to  $|\psi_\alpha(x)|^2$  and calculate  $E(\alpha)$  and

$$\chi = \frac{\langle \psi_\alpha | (1 + \alpha H)^{-1} | \psi_\alpha \rangle}{\langle \psi_\alpha | \psi_\alpha \rangle}. \quad (\text{F.4})$$

$E(\alpha)$  is obtained by averaging over the chosen configurations the local energy corresponding to  $\psi_\alpha$ , namely  $\langle \psi_\alpha | \hat{\mathcal{H}} | x \rangle / \langle \psi_\alpha | x \rangle$ , whereas  $\chi$  is obtained by averaging over the same configurations  $\psi(x) / \langle x | (1 + \alpha \hat{\mathcal{H}}) | \psi \rangle$ . Given  $\chi$ , it is straightforward to compute  $h_2$  as

$$h_2 = \frac{(\chi^{-1} - 2)(1 + \alpha h_1) + 1}{\alpha^2}, \quad (\text{F.5})$$

and finally, using  $h_1$  and  $h_2$  and  $E(\alpha)$ , the highest moment  $h_3$  can be calculated as

$$h_3 = \frac{E(\alpha)(1 + 2\alpha h_1 + \alpha^2 h_2) - h_1 - 2\alpha h_2}{\alpha^2}. \quad (\text{F.6})$$

Notice that the most difficult energy moment  $h_3$  is given by sampling an energy expectation value, which is by far statistically more accurate compared to the direct determination of  $h_3$ .

Given the values of  $\chi$ ,  $h_1$  and  $E(\alpha)$ , Eq. (F.3) provides the exact value of  $\alpha_0$  within the statistical uncertainties, that are the smaller the nearer is  $\alpha$  to the optimal value  $\alpha_0$ . Typically two or three attempts are enough to reach an accurate determination of  $\alpha_0$  when the condition

$$\chi = \frac{1}{1 + \alpha_0 E(\alpha_0)}, \quad (\text{F.7})$$

which is true in general only for the eigenstates of the Hamiltonian, is exactly fulfilled by the optimal one Lanczos step wavefunction.

# Bibliography

- [1] H. Bethe, *Z. Phys* **71**, 205 (1931)
- [2] E. J. Neves and J. F. Perez, *Phys. Lett. A* **114**, 331 (1986).
- [3] P. W. Anderson, *Science* **235**, 1196 (1987).
- [4] J. D. Reger and A. P. Young, *Phys. Rev. B* **37**, 5978 (1988).
- [5] P. Chandra, P. Coleman, and A. I. Larkin, *Phys. Rev. Lett.* **64**, 88 (1990).
- [6] H. H. Weitering, X. Shi, P. D. Johnson, J. Chen, N. J. DiNardo, and K. Kempa, *Phys. Rev. Lett.* **78**, 1331 (1997).
- [7] C. S. Hellberg and S. C. Erwin, *Phys. Rev. Lett.* **83**, 1003 (1999).
- [8] R. Melzi, P. Carretta, A. Lascialfari, M. Mambrini, M. Troyer, P. Millet, and F. Mila, *Phys. Rev. Lett.* **85**, 1318 (2000).
- [9] P. Carretta, private communication.
- [10] Q. F. Zhong and S. Sorella, *Europhys. Lett.* **21**, 629 (1993).
- [11] P. W. Anderson, *Phys. Rev.* **86**, 694 (1952).
- [12] B. Bernu, C. Lhuillier, and L. Pierre, *Phys. Rev. Lett.* **69**, 2590 (1992); B. Bernu, P. Lecheminant, C. Lhuillier, L. Pierre, *Phys. Rev. B* **50**, 10 048 (1994).
- [13] E. Manousakis, *Rev. Mod. Phys.* **63**, 1 (1991).
- [14] N. Trivedi and D. M. Ceperley, *Phys. Rev. B* **41**, 4552 (1990).
- [15] H. J. M. van Bommel, D. F. B. ten Haaf, W. van Saarloos, J. M. J. van Leeuwen, and G. An, *Phys. Rev. Lett.* **72**, 2442 (1994); D. F. B. ten Haaf, H. J. M. van Bommel, J. M. J. van Leeuwen, W. van Saarloos, and D. M. Ceperley, *Phys. Rev. B* **51**, 13 039 (1995).

## 108 Bibliography

- [16] S. Sorella, Phys. Rev. Lett. **80**, 4558 (1998);
- [17] S. Sorella and L. Capriotti, Phys. Rev. B **61**, 2599 (2000).
- [18] E. Lieb and D. Mattis, J. Math. Phys. **3**, 749 (1962).
- [19] W. Marshall, Proc. R. Soc. London Ser. A **232**, 48 (1955).
- [20] R. A. Horn and C. R. Johnson, *Matrix Analysis* (Cambridge University Press, 1985).
- [21] J. Richter, N. B. Ivanov, and K. Retzlaff, Europhys. Lett. **25**, 545 (1994).
- [22] P. Azaria, B. Delamotte and D. Mouhanna, Phys. Rev. Lett. **70**, 2483 (1993).
- [23] H. J. Scultz and T. A. L. Ziman, Europhys. Lett. **18**, 355 (1992); H. J. Scultz, T. A. L. Ziman, and D. Poilblanc, J. Phys. I (France) **6**, 675 (1996).
- [24] P. W. Anderson, in *Basic Notions of Condensed Matter Physics* (The Benjamin/Cummings Publishing Company, Menlo Park, CA, 1984).
- [25] H. Neuberger and T. Ziman, Phys. Rev. B **39**, 2608 (1989).
- [26] D. S. Fisher, Phys. Rev. B **39**, 11 783 (1989).
- [27] P. Hasenfrantz and F. Niebermayer, Z. Phys. B **92**, 91 (1993).
- [28] C. Lavallo, S. Sorella and A. Parola, Phys. Rev. Lett. **80**, 1746 (1998).
- [29] S. Chakravarty, B. I. Halperin, and D. Nelson, Phys. Rev. Lett. **60**, 1057 (1988).
- [30] P. W. Anderson, Mater. Res. Bull. **8**, 153 (1973).
- [31] A. Auerbach, *Interacting electrons and quantum magnetism* (Springer-Verlag, New York, 1994); A. Auerbach, F. Berruto and L. Capriotti, in *Field Theories for Low-Dimensional Condensed Matter Systems* edited by G. Morandi, P. Sodano, A. Tagliacozzo, and V. Tognetti (Springer-Verlag, Berlin/Heidelberg, 2000).
- [32] P. Sindzingre, P. Lecheminant and C. Lhuillier, Phys. Rev. B **50**, 3108 (1994).
- [33] S. Liang, B. Doucot, and P. W. Anderson, Phys. Rev. Lett. **61**, 365 (1988); B. Sutherland, Phys. Rev. B **37**, 3786 (1988).
- [34] S. R. White, Phys. Rev. Lett. **69**, 2863 (1992); Phys. Rev. B **48**, 10 345 (1993).

- [35] D. M. Ceperley and B. J. Alder, *Phys. Rev. Lett.* **45**, 566 (1980).
- [36] L. Capriotti, A. E. Trumper, and S. Sorella, *Phys. Rev. Lett.* **82**, 3899 (1999).
- [37] L. Capriotti and S. Sorella, *Phys. Rev. Lett.* **84**, 3173 (2000).
- [38] C. Lanczos, *J. Res. Nat. Bur. Stand.* **45**, 255.
- [39] E. Dagotto, *Rev. Mod. Phys.* **66**, 763 (1994).
- [40] G. Grosso and G. Pastori Parravicini, *Solid State Physics* (Academic Press, 2000).
- [41] G. H. Golub and C. F. Van Loan, *Matrix Computations* (The John Hopkins University Press, Baltimore and London, 1996).
- [42] J. K. Cullum and R. A. Willoughby, *Lanczos algorithms for large symmetric eigenvalue computations* (Birkhauser, Boston, 1985).
- [43] F. Becca, *Ph.D. Thesis* (SISSA, Trieste, 2000).
- [44] J. W. Negele and H. Orland, *Quantum Many-Particle Systems* (Addison Wesley Publishing Company, 1988).
- [45] N. Metropolis, A. W. Rosenbluth, M. N. Rosenbluth, A. H. Teller, and E. Teller, *J. Chem. Phys.* **21**, 1087 (1953).
- [46] E. S. Heeb, and T. M. Rice, *Europhys. Lett.* **27**, 673 (1994); E. S. Heeb, *Ph.D. Thesis* (ETH, Zürich, 1994).
- [47] M. Calandra and S. Sorella, *Phys. Rev. B* **57**, 11 446 (1998).
- [48] D. M. Ceperley and B. J. Alder, *J. Chem. Phys.* **81**, 5833 (1984).
- [49] P. Fazekas and P. W. Anderson, *Philos. Mag.* **30**, 423 (1974).
- [50] T. Oguchi, H. Nishimori, and Y. Taguchi, *J. Phys. Soc. Jpn.* **55**, 323 (1986)
- [51] H. Nishimori and H. Nakanishi, *J. Phys. Soc. Jpn.* **57**, 626 (1988); **58**, 2607 (1989); **58**, 3433 (1989).
- [52] M. Imada, *J. Phys. Soc. Jpn.* **56**, 311 (1987); **58**, 2650 (1989).
- [53] R. Deutscher, H. V. Everts, S. Miyashita, and M. Wintel, *J. Phys. A* **23**, L1043 (1990).

## 110 Bibliography

- [54] P. W. Leung and K. J. Runge, *Phys. Rev. B* **47**, 5861 (1993).
- [55] V. Kalmeyer and R. B. Laughlin, *Phys. Rev. Lett.* **59**, 2095 (1987).
- [56] D.A. Huse and V. Elser, *Phys. Rev. Lett.* **60**, 2531 (1988).
- [57] R. Singh and D. Huse, *Phys. Rev. Lett.* **68**, 1766 (1992).
- [58] N. Elstner, R. R. P. Singh, and A. P. Young, *Phys. Rev. Lett.* **71**, 1629 (1993).
- [59] K. Yang, L. K. Warman, and S. M. Girvin, *Phys. Rev. Lett.* **70**, 2641 (1993).
- [60] M. Boninsegni, *Phys. Rev. B* **52**, 15 304 (1995).
- [61] T. Oguchi, H. Kitatani, and H. Nishimori, *J. Phys. Soc. Jpn.* **56**, 3858 (1987).
- [62] Th. Jolicoeur and J. C. Le Guillou, *Phys. Rev. B* **40**, 2727 (1989).
- [63] S. J. Miyake, *J. Phys. Soc. Jpn.* **61**, 983 (1992).
- [64] A. Chubukov, S. Sachdev, and T. Senthil, *J. Phys.: Condens. Matter* **6**, 8891 (1994).
- [65] L. O. Manuel, A. E. Trumper and H. A. Ceccatto, *Phys. Rev. B* **57**, 8348 (1998).
- [66] I. Ritchey and P. Coleman, *J. Phys.: Condens. Matter* **2**, 9227 (1990).
- [67] G. Baskaran, *Phys. Rev. Lett.* **63**, 2524 (1989).
- [68] M. Takahashi, *Phys. Rev. B* **40**, 2494 (1989).
- [69] J. E. Hirsch and S. Tang, *Phys. Rev. B* **40**, 4769 (1989).
- [70] A. E. Trumper, L. Capriotti, and S. Sorella, *Phys. Rev. B* **61**, 11 529 (2000).
- [71] F. Franjic and S. Sorella, *Prog. Teor. Phys.* **97**, 399 (1997).
- [72] L. Capriotti, R. Vaia, A. Cuccoli, and V. Tognetti, *Phys. Rev. B* **58**, 273 (1998); L. Capriotti, A. Cuccoli, V. Tognetti, P. Verrucchi, and R. Vaia, *Phys. Rev. B* **60**, 7299 (1999).
- [73] E. Dagotto and A. Moreo, *Phys. Rev. Lett.* **63**, 2148 (1989).
- [74] P. Chandra and B. Doucot, *Phys. Rev. B* **38**, 9335 (1988).
- [75] H. A. Ceccatto, C. J. Gazza, and A. E. Trumper, *Phys. Rev. B* **45**, 7832 (1992).

- [76] A. E. Feiguin, C. J. Gazza, A. E. Trumper, and H. A. Ceccatto, Phys. Rev. B **52**, 15 043 (1995).
- [77] M. P. Gelfand, R. R. P. Singh, and D. A. Huse, Phys. Rev. B **40**, 10 801 (1989).
- [78] R. R. P. Singh, Z. Weihong, C. J. Hamer, and J. Oitmaa, Phys. Rev. B **60**, 7278 (1999).
- [79] M. Zithomirski and K. Ueda, Phys. Rev. B **54**, 9007 (1996).
- [80] N. Read and S. Sachdev, Phys. Rev. Lett. **66**, 1773 (1991); S. Sachdev and N. Read, Int. J. Mod. Phys. B **5**, 219 (1991).
- [81] F. Figueirido, A. Karlhede, S. Kivelson, S. Sondhi, M. Rocek, and D. S. Rokhsar, Phys. Rev. B **41**, 4619 (1989).
- [82] F. D. M. Haldane, Phys. Rev. Lett. **61**, 1029 (1988).
- [83] I. Affleck, Phys. Rev. B **37**, 5186 (1988).
- [84] V. N. Kotov, J. Oitmaa, O. P. Sushkov, and Z. Weihong, Phys. Rev. B **60**, 14 613 (1999).
- [85] M. S. L. du Croo de Jongh, J. M. J. van Leeuwen and W. van Saarloos, e-print cond-mat/0002116.
- [86] G. Santoro, S. Sorella, L. Guidoni, A. Parola, and E. Tosatti, Phys. Rev. Lett. **83**, 3065 (1999).
- [87] F. D. M. Haldane, Phys. Rev. B **25**, 4925 (1982); **26**, 5257 (1982).
- [88] G. Castilla, S. Chakravarty, and V. J. Emery, Phys. Rev. Lett. **75**, 1823 (1995).
- [89] S. Eggert, Phys. Rev. B **54**, 9612 (1996).
- [90] M. Calandra, *Ph.D. Thesis* (SISSA, Trieste, 1999).